VELOCITY FIELDS IN MAGNETICALLY DISTURBED REGIONS OF THE Hα CHROMOSPHERE

Thesis by

Phillip Howard Roberts, Jr.

In Partial Fulfillment of the Requirements

For the Degree of

Doctor of Philosophy

California Institute of Technology

Pasadena, California

1970

(Submitted October 21, 1969)

ACKNOWLEDGEMENTS

It is my pleasure to thank my research advisor, Professor R. B. Leighton for his encouragement, patiente and help in this project. Without his suggestions many of the mechanical and electronic difficulties encountered in constructing the apparatus would have taken much longer to overcome.

I would also like to thank Dr. Alan Title for help in gathering data and for many useful discussions during the design of the apparatus and interpretation of the data. The work of Mr. Haren Fisher and Mr. Stephen Browne in gathering the data is appreciated as is the great amount of help of Mr. Browne in constructing the apparatus.

I am indebted to Dr. Charles Hyder for permission to use and reprint his spectrum which was of great assistance in interpreting my data.

I am also grateful to Dr. H. Zirin for several helpful discussions, and for the use of his laboratory facilities on many occasions, and the free use of his data. I wish also to thank Drs. D. Bohlin and S. Weart for several useful discussions.

Special gratitude is also due to my wife Joan whose help in data reduction and typing has greatly shortened the time required by this project, and whose courage in the face of many disappointments and trying circumstances has made this work possible.

ABSTRACT

A cancellation machine has been constructed to automatically produce the cancellation required by the method of Leighton in making Doppler movies. Various adaptations of the machine allow rapid data reduction to the 16 mm print required for cinema viewing. The preliminary data gathered in 1966 and 1967 has been reduced. These data consist mostly of Hα Doppler movie pairs, and some Zeeman movie pairs, of sunspot regions. A new calibration technique for inferring Doppler velocities from cancellation densities has been developed. This technique extends the calibration to large Doppler shifts with no less in accuracy.

Doppler movies taken in Hα, .070 nm from the core, show a long lived flow region connecting spots of opposite magnetic polarity in newly developing sunspot regions. The flow regions consist of a series of parallel arched filaments about 2 Mm thick by 23 $\pm$ 8 Mm long which are found also in the Hα core superimposed upon bright plage. The material in the arches is shown to flow downward along the legs of the arch from its center. The average height of the arches is 2 to 4 Mm depending upon the method of calculation. Velocities of 35 km/s inferred in the arches are consistent with those expected from frictionless descent from the top of the arch. An ascent velocity of about 5 km/s of the arch center is also consistent with the data. The material flow is not a mass flow from one leg of the arch to another as previously reported by other observers.

A discussion of other minor discrepancies of this work with that of previous observers points out certain possible sources of error in both their work and this.

A physical model for the arches is proposed, whereby they consist of material trapped by magnetic lines of force which are emerging from the photosphere in the forming sunspot region. This material then flows downward along the arched lines of force as they rise. The subsurface magnetic field energy is shown to be sufficient to raise the material to the heights inferred for the arches, but insufficient to raise the temperature of the photosphere at the feet of the arches by more than about 7° K. The average lifetime of an arch is about thirty minutes yet the rise and decay times indicated by the data are shown to be about five minutes. Two possible explanations are offered for this discrepancy, one involving a great optical depth and the other a series of arches superimposed. Several suggestions are made for further persuing this phenomenon.

The study of Tile of velocity features in the Hα chromosphere of the quiet sun has been extended to active regions. The results for network regions near the sunspots corroborate those of Title. A mean lifetime of 215 ± 9 s was found for upflow events and 371 ± 30 s for downflow. In the regions covered by bright plage in the Hα core photographs the mean lifetime in a majority of both upflow and downflow events was 217±71 s and 211 ± 91 s respectively.

TABLE OF CONTENTS

Part I Introduction

The principal observations upon which this thesis are based were made in the summer of 1966 at the Sixty Foot Solar Tower of the Mount Wilson Observatory with a spectroheliograph camera constructed by A. M. Title.

This camera, together with a new automatic cancellation machine extensively modified from a commercial slide copier, allows rapid production of Zeeman or Doppler movies. The basic idea behind the technique used in the production of the movies is that developed by R. B. Leighton for making Zeeman and Doppler plates. The implementation of the idea, however, is based on an alternative set of techniques applicable only to film in a practical way.

The reasons for building the cancellation machine (Film Copier) and the basic ideas behind the technique which it automates are discussed in Part II. This section also includes a discussion of the advantages and disadvantages of the machine with respect to more traditional techniques. A set of instruction manuals and a very detailed discussion of the machine and associated system may be found in the Appendices. Included there is a detailed discussion of the design considerations that went into the machine in Appendix I. Appendix II explains the controls of the Film Copier in enough detail to allow a novice to operate it. Appendix III explains in detail how to cancel a film to get a Doppler or Zeeman movie. Appendices II and especially III contain many useful photographs and sketches which clarify and illustrate the operation of the Film

Copier and the cancellation method. Appendix IV explains some of the difficulties encountered in construction of the machine, so that some of the reasons behind the design details of Appendix V are clarified.

The routine procedures used in observing the sun and in reducing the 70 mm data to 16 mm projection positive movies are explained in Part III including briefly the cancellation procedures. Many of the problems encountered in the reduction and analysis of these preliminary data have led to the suggestions for improvement of future data which are included at the end of Part VII.

In 1944 Ellison (14) noticed the plage loop regions discussed in Part IV and interpreted the motion in the loops as flow from one leg of the arch to the other. Ellison also looked for examples of this phenomenon on the solar limb. In 1967 Bruzek (10, 11) reported a study of these regions made with data taken in 1966 including some of the same spot groups that this thesis uses. At that time Bruzek also interpreted the flow as Ellison had. Recently Zirin and Weart have noted these features and seen that they are more complex in magnetically more complex regions. In this work we show that the arches are very flat and that the flow is downward in both arch legs as Bruzek has recently realized (11). A fairly simple and consistent model emerges for these regions and is discussed in the latter sections of Part IV.

In 1966 Title described the small jets of upward and downward flowing material seen in Doppler movies of the network of the quiet

sun. Part V extends this study to the network near active regions and to the active regions themselves.

In order to use the preliminary data already obtained and to extend the calibration range of the cancellation technique to large Doppler shifts, a new calibration technique was developed. This technique along with a brief study of the effects of profile broadening on calibration is contained in Part VI. Part VI also discusses the accuracy attained with the new cancellation machine.

Part II The Cancellation Machine

Introduction

In 1958 R. B. Leighton developed a method for making Zeeman spectroheliograms in which the density of the plate was directly related to the Zeeman splitting of the observed line. (1) The method was to obtain a pair of identical images on the entrance slit of the spectroheliograph (SHG) using a beam splitter, then set the grating and exit slit on the wing of a suitable line. An arrangement of a quarter-wave plate and some polaroid filters removed light of opposite circular polarization from the two images. Thus, the effect of the Zeeman splitting of the line on the intensity received at each picture was opposite.

The method was soon extended to making Doppler spectroheliograms in which the density of the image was directly proportional to the Doppler shift in the line. (2) In this method a pair of glass blocks allows the shifting of the apparent position of the two halves of the exit slit as seen from the grating so that these two halves transmit different wavelengths. By putting the two wavelengths in opposite wings of a line, any Doppler shift in the line will cause opposite effects on the two pictures.

Both of these methods require subtraction of the two pictures to obtain the final Zeeman or Doppler picture. The procedure is to make a unit contrast ($\Gamma = 1$) contact print of one of the pictures and to lay it on the other picture so that corresponding image points are

in emulsion to emulsion contact. The latter procedure is called cancellation since all undesired signals are cancelled out and ideally become invisible. The cancellation technique has led to several important discoveries including the five minute oscillation of the upper photosphere,(2,3,4) the supergranulation pattern,(2,3,5,6) the distribution properties of solar magnetic flux, (1,3,5,6,7) some correlations between the magnetic field and structure visible in various wavelengths (1,3,5,6,7) and some properties of small upflow and downflow regions on the quiet sun in Hα (8).

In 1963, Title constructed a pair of 70 mm film cameras to replace the plate holder at the exit slit of the SHG and record the pairs of pictures on separate 70 mm film strips (8). This system with its automatic film advance and SHG control allowed time-lapse Doppler or Zeeman data to be obtained. The data were reduced by a somewhat tedious and time-consuming operation, which involved manually aligning each of the two films in cancellation frame by frame. A set of independent guides for the two films could be adjusted so that as each pair of frames was brought into position below the copy camera, the correct position for copying and cancellation could be felt.

The research leading to this thesis was begun with the hope that a simple automatic procedure for cancelling film strip pairs to make Doppler or Zeeman movies could be built and used for an analysis of velocity or magnetic field changes in active regions. This field of research was essentially untouched, since movies obtained until then had been taken during solar minimum for a study of the quiet sun.

The summer of 1966 was spent considering the alternative methods of automating the cancellation process and collecting Doppler movie pairs in the wings of the Hα line in regions surrounding sunspot groups. These were set aside to await completion of the machine.

A complete discussion of the methods and apparatus for obtaining Zeeman and Doppler plates can be found in Parts I and II of R. W. Noyes's thesis (1963). The design and operation of the Dual 70 mm Camera used in gathering movie data is described in detail in the Appendices of A. M. Title's thesis (1966). A similar description of the construction and operation of the cancellation machine is contained in Appendices I through V of this thesis. (See Figures A1-A8)

The Advantages of the Film Copier

The automatic cancellation machine (called the Film Copier) was constructed and debugged during 1967 and 1968. It was expected to make data reduction about as rapid as its acquisition. The Film Copier was also expected to make time displacement movies practical. In this method a movie is subtracted from itself but with frame i cancelled against frame i + s , where several values of s were to be tried. Another important possibility may be that it is now practical to try doubly cancelled Zeeman and Doppler movies.

The Film Copier has several major advantages. First, it is easy to set up and automatically does all the tedious and repetitive labor in movie reduction without mistakes. It automatically aligns

the unit contrast index copy with the original to achieve cancellation. The relative alignment of the two films is the same from frame to frame and all frames have the same development. Thus changes from frame to frame must be due to changes on the sun since any errors in processing are constant for all frames. Second, and perhaps most important is that with the Film Copier, a movie pair obtained on Mt. Wilson in a morning's run could be viewed as a cancellation movie with a 16 mm projector on the same day, although this has not yet been done. The different procedures involved in making the 16 mm movie from the 70 mm movie pair received from Mt. Wilson require about three hours of efficient work to complete. This allows the observer to learn from his own mistakes in time to improve the next observation. Previously, such difficulties as jitter in the image guider or poor calibration data were not discovered until after the observing season, when sufficient time for the reduction task was available. Third, the Film Copier is versatile having several different uses. The Copier not only processes 70 mm film for making the cancellation movie doing the necessary realignment for cancellation, but also will copy 35 mm movies to 16 mm. Finally, another modification of the Film Copier allows it to be used as a 70 mm film strip projector. In conjunction with the automatic features of the Transport Unit, successive frames may be projected automatically in register. A photometer looking through a small hole in a cardboard screen allows readings of density versus time at areas of interest on the 70 mm frame. Once set up as in Figure 2 a whole series of readings

of successive frames at a given photometer position may be recorded including multiple readings on each frame for consistency checks. This same basic set up allows cancellation pairs to be projected for printing to paper or viewing or photometry. This eliminates one basic disadvantage of film over plates, which is that the cancellation film pair can not be glued together in register and then easily projected.

The major disadvantage of the system has been only that it required two years instead of the expected six months to construct and make operational. A second disadvantage is that should the machine fail electronically, a more competent repairman will be required than would be the case for a nonelectronic control system.

Part III The Data

Introduction

Most of the data taken for this thesis were considered to be exploratory in nature. The expectation was that as soon as the data were reduced by the cancellation machine under consideration, they would serve as a guide in an observation program. Doppler movies of disturbed regions on the sun appeared to be a new and uncharted field of exploration so data were gathered in sunspot regions.

Observations

During the summers of 1966 and 1967, the Dual 70 mm Camera, constructed by Alan Title, was used to take data for Doppler and Zeeman movies. Most of the Doppler data was taken at an offset of .070 nm from the core of the Hα line. The bandpass of the spectroheliograph was set at .011 nm. The time resolution as always was a function of solar altitude, but the average time was about 27.5 seconds. The time resolution was usually 20 seconds per frame after the sun had risen for an hour.

The usual procedure after aiming at the largest spot visible, was to take the first one or two movie frames with no offset from the Hα core. Excepting minor optical aberrations, this produced identical images on the first frames of both the wing movies. When the cancellation movie is to be made, these pictures aid in the alignment procedure and serve as a check on the final results. The bulk of the

movie was run at the prescribed offset from the core of Hα in the early hours after dawn. At the end of breakfast or whenever the seeing seemed to get worse, the movie was halted and a line profile taken with the line shifter at zero and line speed set for good exposure at the Hα core.

The Zeeman data were obtained in the wing of the Ca 610.3 nm line using Kodak 2485 film, and using a specially built quarter-wave plate rotator. The first few frames were taken with the quarter-wave plate set at 0 so that both images would be identical. Unfortunately, the Zeeman data were taken in the Fall of 1967, when a succession of cold fronts was passing through the area causing the seeing to be generally poor. This poor seeing combined with the lack of fiducial marking of the first frames, the low contrast and large grain of the image, and the complex nature of the required reduction procedure, has deterred reduction of the data until better data are obtained. It should be said that had the cancellation machine been operational during the time of observations, many of the procedural difficulties would have become apparent in time to improve later data acquisition.

Preliminary Data Reduction

Most of the data were finally reduced in the late Summer and Fall of 1968 when the Film Copier was finally debugged. The violet wing was always copied at unit magnification with the Dual 70 mm Camera in re-register to give a Doppler cancellation which with the

red wing data was run through the machine face-to-face with sprocket holes aligned. Figure A2 shows the setup for the 70 mm camera. This Doppler bi-pack was copied onto 35 mm High Contrast Copy film, using the Film Copier as shown in Figure A3. The wing movies were copied similarly onto 35 mm film. These 35 mm copies were spliced together in triplets, so that the Doppler movie preceded the violet and red wing movies from which it was made. These triplets were then spliced together in calendar order to make a master movie.

The 35 mm movie was sent to Perfect Film Laboratories (formerly Pathé, now Berkey Pathé) for reduction printing to 16 mm, so that the movie could be viewed with ordinary projection equipment. In the resulting 16 mm Doppler movie, lighter than average features represent downflow of gas on the sun, and darker regions represent upflow, provided the features are absorbing.

After the 16 mm movies were viewed, interest centered on certain days. The Pathé movies were not calibrated with a step wedge and in fact were often of poorer quality than the originals would indicate was warrented. In addition, some of the original movies had errors due to bugs in the Film Copier that were later eliminated after these movies had been copied by Pathé. Because of these problems it was desirable to improve some of the 16 mm movies. A 16 mm Bell and Howell camera was adapted to the Optical Printer to allow inhouse production of 16 mm movies. In the future this camera adaptation will allow cinema viewing of the data on the same day it is obtained. Figure A6 of Appendix IV shows the 16 mm camera set-up.

Since this method eliminates the 35 mm camera altogether, the violet and red wing movies are positive with a white sun against black sky, and the bright Doppler features are approaching while the dark ones are receding.

Part IV A Study of Plage Loop Regions

The Appearance and Form of the Plage Loop Regions

Intensive viewing of the Doppler movies finally led to the discovery of some flow regions near sunspots having unusually long lifetimes. These regions can last for at least a day or more. They are easily seen and rather conspicuous in Doppler stills, but do not attract the attention of the casual observer in movies, since they are a fairly constant feature in a sea of distracting motion. A search of the movies finally yielded six independent examples of this phenomenon of which three are shown in Figures 2, 3, and 4. A comparison with the Hα core frames taken daily for alignment showed that these regions were the "bright loop regions" of Zirin (12) found in newly developing sunspot groups. The plage loops are only found in newly developing sunspot groups and often begin with the first pores or even precede them according to Zirin and Weart. (13) The lack of more than six examples in the present data is due to the fact that the largest sunspot groups on the disk were systematically photographed rather than the newest. This selection effect prevented more data on the arches since a sunspot group had to be about three days old before it could be large enough to attract attention.

The plage loop regions consist of a series of more or less parallel arches connecting leading and following sunspot groups, apparently along lines of magnetic force. In the Hα core the arches are imbedded in the bright plage of the active region between the

spots as shown schematically in Figure 1. The loops appear there as dark striations or filaments on the plage. In the violet and red wings of Hα the legs of the arches appear as dark filaments between the sunspots. The legs visible in the red wing are not visible in the violet wing and vice versa as sketched in Figure 1. Those filaments visible in one wing are lined up more or less in a row near one magnetic polarity of sunspots while those visible in the opposite wing are lined up near the sunspots of opposite polarity in the group. In the Doppler cancellation the filaments from both the violet and red wing pictures may be seen; however, those visible only in the violet wing are lighter than average, while those visible only in the red wing remain darker than average. The above descriptions are shown as a series of sketches in Figure 1 which has the same format as the three photographs, Figures 2, 3 and 4. The arches themselves are filaments having dimensions of about 23 by 2 Mm in projection upon the solar surface. The arches apparently are optically-dense, cool hydrogen which flows down both legs of the arch while the arch itself may rise slowly. The flow is not, as previously interpreted by other observers, a mass flow from one spot to another; although a casual interpretation of the phenomenon will almost always give that result because of a tendency to confuse "line-of-sight" with "solar vertical". The flow may reach speeds of 40 km/s as interpreted from the Doppler shifts indicated in the movies using a calibration factor based on the spectrum received from C. L. Hyder.

The plage loop regions in the 1966 data have three to nine

The top sketch represents the plage loop region as seen in the Hα core. The white area is bright plage. The large dark areas are sunspot umbras. The arches show as dark lines on the plage. The shaded area represents background structure.

The second sketch represents the same region as seen in the red wing at Hα +.07 nm. The receding legs of the arches are visible as short lines and blobs near the top group of spots. The stripes radiating from the large sunspots are penumbras.

The third sketch represents the same region as seen in the violet wing of Hα. The approaching legs of the arches are visible near the large sunspot at the bottom.

The bottom sketch shows the expected cancellation print or Doppler picture of the same region. The approaching legs are now lighter than average and the receding legs darker. The sunspots ideally disappear altogether.

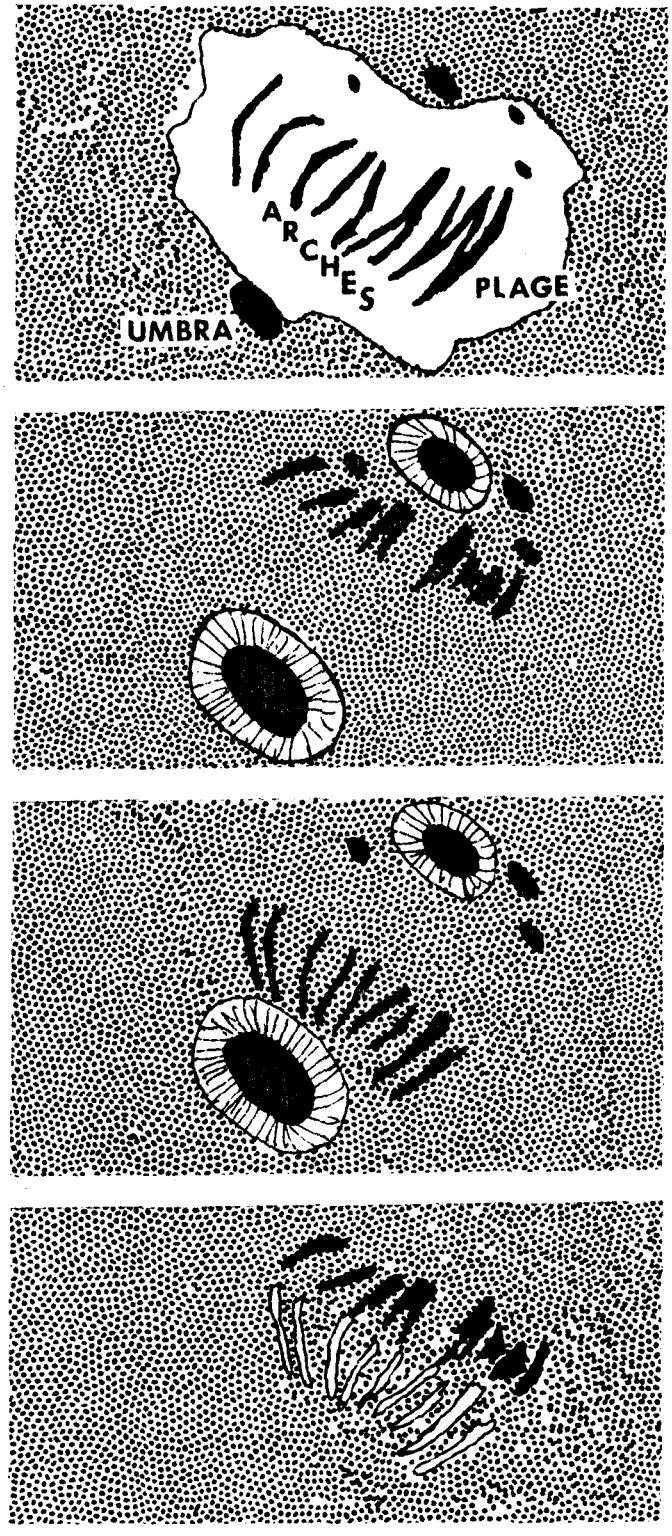

Figure 1. An Idealized Sketch of a Plage Loop Region

Figure 2

Data from July 4, 1966 shows a plage loop region. The length of the fiducial marks correspond to 10 Mm on the solar disk.

Top	Hα core
Second	Hα +.070 nm (red wing)
Third	Hα -.070 nm (violet wing)
Bottom	Doppler (red minus violet)
	Approaching features are white

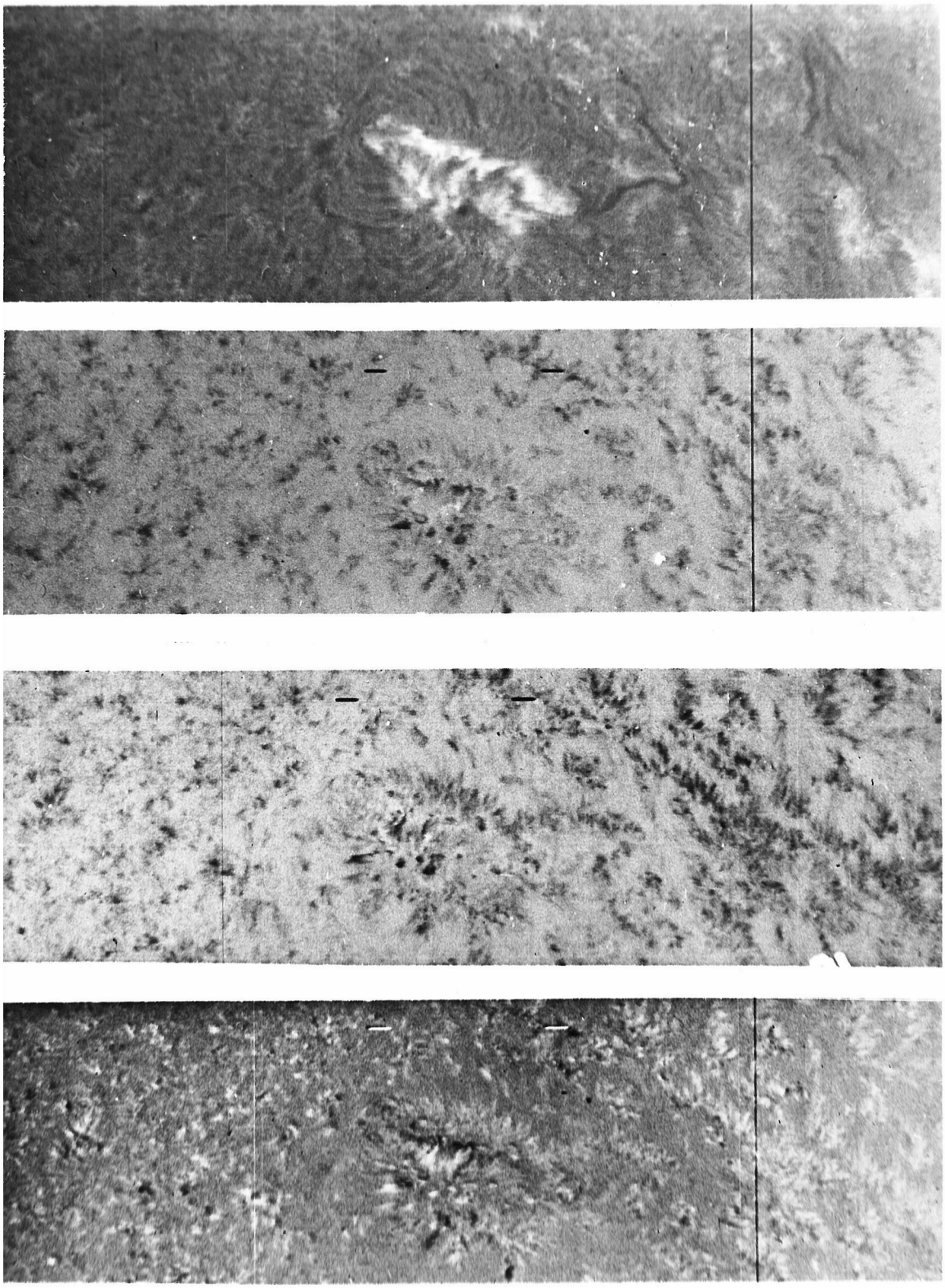

Figure 2. Data From 4 July 1966

Figure 3

Data from July 31, 1966 shows a plage loop region on the right. Note the long filament at the left of this group, which can be seen in the Hα core as an unbent letter J pointing to the big spot. This filament is connecting widely spaced opposite legs in the Doppler frame. Note also how the big filament in the left hand group falls in a clear lane in the Doppler frame. This phenomenon was seen many times.

Top	Hα core
Second	Hα +.070 (red wing)
Third	Hα -.070 (violet wing)
Bottom	Doppler (red minus violet)
	Approaching features are white, except those corresponding to bombs in the wing frames.

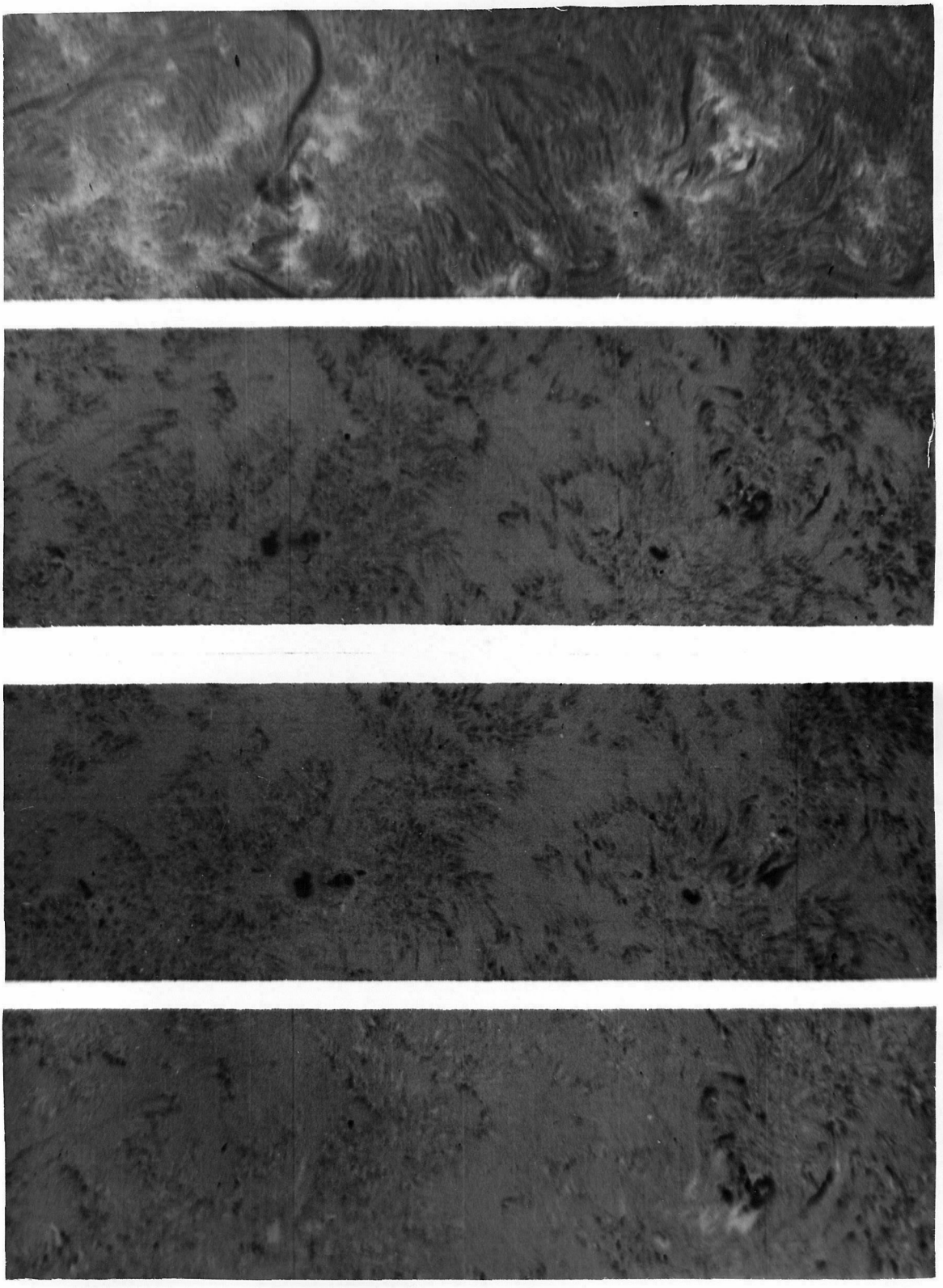

Figure 3. Data From 31 July 1966

Figure 4

Data from August 26, 1966 shows a plage loop region. Fiducial marks correspond to about 10 Mm on the solar disc.

Top	Hα core	
Second	Hα +.070 nm	(red wing)
Third	Hα -.070 nm	(violet wing)
Bottom	Doppler	(red minus violet)
	Approaching features are white.	

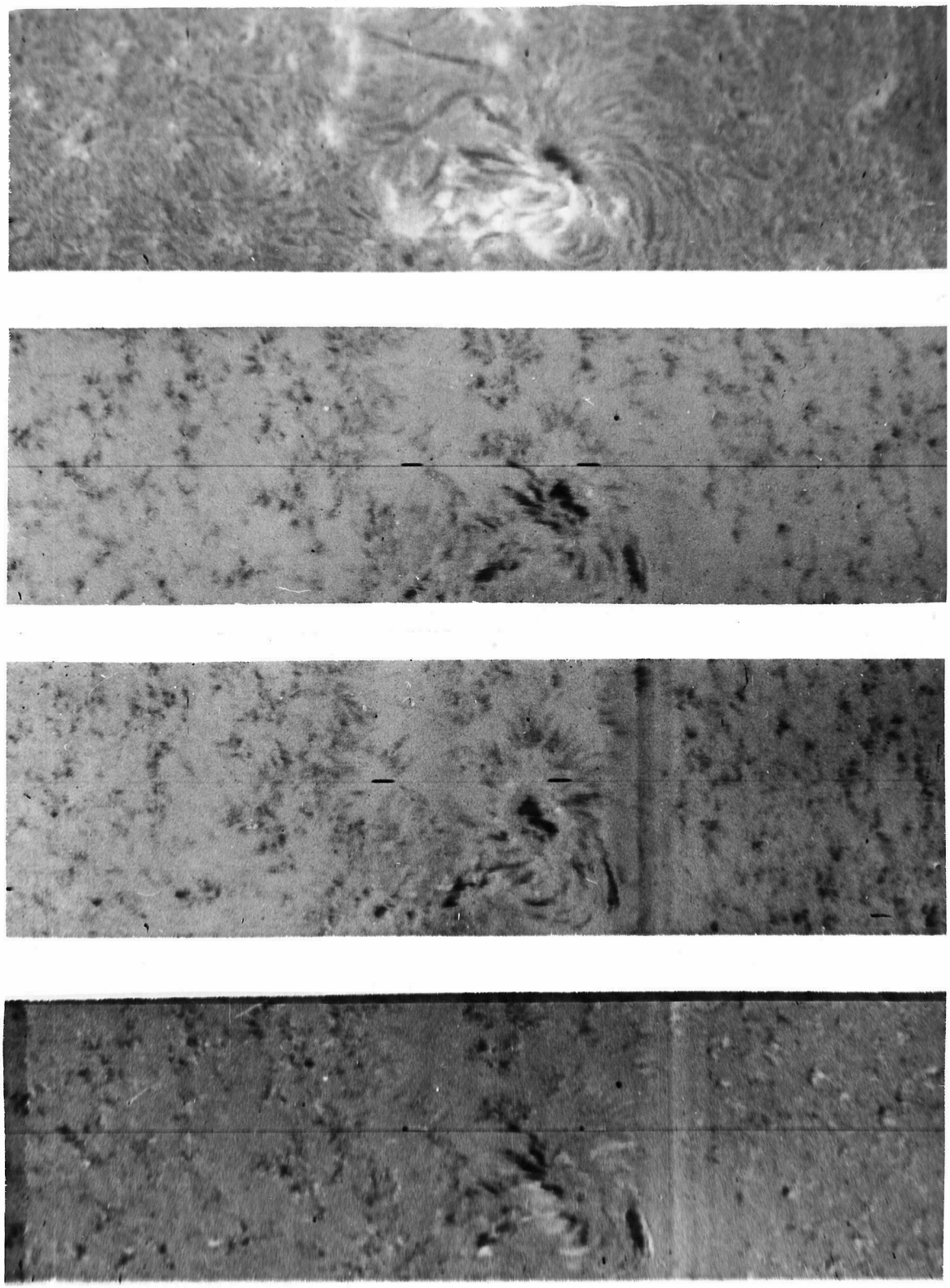

Figure 4. Data From 26 August 1966

filaments and would probably show more of them under better resolution. More arches are often found in younger regions. The above count does not include arches having only one visible leg and thus would ignore those arches having a large invisible center gap in the Doppler pictures. The plage loop regions are smaller than sunspot groups themselves since they lie between leading and following sunspot groups and do not in general seem to connect to any sunspot proper. The dimensions of plage loop regions are from 15 to 40 Mm perpendicular to the arches and are the same dimensions as the arch length parallel to them.

As seen in the Doppler movies the plage loop regions consist of a series of arches as in the Hα core. However, the striking feature is that the opposite legs of each arch have opposite Doppler shifts. All arches of a given region show the same flow pattern. The arches as a whole show an average projected length of 17 $\pm$ 6 Mm. The approaching legs of the arches are dominant averaging 63 $\pm$ 10% of total length projected, at about 45° from vertical, along the line of sight. Although the scatter indicated might allow for many cases of receding legs being longer than approaching legs, only two out of the thirty-five arches measured showed this. The bulk of the cases showed an approaching leg of about twice the projected length of the receding one. About 25% of the cases showed nearly equal leg lengths. The fact that the scatter in the projected total lengths is 35% of the average, whereas the scatter in the percentage of the total length of the approaching legs is only 10%

is because the size of arches varies more than their proportions.

Several cases of thick filaments occurred but these are probably just unresolved filament pairs. Most of the filaments were about 2 Mm thick. Often the red shifted or receding legs appeared to be clumped together. Many cases could also be seen where the two legs of an arch did not meet and yet seemed to be connected by an invisible thread. The invisible thread can in fact be found on the Hα core alignment frame. The best example of this was photographed on July 31, 1966. These invisible connections in the Doppler movies would be consistent with a transverse velocity at the top of the arch or with no velocity.

The inequality of the lengths of approaching and receding legs of an arch is easily explained with the help of the model sketched in Figure 5. As would be expected from the shape of a symmetrical arch when viewed from an angle, the part of the arch closest to the observer has the largest projection along the line of sight. If the flow is downward in both legs and the viewing angle large enough, the nearer leg will flow toward the observer while the farther one will flow away. In this way the approaching leg always has a larger projection along the line of sight no matter toward which limb the phenomenon is found. Clearly too, the phenomenon should appear as receding in both legs when it is found near the center of the disk and thus viewed from a small angle to the local vertical.

The difficulty with the sketch at the bottom of Figure 5 is that the flow is seen to be always from the center of the disk to

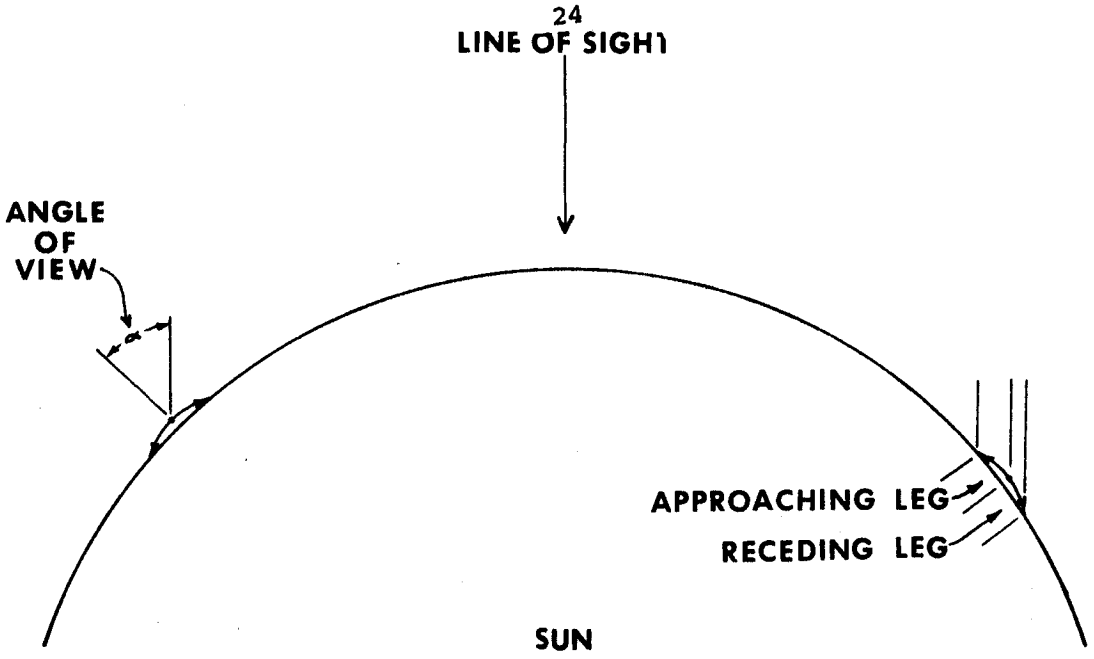

ACTUAL GEOMETRY OF TYPICAL ARCHES

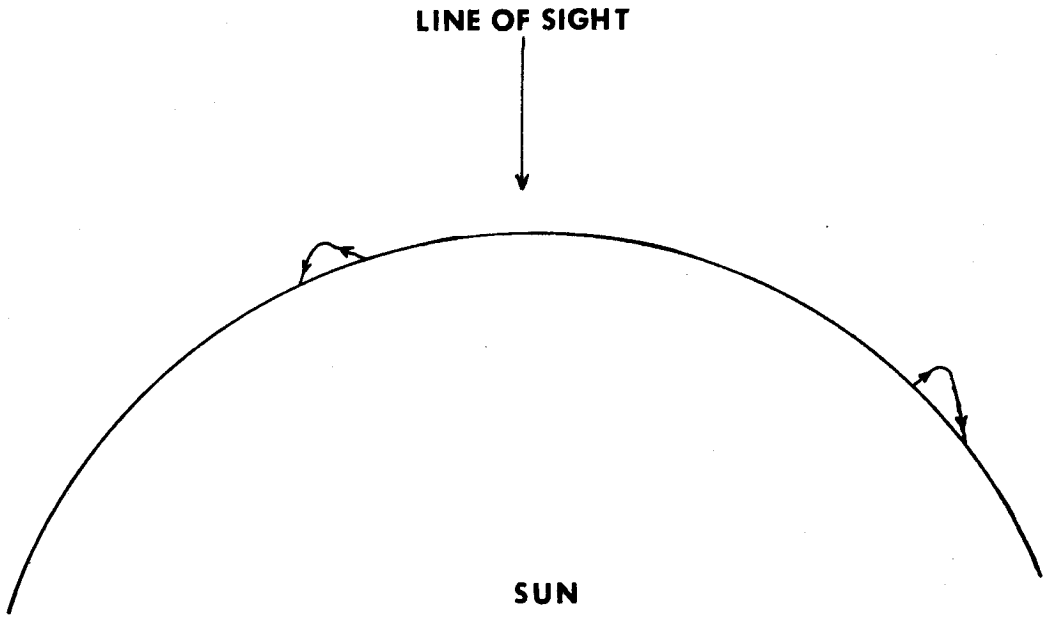

INCORRECT INTERPRETATION OF THE ABOVE GEOMETRY

Figure 5. Models of Plage Loops As Viewed Obliquely

the limb when that model is accepted. Clearly, this would mean that the phenomenon was controlled by the location of the earth in its orbit since that is what defines the center and limb of the solar disk. Such an effect may surely be discounted.

Determination of the Correct Geometry of the Arches

The most inviting model, consistent with the general appearance of these arches, is that matter is flowing out of the solar surface, ascending to the top of the arch and then descending in the opposite or receding leg. This model is however based on the simple mistake of thinking of solar vertical as being equivalent to the line of sight.

Proceeding on the false assumption that the flow was from the approaching leg to the receding one, as earlier observers including Ellison (14) and Bruzek (9, 10) had done, it appeared that the ascending legs of the arches were always nearer the preceding spots and the descending legs nearer the following spots in a given group. Of the six examples eventually discovered in the 1966 data, two proved to be counter-examples to the above hypothesis. These two counter-examples, however, were peculiar in another respect. Both had negative axial tilts, which means that the following spots were closer to the solar equator than the preceding spots. This meant that in all six cases the flow would be from the equator toward the pole. One group was the source of a class three flare within two

days after the arches were observed. It thus seemed worthwhile to investigate possible correlations of the flow directions in the plage loop regions with the axial tilts of sunspot groups and with the occurrence of large flares. A search through some of the data taken through the Hallé filter by Dr. Zirin's group yielded seven more independent samples. For these the time, McMath plage number, hemisphere, direction of flow and distinctness or clarity of each plage loop region were recorded.

The directions of the supposed flow were measured by blinking the wave length scans in the Hα movies of Dr. Zirin. The usual method was to find a day on which a few frames taken at Hα + .05 nm followed by a few taken at Hα -.05 nm were interspersed in the Hα movie. A scan of the Hα frames would indicate the existence of a plage loop region. By running the film back and forth between the Hα +.05 nm and the Hα -.05 nm frames, an impression of material jumping from one set of legs of the arches to the other was created. The direction of the jump as the movie goes from Hα -.05 nm would be the direction of material flow. The Solar Geophysical Data of the E.S.S.A. Research Laboratories allowed the polarities, tilts, plage numbers and location of sunspot groups in the movies to be determined.

Wherever possible several measurements were taken of each region to check consistency. Except where the clarity of the data was poor, all results were self-consistent. Of the nine self-consistent cases, six had positive axial tilts and flow was poleward from preceding to following groups. Of the other three cases with

negative tilts, two showed reversed flow from following to preceding. Thus, of a total of fifteen examples, fourteen showed flow from equator toward pole. This fact should have been a clue that the phenomenon was a manifestation of the angle between the local vertical and the line of sight; however , the symmetry about the equator also indicated a connection to the differential rotation which has similar symmetry. No particular correlation between the flow directions and large flares was found which is understandable.

The idea that the flow ascended in one leg and descended in the other was destroyed by an investigation following the receipt of a spectrum of an arch taken by C. L. Hyder of Sacramento Peak Observatory. The spectrum and a slit jaw photograph are shown in Figure 6. Hyder's spectrum was taken 15° from the center of the solar disk and showed descending flow in both arch legs, and an upflow in the center of the arch. Ellison had also cited such a case. A composite drawing was made to determine the location of each sunspot group in which arches were seen. Inclusion of the supposed mass flow vectors yielded the result shown in Figure 7.

All arches seem to flow from the disk center to the limbs as would be expected according to Figure 10. A check of the E.S.S.A. data confirmed that this was the case for all of Zirin's data too. Bruzek has made a similar analysis of his data and seen a consistent center to limb effect. (11) His interpretation also indicates that the flow is downward in both arch legs.

It is interesting to consider the a priori chance that of

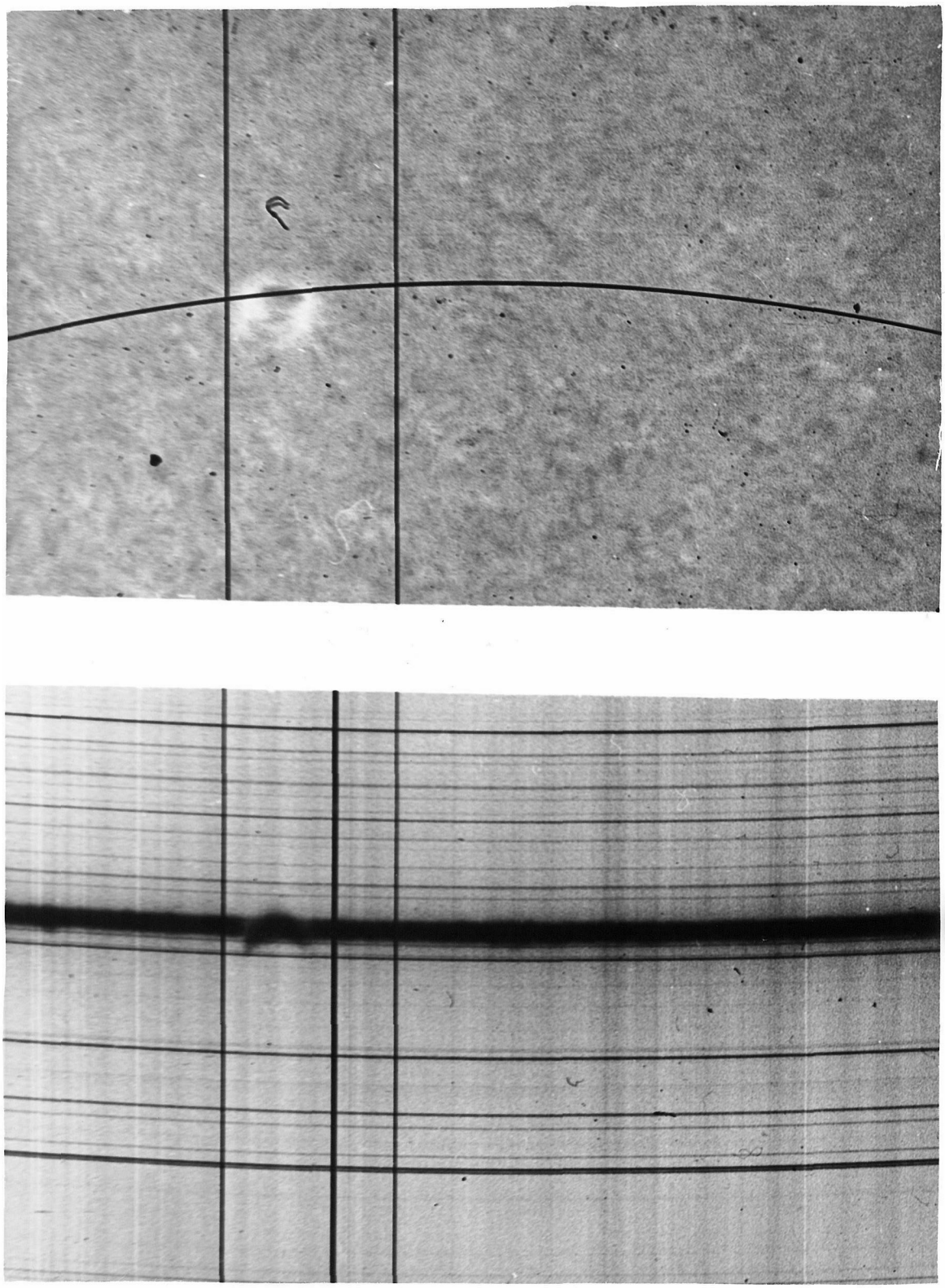

Figure 6. Spectrum and Slit Jaw Photograph With an H Filter Showing a Plage Loop Region

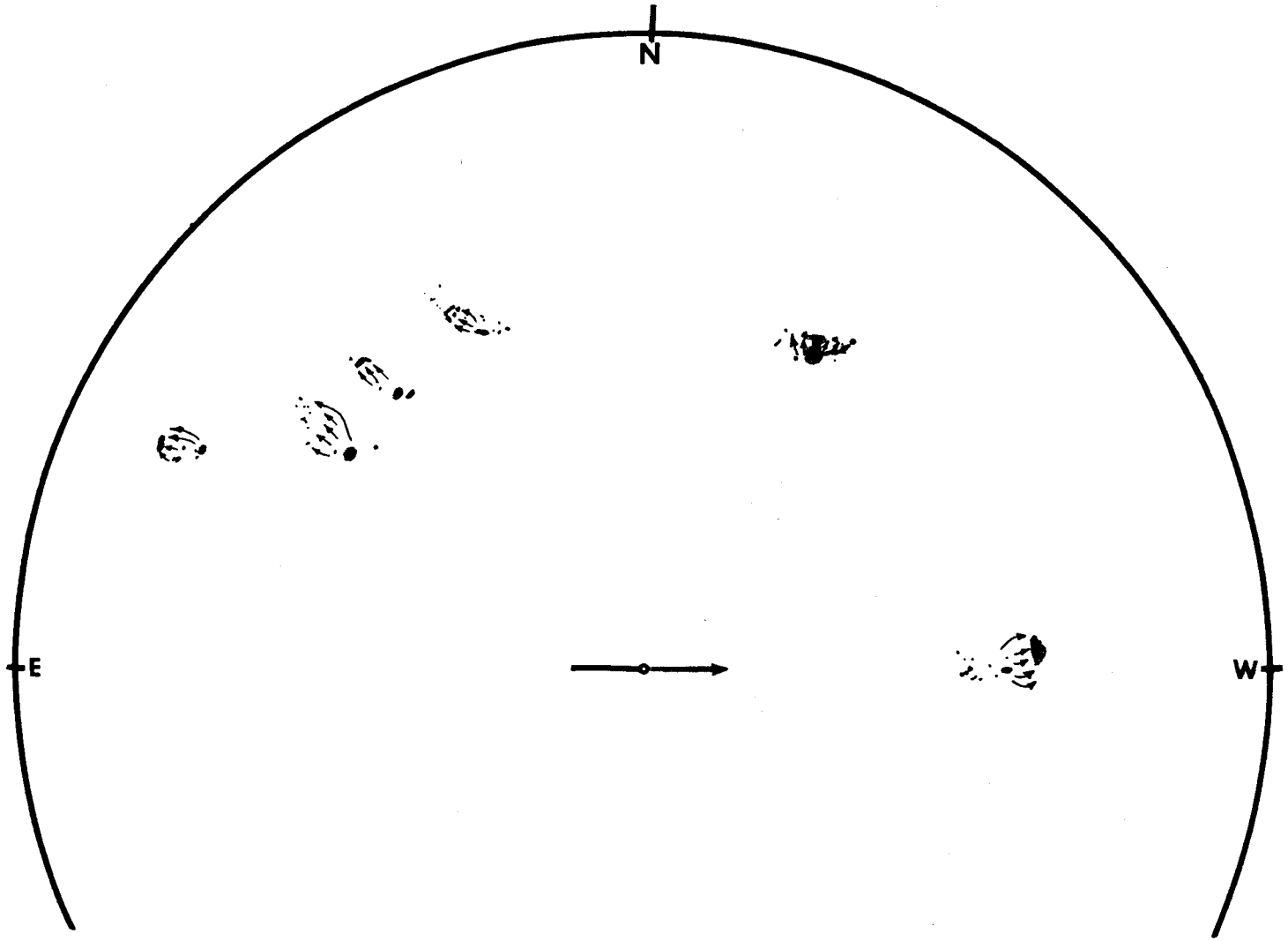

Figure 7. Composite Sunspot Drawing For 6 Groups Having Plage Loops. Arrows Indicate Supposed Mass Flow Which Always Goes From Disc Center to Limb.

four normally tilted and two reverse tilted sunspot groups, the four would be observed on the east limb and the two on the west limb. The chance is .016 which is rather poor luck since it led to a search for tilt correlations rather than to a correct interpretation of the phenomenon.

Calculations of the Average Height of the Arches

It is possible to calculate the average height of these arches within a factor of about two using the model above. The arches cannot be high in comparison to their length. If they were, then the rising center, indicated by the spectrum, would tend to obscure the leg nearest the limb and the arch would appear to rise near the limb and fall near the center of the disk. Therefore, the arches are low in comparison to their length. The approaching and receding velocities and the lengths of the approaching and receding legs are not equal on the average. If the discrepancy is due to the filaments being arches, then the arch height, h, may be estimated using the following derivation based on the geometry of Figure 8.

Assuming the velocities measured were near the center of the legs, we can write the following three equations.

$$V_a = V \sin(\alpha - \theta/2) \qquad (1)$$

$$V_r = V \sin(\alpha + \theta/2) \qquad (2)$$

$$L = 2h \cot(\theta/2) \cos \alpha \qquad (3)$$

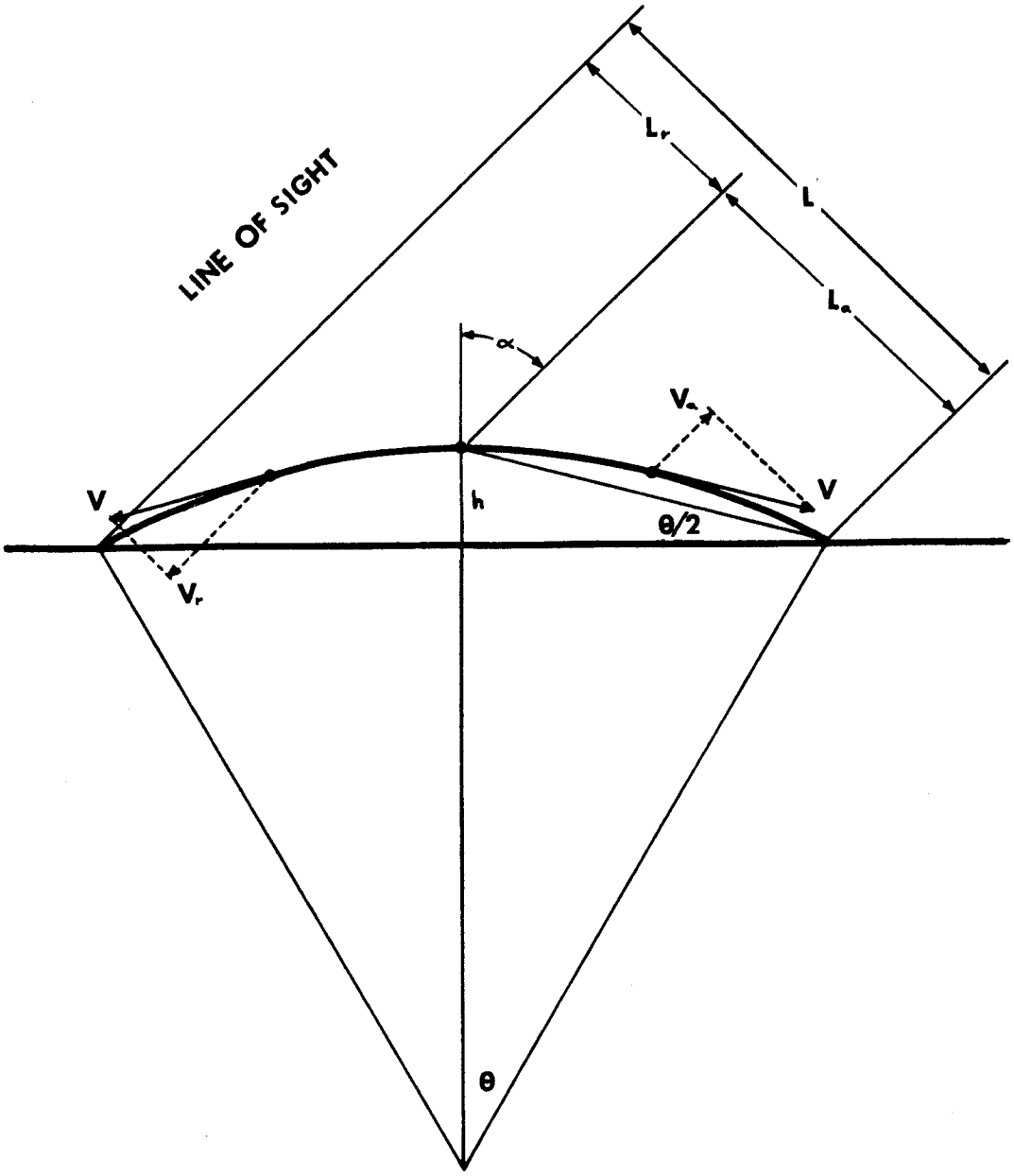

Figure 8. Detailed Model of the Geometry of

An Arch As Viewed Obliquely

By eliminating the unknown quantities V and θ we get equation (4).

$$h = \frac{L}{2} \tan \alpha \sec \alpha \frac{V_r - V_a}{V_r + V_a} \qquad (4)$$

L is the length of the arch projected along the line of sight, α is the angle between solar vertical at the arch and the line of sight, and V_a and V_r are the maximum velocities of approach and recession respectively, measured presumably at the center of each leg. Taking $\alpha = 40°$ for the arches used and taking the average velocities and lengths previously mentioned, an average arch height of about 2 Mm results.

The discrepancy between the average length of the approaching and receding legs of the arches as projected along the sightline, again allows an estimate of the height of the arches. Figure 8. yields the following equations

$$L_a = \frac{L}{2} \sec(\theta/2) \cos(\alpha - \theta/2) \qquad (5)$$

$$L_r = \frac{L}{2} \sec(\theta/2) \cos(\alpha + \theta/2) \qquad (6)$$

These together with equation (3) can be solved for h eliminating θ and L.

$$h = \frac{L_a - L_r}{2 \sin \alpha} \qquad (7)$$

L_a and L_r are the projected lengths of the arch legs and h and α have their previous meanings. Using the average lengths previously mentioned and using $\alpha = 45°$, we get a height of about 3 Mm, in fair

agreement with the previous value.

The heights above are arrived at assuming the filaments are true circular arches, the flow is symmetric about local vertical and that the arch is not rising. If the filaments have other plausible geometries, the true heights will differ from that derived by a small amount. If the center were rising as Hyder's spectrum indicated, then the difference between approaching and receding velocities would be lessened, whereas the dominance of the approaching leg in the total length would be augmented. Thus a rising arch would tend to have a height measured by a formula (4) that was lower than the same height calculated by formula (7). By introducing the upward velocity of the arch into the calculation, the discrepancy can be eliminated. The exact functional form of the upward velocity and flow velocities as a function of arc length have considerable effect on the discrepancy. Simplified models give upward velocities from 2 to 4 km/s. This too is in good agreement with Hyder's spectrum.

The statistical spread of the data would allow that some heights might be as small as zero or as large as 6 Mm. Zero heights or level filaments are hard to reconcile with flow which is presumably driven by gravity. It should be kept in mind however that asymmetry in the flow or shape of a filament could be responsible for specific filaments having indicated heights of zero. It is the expectation that asymmetry in the individual filaments will be cancelled on the average, that makes the average useful.

An analysis of the spectrum allowed a third independent method of estimating the height of the arch in the spectrum. The maximum recession velocities were at the ends of the arch and given by Doppler shifts of .03 nm and .09 nm. A derivation similar to that for formula (1) but taking the values for V_a and V_r at the ends of the legs rather than the centers, leads to equations (8) and (9) in place of (1) and (2).

$$V_a = V \sin (\alpha - \theta) \tag{8}$$

$$V_b = V \sin (\alpha + \theta) \tag{9}$$

Using these with equation (3) yields

$$h = \frac{L}{2} \tan\left\{\frac{1}{2} \arctan\left[\left(\frac{V_r - V_a}{V_r + V_a}\right)\tan \alpha\right]\right\} \tag{10}$$

The result is a height of 2.6 Mm taking L=20 Mm, V_r =40.5 km/s, V_a = -13.5 km/s and $\sin\alpha$ =.27 from the spectrum and accompanying data.

Another method of determining the height of this arch is to assume conservation of energy in the falling matter. If v is the average of the two recession velocities and L is the length of the arch, then since cos α = .97 ≈ 1, we get the following equation for the angle of the legs with the solar surface.

$$\tan(\theta/2) \sin^2\theta = \frac{v^2}{gL} \tag{11}$$

Trial and error on a slide rule leads to θ = 39° which in turn gives h = 3.5 Mm with either of the two formulas used in deriving equation (5).

$$h = v^2/2g \sin^2\theta = \frac{L}{2} \tan(\theta/2) \qquad (12)$$

Velocities in the Arches

Velocities were measured in the arches using the standard calibrating technique based on an average line profile. An aperture corresponding to 1 Mm on the sun was used, which is about the resolution limit of the movie. The aperture allowed measurement of the density of the cancellation picture over an area on the film corresponding to about 1 Mm on the sun. This density in turn gave an average velocity over that area. The average maximum approaching velocity in 22 arch legs was 8.6 $\pm$ 2.7 km/s as measured. The average maximum receding velocity was 12.7 $\pm$ 4 km/s. These velocities are as projected along the line of sight from three spot groups all nearly 40° from the center of the solar disk. Extreme values of 14 km/s approaching and 20 km/s receding were measured. The model of Figure 10 also easily explains the dominance of the receding versus the approaching velocities. If the arch is symmetric as supposed and if the downward flow speed is symmetric in both arch legs, then the velocity component along the line of sight is larger for receding velocities than for approaching ones, because the receding leg is more nearly parallel to the line of sight.

In an active region it may be argued that the profile of some unique feature is not at all like the average. If the profile is broader, the measured velocities will be too low. If the profile is

shallower, the maximum spread of density with velocity will be less. If the profile is asymmetric, then the macroscopic velocity is not well defined so the velocity measurement will have little meaning, except perhaps to indicate the direction of the prevailing microscopic currents. Finally, if the profile is in emission above the continuum, the sign of the velocities will be mistaken unless the original data are checked for this possibility. For these reasons it is clear that a study of spectra of active regions in conjunction with Doppler movies would be a better means of elucidating their velocity behavior quantitatively.

The spectrum showed that the line profile of $H\alpha$ is not broadened to any significant degree in the arch-shaped filaments. The profile instead shows two distinct components, one at the usual wavelength and the other at some large Doppler shift. Since the two peaks are of approximately equal intensity and normal width, the Doppler velocities measured by the average profile technique are too low by a factor of about two. This does not affect the height measurements previously derived since they depend upon velocity ratios. The line of sight velocities should be reinterpreted from the Doppler movies. The average maximum approach velocity was then about 17 km/s and the average maximum recession velocity was about 26 km/s. The average maximum speed, v, along the arch may be estimated with the following formula which is derived by summing equations (1) and (2), and then solving equation (3) for $\theta/2$ and substituting into the sum.

$$v = \frac{V_a + V_r}{2 \sin \alpha \cos(\arctan(2h/L))} \qquad (13)$$

The result for V_a = 17 km/s, V_r = 26 km/s, α = 40°, L = 17 Mm, and h = 2 Mm, is 35 km/s. This velocity is the velocity attained by an object losing potential energy from a height of 2.3 Mm without friction.

Comparison of the Observations to the Work of Others

In general the measurements of sizes and lifetimes of the arches in bright loop regions corroborate the work of Bruzek and Ellison. The two major discrepancies are that my data indicate maximum flow velocities below 40 km/s rather than above 50 km/s, and indicate flow from the top to the legs of the arches rather than a mass flow from one leg to the other. (9, 10, 14)

Unfortunately Bruzek gives little indication of the confidence he has in his measurements and little discussion of possible error sources. His velocities are apparently determined by tuning a Halle filter offband and noting how far into the Hα wings the arch legs are visible. The Halle filter has a bandpass of .05 nm with side bands and, when tuned offband, the side bands increase greatly in transmission. It may thus be that the legs of the arches follow far into the wings of the line as indicated by the filter adjustment, when in reality, the spectral profile of the arches is merely peaking in a sideband. So, it is not true that seeing filaments at large spectral displacements with a

Halle filter guarantees that the phenomenon has precisely the corresponding velocity. On the other hand, Ellison was able to see filaments with velocities of up to 70 km/s with a spectrohelioscope, which has no sideband difficulties. This velocity would indicate an arch of at least 9 Mm height assuming only gravitational energy is available. The best possibility is that the high velocities refer to a few relatively rare arches or to relatively thin arches. In the first case my mere three measured regions totaling about twenty prominent arches may not include a high velocity arch. In the second case, my lack of high resolution might smear out the velocity field causing low values to be read. A major difficulty with the cancellation method is that an average line profile is assumed in calibrating the velocities. The spectrum of Figure 6 indicates that the Hα line splits into 2 components whose intensity sum is about equal to that of the average Hα profile. Since one component remains at the nominal wavelength of Hα , the intensity difference indicated in the Doppler movies will be due only to the shifted component. The calibration procedures should thus be based on the shifted component profile only. This profile appears to be very much like the average except the intensity is less; therefore, the calibration curves for the average profile are good for this profile if the vertical scale is changed to give the correct maximum density.

The calibration curves of Figure 12 are clearly double valued. A maximum or minimum density occurs for a Doppler shift equal to the shifter setting. Thus, a velocity of 0 km/sec cannot be differen-

tiated from either ± 100 km/sec. by merely measuring the density of the Doppler movie. However, since it may be assumed that the solar surface as a whole is stationary and that the velocity field is a continuous function, it follows that no region should be assigned the higher of two possible velocities unless it is surrounded by a region of maximum or minimum density. The assumption of a continuous function for the velocity field may not be true in a practical sense, however. If the shear layer surrounding a fast column of gas is thin compared to the image resolution due to seeing, then the expected peak in the transmission could be washed out. Since the seeing at Mt. Wilson is seldom better than 1" of arc, a shear layer substantially less than 700 km thick could easily pass undetected. For small columns of diameter 2 or 3 Mm, an undetectable shear layer seems entirely consistent with the scale of the phenomenon. However, if the phenomenon seems ordinary in other respects, it is simpler to assume the lower velocity value.

In the case of the arches the argument favoring thin shear layers to explain the discrepancy between the Doppler velocities measured from the movies and those obtained by earlier observers has the following difficulty. In an arch the central high velocity column undergoes acceleration so that a range of components along the line of sight occurs. At some point then the arch should exhibit the maximum density of the calibration curve. In some of the measurements of velocities the density might be as high as the maximum, thus the very high velocities may have been photographed in the

movies. However, as Table 1 shows, the relative density on the film of the arches measured for August 26, 1966, was always greater in absolute value for shifter settings at $\pm$ .070 nm than for settings at $\pm$ .084 nm. That is, the arches show with greater contrast at $\pm$ .070 nm as would be expected if the lower velocities are correct. If the higher velocities were correct, the greater offset would yield the higher contrast.

Other attempts have been made to observe the bright loop regions on the limb of the sun. (8) Since the results of all estimates of the height of the arches give results between 2 and 4 Mm, the arches are thus very low and would be difficult to see with limb observations. This difficulty is even worse because the arches tend to be set in an east to west direction giving a poor profile on the east or west limb. In any case, limb photographs should at most show little mounds in the upper chromosphere or lowest corona. The troubles of earlier observers in identifying the bright loop phenomena on the solar limb are now easily understood.

A Physical Model of the Arches

Energy Considerations

It is of some interest to discuss the possible physical origins of the bright loop regions. Considering that the filaments are along the magnetic field and are found only in newly developing sunspot groups, the most reasonable possibility is that the magnetic field erupts from below the surface, in the manner of Babcock's model (15)

and lifts dense photospheric matter up into the chromosphere. As this magnetic loop forms, the material flows down being confined to follow the magnetic lines. It is clear that this model would account roughly for the shape of the arches and their time of appearance in spot formation. Moreover, the model indicates an energy source to lift the material. It is of interest to consider whether a flux tube might have enough free energy to lift much matter to the heights indicated by the previous calculations. The following discussion shows that this is the case.

Consider a flux tube of area A, length L and uniformly distributed flux Φ . It contains an energy W given by the integral

$$W_1 = \int \frac{\vec{H}\cdot\vec{B}}{2\mu_o} d^3x = \frac{\Phi^2}{2\mu_o A} \frac{L}{} \qquad (14)$$

We may estimate the energy released when the tube rises and the flux expands into free space, by solving for the field energy of two magnetic monopoles. In order to be certain that the infinite self energy terms are disposed of properly, one must use a uniform monopolar surface charge on a spherical surface of such radius r, that the B field has the same value at that radius that it did in the flux tube. Finally, since the flux may only expand into the vacuum above the solar surface, the integral of the B field over half the monopolar surface of the sphere must give the flux in the original tube. Thus we get equations (15) and (16) for one sphere.

$$B(r) = \frac{\Phi}{A} = \frac{\Phi}{2\pi r^2} \tag{15}$$

$$B(r' \geq r) = \frac{2\Phi}{4\pi r'^2} \tag{16}$$

The energy in this field is W_2

$$W_2 = \int \frac{B^2}{2\mu_0} d^3x = \left(\frac{2\Phi}{4\pi}\right)^2 \frac{4\pi}{2\mu_0} \int_r^\infty \frac{r'^2 dr'}{r'^4} \tag{17}$$

which for both spheres is given by equation (18).

$$W_2 = \frac{\Phi^2}{\mu_0 \sqrt{\pi A/2}} \tag{18}$$

For two monopolar spheres of opposite polarity, an amount of field energy equal to the work done in attracting the two spheres to a distance L, from infinity is lost. The force of attraction is

$$F = \frac{(2\Phi)^2}{4\pi\mu_o r'^2} \tag{19}$$

Thus the work must be

$$W_3 = \frac{(2\Phi)^2}{4\pi\mu_0 L} \tag{20}$$

Putting equations (18) and (20) together and considering only half the energy, since the other half is due to hypothetical image flux below the solar surface, we get

$$W_4 = \frac{\Phi^2}{2\mu_0}\left(\frac{\sqrt{2}}{\sqrt{\pi A}} - \frac{1}{\pi L}\right) \tag{21}$$

Combining equations (15) and (21) we obtain the available energy release W.

$$W = \frac{\Phi^2}{2\mu_o}\left(\frac{L}{A} + \frac{1}{\pi L} - \frac{\sqrt{2}}{\sqrt{\pi A}} \right) \qquad (22)$$

Taking $\Phi = B \cdot A$ we can get the result in terms of directly measurable quantities.

$$W = \frac{B^2 AL}{2\mu_0}\left(1 - \sqrt{\frac{2A}{\pi L^2}} + 2\frac{A}{\pi L^2} \right) \qquad (23)$$

Taking typical values for B, L, and A of B = 1000 gauss, and A = 50 Mm^2 for a sunspot umbra and L = 30 Mm for sunspot separations, we get W = 5 x 10^{24} Joules. If we take this energy and lift a mass to the height of the arches we can lift 6 x 10^{15} kg. This mass weighs 1.6 x 10^{18} Nt, which if distributed over the area of a bright loop region corresponds to a pressure of 4000 Nt/m^2. This pressure is typical of the upper photosphere at an optical depth of .15. (17) Since the arches show as filaments it may be that the energy is concentrated in these. If the magnetic field measurements of sunspots give 1000 gauss for the line of sight component, then it may be that the typical field for a sunspot should be higher when the transverse component is accounted for. In any case it is not difficult to hypothesize release energies sufficient to lift the entire photosphere from an optical depth of one to an altitude of 3 Mm especially with some hydrostatic pressure from below. In any case there is sufficient energy to lift a large fraction of the photosphere ten to twenty scale heights into the middle or upper chromosphere.

The model also allows some other predictions concerning energy balance to be made. If the energy available in the magnetic field is dissipated in the impact of material falling down the legs of the arches and hitting the photosphere, then an estimate can be made of the heating effect of this. If a plage loop region has an average of seven bright loops per half hour for three days, then a total of about 1000 loops will be formed, each of these having two legs of say 4 Mm^2 cross sectional area and lasting one half hour. The power dissipation per unit area is then 3×10^5 W/m . The luminosity of the sun is about 6.4×10^7 W/m^2 so that the power ratio is 4.7×10^{-3} If the heat increased the luminosity of the sun at the arch ends, then the temperature rise required would be about 7°K for light coming from an optically deep layer in white light. Since the arches are 10 or 20 scale heights high, the matter falling down them achieves kinetic energy sufficient to raise its own temperature by a factor of 10 or 20. Of course much of this energy will be transferred to the stationary gas at the arch ends. In fact, only when this gas hits the region of the atmosphere where the densities are about equal to its own will the dissipation become large. It appears then that the excess energy will be hard to see in white light. Many small bright points called bombs, visible especially in the violet wing of Hα , are seen near to plage loop regions. It is possible that some of these are caused by this dissipation. However, a great deal of other violent activity occurs nearby to these regions, so no conclusions can be reached in that matter yet.

Lifetime Considerations

Since there seems to be sufficient energy in the magnetic field to account for the lifting of matter in the arches, it is of interest to see if we can account for other features of the arches. The arches seem to undergo changes with a time of 300 seconds and to have lifetimes of about 2000 seconds. If the matter in the arches flows down the legs without friction, then the position as a function of time for a particle of fluid would be

$$X = X_0 \exp(t/T) \qquad (24)$$

X is the position of the particle with respect to the arch center; X_0 is the position at which t= 0 and dx/dt = 0; and T is the square root of the arch radius divided by gravity. Since the arch radius is about L, or 20 Mm, the constant T is about 300 seconds. If X is half the length of an arch, then we have

$$X_0 = L/2 \exp(-t/T) \qquad (25)$$

which shows that the arch has a decay time of 300 s for density loss. According to Kuiper (18) the density at 3 Mm above the photosphere is 10^{-5} that at the photosphere. The dense matter lifted to that height might be expected to be optically deep in Hα and thus very visible. If the arch is optically deep when first formed, it should remain visible for awhile and then as the optical depth in Hα reaches one, it should disappear suddenly in about five minutes. In any case the arch should show appreciable change in shape or size in

a five minute time interval. The arches do appear to show movement on such a time scale and to disappear rather suddenly. It is difficult to say however how much seeing difficulties affect the observations.

There is a problem with this model in accounting for the half hour lifetime of a typical arch. The optical depth argument above has the difficulty that the spectrum of Figure 6 does not look as intense in the arch legs as might be hoped. The center of the arch is optically deep however and since it feeds the legs it may be that they are in a temporary sort of steady state. In other words although the legs are optically thin, they may remain visible as long as a supply of material from the arch top continues.

The spectrum also indicates that the arch center is rising at about 5 km/s. If this velocity were constant for 1800 seconds, a height of 9 Mm would result, which is in disagreement with the observations. Therefore, a time scale of much less than 2000 s is indicated for the birth of an arch, unless the upflow is caused by some invisible steady state source. Such a source might be a series of arches coming up in the same location, one underneath the next. In that case no great optical depth need be assumed to account for a 2000 s lifetime. Instead one merely assumes that the arches in such a series come at intervals less than 300 or so seconds and that the source of the series lasts for about 2000 seconds. It is of course possible that the arches pass through a brief time during which the center rises and a long time during which it does not. A

Doppler movie of a plage loop region near the disk center with an hour or so of good seeing should clear up these questions.

If the multiple arch model is correct and the arches are rising one underneath the other, then the number of arches is five or more times as many as there appear to be. In this case it would seem that a given arch does not correspond to as much flux as would be the case for the optically deep model. This would indicate that a few brief arches should be visible for very small sunspot groups, or may even precede the appearance of the first spot in a group. If magnetic field measurements are made then, one would expect the optically deep model would show greater magnetic fields by a factor of about five than would be the case for the multiple arch model.

Part V Study of Upflow and Downflow Near Sunspots

Introduction

A study of the lifetime of prominent upflow and downflow features near sunspots was carried out for comparison to the work of A. M. Title, who made a similar study of features in the undisturbed regions. The results show that velocity features in disturbed regions last longer on the average than they do in quiet solar regions. Furthermore, a large percentage of the upgoing features do not behave in the regular manner that Title described.

Title found a class of upgoing features with a 113 $\pm$ 3.4 second mean lifetime and a definite velocity history. The velocity peaked in the first thirty seconds and then slowed down for the next ninety or so seconds. About one fourth of these events were followed immediately by a repetition so that these "double" events had a mean lifetime of 236 $\pm$ 8 seconds. No "triple" events were observed. The downflow showed no simple life history. Typical downflow features lasted about six to nine minutes, although about 20 percent of them lasted over 15 minutes and a few lasted more than 40 minutes.

Selection of Data

For this study two runs of long-lasting, good seeing were chosen. Each contained a mature active region about one week old. Any features resembling large loops or arches were ignored since these were rare and certain to be quite different from the features Title studied. It was felt that such features would require a

separate study involving more data than was available for statistical significance.

The prominent features were divided into four classes according to two criteria. The first criterion was whether the feature was moving up or down. The second was whether the feature was associated with light or bright plage in the Hα core. Bright plage is almost always associated with sunspot regions, whereas light plage is associated with the chromospheric network and can be found on the quiet sun. It seems generally to be the case that the areas where velocity activity is found are those that are brighter than average in the Hα core. This is in agreement with Title's finding that the velocity features are associated with the rosette structure of the Hα wings. The rosette structure is seen as a network of dark features in the Hα wings. Since it is the dark features which are associated with the velocity field in Doppler pictures, it is not surprizing that the velocity features uniformly fill the area underneath bright plage. The velocity features themselves are not nearly as spatially dense as the dark features in the wings. This means that most of the dark features are stationary. In Doppler pictures the areas underneath bright plage do not appear to be as high in contrast as they do in the regular network. This indicates that the velocities are smaller although the spatial density of velocity features is greater than in the network areas.

Data Reduction

A computer program was written to reduce the data in the databook which contained the timing information associated with the pictures. The main body of this program allows convenient entry of the databook data, and performs consistency checks. Most data sets contain anomalies, and most of these are obvious human errors, though some are mechanical errors. The data were corrected to eliminate inconsistencies in the most plausible way. Typical of this sort of discrepancy is the apparent recording of a clock time that is inconsistent with other records by exactly one minute. Most of the mechanical errors are apparently due to fluctuations in the drive speed or in the microswitch stops of the SHG, or possibly in the speed of film advance. Since the time per frame is always a multiple of four seconds, a slight fluctuation of any of the previous operations could cause an unnoticed change of four seconds in the time of some frame. One or two four second errors are common in 100 frames.

Once the data are cleaned up in the most plausible way, the program can be used to get lists of frame numbers versus clock time or to get the time interval between the start of any two frames.

The basic lifetime data gathered from the Doppler movies was a list of number pairs. The first number of the pair was the frame number on which a velocity feature first appeared. The second number was the first frame number on which it later disappeared. From this list of numbers the computer prepared a list of lifetimes in seconds based on data recordings. Another program took this list and sorted it into ascending lifetime order. This program also would compute

average lifetimes, and generate histogram data for any given sorting interval.

Since the raw data gave a very large scatter about its average due to a few very long lived events in each category, an objective means was needed of forming a meaningful average. If the long lived events were caused by some unique mechanism, then they should be studied separately, while the remaining bulk of the data should be treated as a unit. The method used to isolate the "unique" events was to first form the average lifetime, T, and scatter σ according to equation (26) and (27)

$$T = \frac{1}{n} \sum_{i=1}^{n} T_i \tag{26}$$

$$\sigma = \sqrt{\frac{1}{n} \sum_{i=1}^{n} (T_i - T)^2} \tag{27}$$

Second, all those T_i such that either $T_i < T-2\sigma$ or $T_i > T+2\sigma$ were eliminated. Finally n was changed to equal the number of remaining events. This process was repeated until a set of events was obtained such that all T_i were within the 2σ limits. The number of events eliminated by this process for each category is indicated in the last part of Table 2. The average and scatter finally arrived at are those quoted in the Table and elsewhere in this thesis.

Minimization of Selection Effects

In choosing prominent upflow and downflow features, several

difficulties arise. The most obvious of these is the definition of the word "prominent". No totally satisfactory answer to this problem was devised. Both size and contrast enter into the selection. A larger velocity element is likely to appear darker because it is less affected by light scattered from nearby. A feature next to one of opposite velocity is likely to appear darker than otherwise just because it contrasts with its surroundings. Another factor is the impatience of the observer. After the most prominent features are selected, progressively less and less prominent features are selected. If a good statistical sample is not obtained from the most prominent features, the observer will tend to relax his requirements. The difficulty here is that it is likely that a given sample taken may not be completely representative of any objective criterion of prominence.

Several other factors entered into the lifetime measurements. The first was that any feature found only on one frame was rejected as being probably a speck of dirt or a picture of one on that frame. Thus, even real features of very short lifetime would have been rejected as out-of-focus dirt. Besides features found only on one frame, any other feature which looked like dirt or lint was rejected. It is possible that one or two such dirt specks were included in the data if they looked sufficiently normal. Such a speck would have to become lodged slightly out of focus on some glass surface near the film and then be dislodged a few frames later. Even so, such a speck would probably betray itself by seeming too constant in inten-

sity or by failing to fluctuate in position in phase with the guider errors.

This brings us to the second factor affecting lifetimes which is the guider that makes the telescope follow the sun. The operation of the guider was not particularly good during the summer of 1966 when the data were obtained. As a result the solar image is seen to dance back and forth with an amplitude of roughly 2 Mm. Since most of the features had diameters of only 2 and 4 Mm, this meant that a feature could not be followed by simply encircling it with a pencil mark and noting the number of frames in which it appeared within the circle. Title's key photograph method was similar to the above procedure, and was possible because of the good operation of the guider at that time. In order to try to compensate for the guider drift, the viewing screen was mounted to a screw jack allowing it to be moved up or down in the Z direction at the twist of a knob. The jack in turn was mounted on a table with an x-y motion allowing motion in the two horizontal directions at the turn of cranks. With the projector pointing in the x direction, the y and z motions of the screen could be used to keep the umbra of the spot group shining on a particular point of the screen. This compensated to first order the apparent disk motions caused by guider drift. On any frame, however, the picture is set down in a scan and thus guider errors introduce shear and compression or expansion distortion into the picture. As a result of these, the first order correction was insufficient; many features could be followed by eye from frame to frame,

yet would not stay stationary on the screen with respect to the umbra. This introduces another psychological element into the lifetime measurements. Using the umbra correction and watching for other evidence of distortion, minimized the reliance on psychological factors to correct for guider error.

A third difficulty lies in deciding on what frame a feature disappeared when it actually faded slowly away. The method used was to actually wait until the feature disappeared totally without doubt. This meant that an up-going feature would often last until it was replaced by a minor downward fluctuation.

A final problem is that some features behaved unusually, showing a morphology that defied simply assigning a lifetime or size to them. For example several features coalesced from two or more features and perhaps later split into several fragments which in turn disappeared at different times. Other features seemed to move around as if they were the spray from a loosely held hose, or as if a succession of jets were being turned on and off. Such features were usually found in or near the edge of the bright plage and may be peculiar to active regions. Fortunately such features as these are not too numerous in comparison to those lifetimes are more definite.

Results

The results of the lifetime studies of these four classes of velocity features are summarized in Table 2 and the histograms of Figure 9. The results show that most of the upflow events last

Table 2

AVERAGE LIFETIME AND SCATTER IN SECONDS	Upgoing Features	Downgoing Features
Bright Plage	217 ± 71	211 ± 91
Light Plage	215 ± 81	371 ± 219
NUMBER OF FEATURES IN SAMPLE		
Bright Plage	60	55
Light Plage	81	67
NUMBER OF FEATURES EXCLUDED TO GET THE FEATURE LIFETIMES WITHIN 2 OF THE AVERAGE		
Bright Plage	12	15
Light Plage	29	7

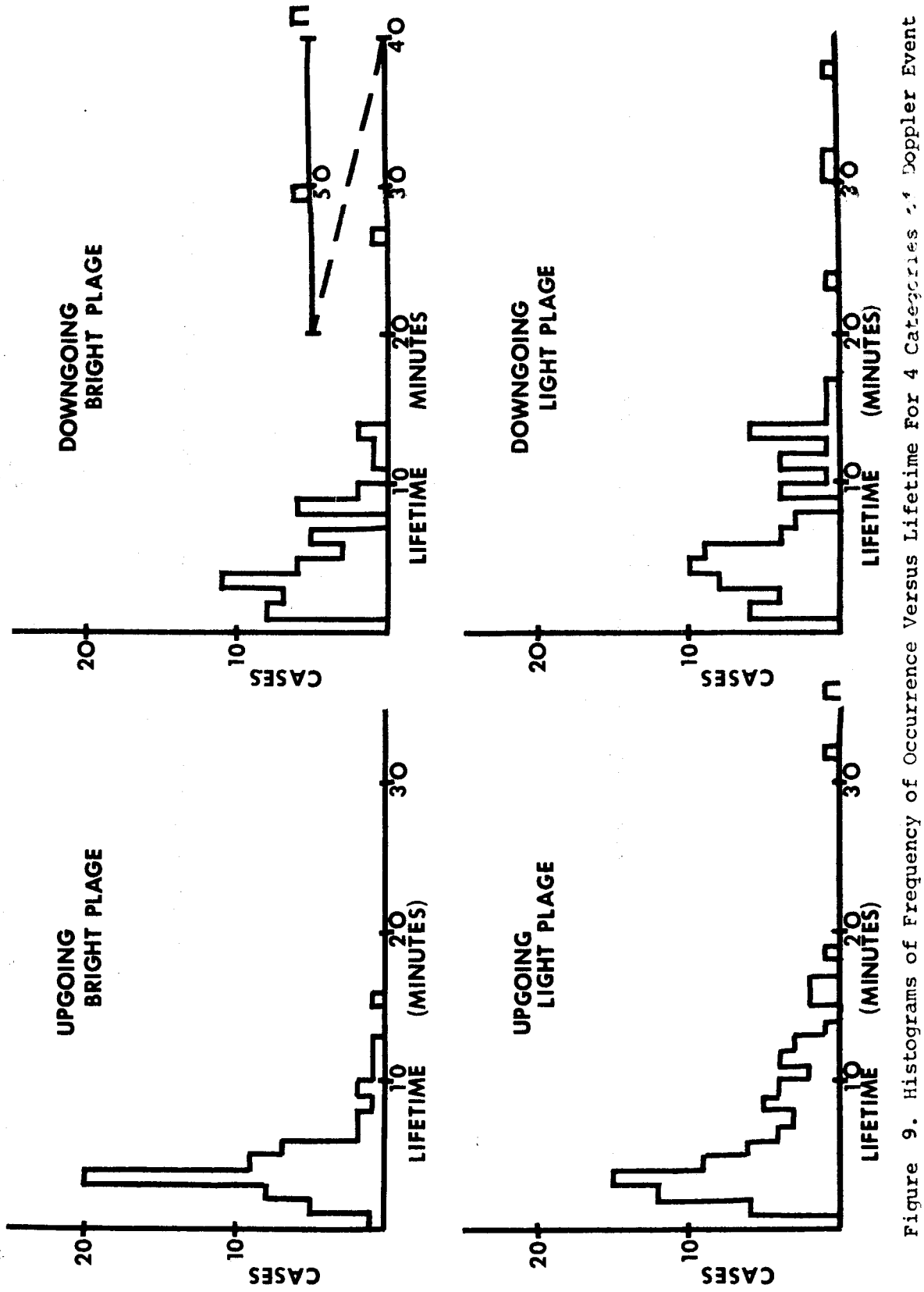

Figure 9. Histograms of Frequency of Occurrence Versus Lifetime For 4 Categories of Doppler Event

about 215 seconds or about twice the value found by Title. The data had a scatter of about one third the average for the upflow events. The standard deviation of the mean itself was about eight seconds, which is about the same percentage deviation as Title found.

In the bright plage regions the best histogram data were obtained, indicating a large fraction of the events lasted between three and four minutes. A similar but less pronounced peak is evident in the light plage features.

Since the results did not show much of the type of upflow noted by Title, a short rerun of the lifetime measurements was done on twenty up-going features in the network. This time a feature was considered to disappear as soon as it could no longer be considered at all prominent, rather than at all existent. The results showed most of the up-going features show life histories similar to those described by Title. The features reached their peak prominence in the first or second frame of the movie and then decayed slowly in the next three or four frames. Eight of the features were "double" events and two were "triple" events.

It thus appears that the difference found between the lifetimes measured here and those measured by Title, are primarily caused by differences in the acceptance threshold for the existence of the feature. Assuming the features were the same as Title observed, if the threshold here were enough lower than Title's to add an extra frame to the count before the peak of prominence, then it would be enough lower to add two or three extra frames at the end of the count. Three

or four extra frames would increase the average lifetime by about 80 to 110 seconds. As a result of this there would be a tendency for "double" events to run together and extend the mean lifetime further. The guider jitter could have caused a few pairs of events, separated a little in space and time, to be considered as one. This would tend to add a background noise, which would be greatest for apparent lifetimes between those for "single" and "double" events. The large percentage of "double" events found here in the sample of twenty is probably partly due to statistical fluctuation and perhaps also to the guider jitter difficulty. The important consideration here is then not that the lifetimes differ or indeed what the exact value of the mean life is. Instead it is that once an acceptance threshold is chosen, a class of up-going features can be found in the network with a fairly well defined lifetime, and a similar velocity history.

Thus, both observations show a class of up-going features in the network of Hα $\pm$.070 nm Doppler movies, having a mean lifetime on the order of three minutes whose standard deviation is about 4% of the mean. Both observations agree that the features reach maximum velocity in the first 25% of their lifetime and slow down for the remainder. Both agree that "double" events appear to be repeated "single" events as described above.

The downflow found in the network was also similar to that found by Title. The mean lifetime of downflow events was measured as 371 seconds which is near the lower limit given by Title. Since

this average does not include seven features of longest lifetime, thus the slightly low value is not surprizing. The large scatter found is indicative of the complexity of the downflow phenomena. No particular pattern was observed in the downflow, and as Title noted several of these events lasted for over thirty minutes.

In the bright plage areas one would expect the greatest chance for results differing markedly from the pattern in the regular network. The upflow events in the bright plage show a pronounced peak in the lifetime histogram at three to four minutes. The 217 second mean lifetime found is remarkably close to that in the network. The greatest difference observed between the bright plage between the bright plage features and the network was the lack of contrast in the bright plage. This would indicate that plage features have lower velocities than network features, or that they have wider profiles than average. If the latter is the case then there may be no real difference between the features in the two regions, since the velocities would be the same in spite of the different appearance in the Doppler movies.

The downflow in the bright plage regions is remarkable for having a class of features with a mean lifetime and deviation from it very like that found for upflow. It should be noted however that several very long lived downflow regions were seen here, which were excluded from the average. A careful study comparing the velocity or visibility of these downflow features as a function of time should be undertaken to see if their behavior is like that of the upflow events.

Part VI Calibration

Velocity Calibration

In order to calibrate the Doppler movies it is necessary to measure the transmission, $T(x,y,\lambda(x))$, of the film as a function of the wavelength, λ, for the line profile taken with each day's data. A sample profile may be seen in Figure 10. The profile is made in the same manner as it was for plates by slowly scanning the spectrograph in wavelength while rapidly making a spectroheliogram of the sun. The fiducial marks were put in at predetermined slit offsets and used to determine $\lambda(x)$.

The Film Copier was set to operate as a microphotometer as shown in Figure 11. The line profile was projected on the screen using the enlarging lens and mirror. An aperture at the film plane reduced the scattered light to an acceptably low level and an aperture in the viewing screen in front of the photocell caused it to measure $\int T(x,y,\lambda(x))\, dy$ over an interval in y corresponding to about 15 Mm on the sun. Although the resulting measurement $T(x, \lambda(x))$ was impossible to integrate with respect to x without removing the λ dependence too, it could be assumed that the y integral had removed the spatial dependence of T provided the structures integrated over were small compared to 15 Mm. This condition holds well except in the Hα core where filaments and plage areas can be found, or in sunspots. These disturbed areas were avoided as much as possible and the procedure for reducing the data was designed to reduce the importance of the Hα core.

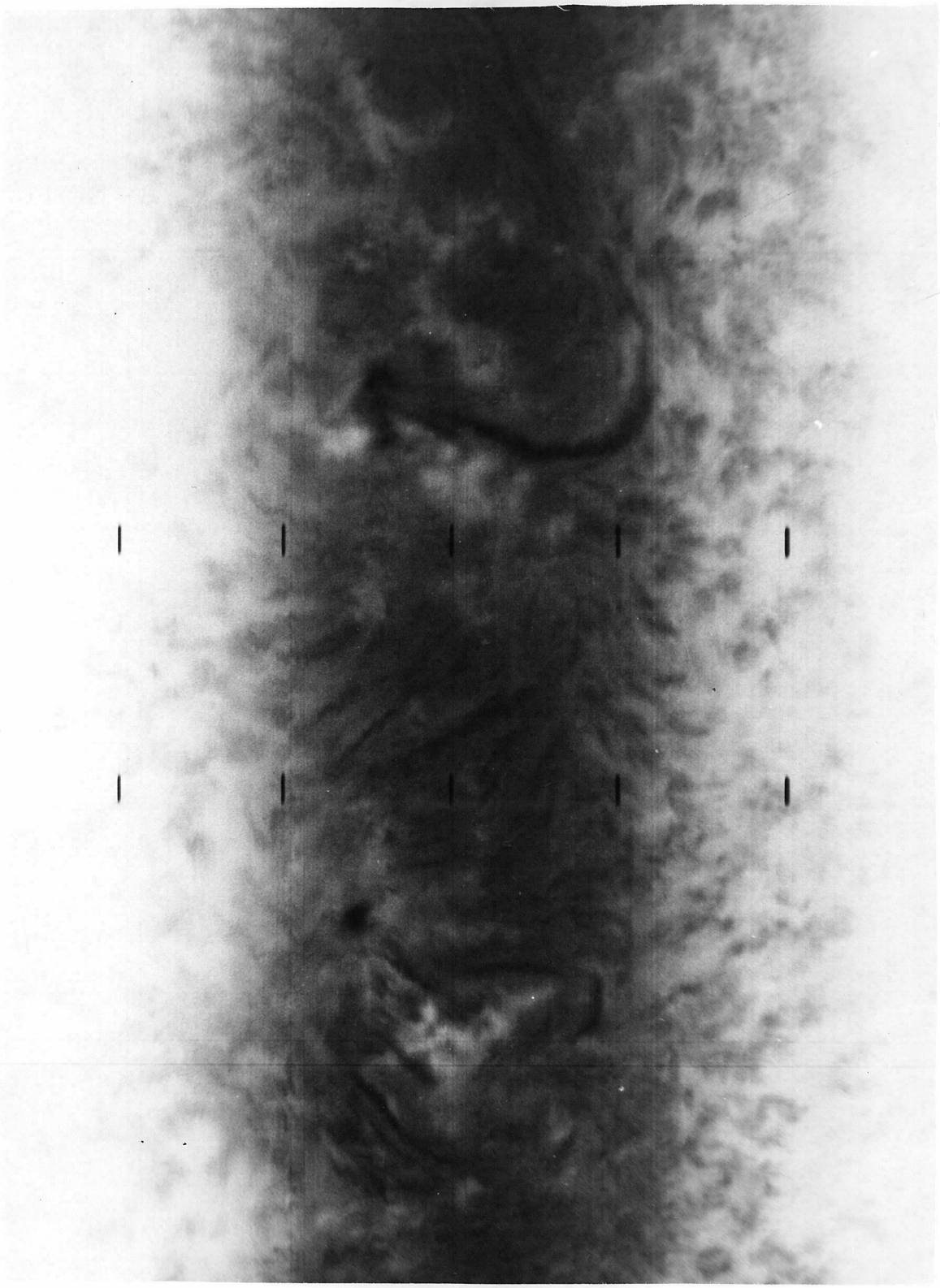

Figure 10. Line Profile of July 31, 1966

Figure 11. The Film Copier as a Microphotometer

A. Enlarging Lens and 45° Mirror

C. Bracket Attachment at Camera Position

M. Photometer

P. Photomultiplier Tube Attached to View Screen

T. Transport Unit

TC Transport Control

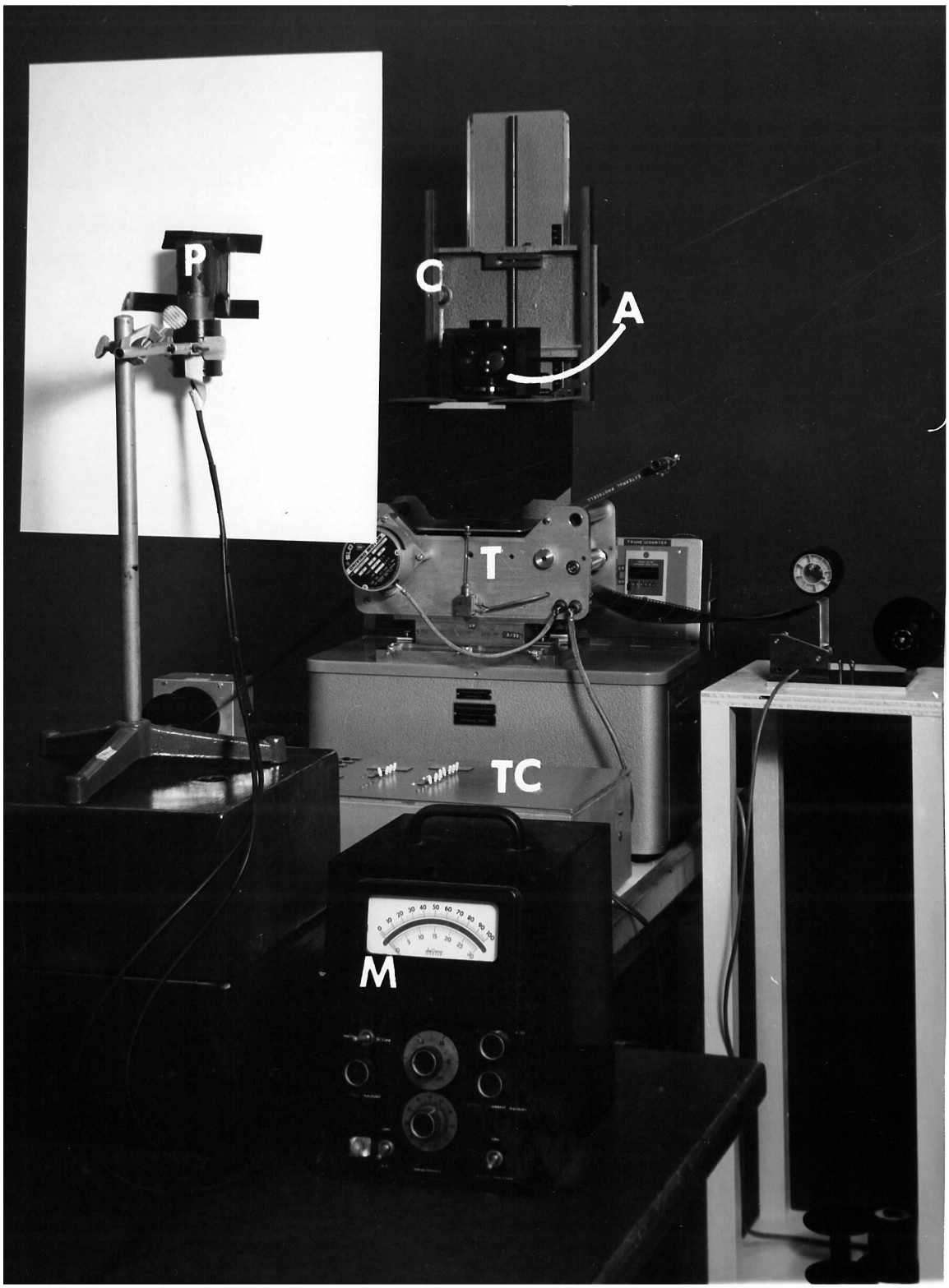

Figure 11. The Film Copier as a Microphotometer

For each profile a set of eleven measures was made at uniformly spaced positions in the profile. This was easily accomplished by setting the advance of the transport stepping motor to five steps per frame. In this way, the profile could be moved a known change in wavelength at the push of a button. Possible intensity fluctuations of the photolamp could be minimized by rapidly going through all eleven measurements and rechecking. The position of the fiducial marks corresponding to particular wavelengths with respect to positions of measurement was noted, and the density of the unexposed film on either side of the profile allowed calculation of the relative transmission of the profile with respect to that of unexposed film.

The line profiles taken on Mt. Wilson at the end of each day's observations extended into the wings just far enough to barely cover the wavelength of observation and occasionally not that far. This meant that the calibration data at the operating wavelength was barely available at best and for large Doppler shifts was missing in either one wing or the other. Since it seemed entirely possible that large Doppler shifts might be encountered in active regions, the first-order curve fitting procedure of R. W. Noyes, requiring only the value of $d(\ln T)/d\lambda$ at the operating wavelength, was not used. Instead a guassian curve of the form $T(\lambda) = a + b \cdot \exp(-(\lambda-\lambda)/\sigma)^2$ was fitted to the profile by a computer program. This program adjusted the parameters a, b, σ and λ to minimize the squares of the percentage errors between the measured values and the values of T predicted by the formula. Since the transmission is low in the wings of the line,

the program weighted the data there in preference to those in the core. Also since it is the ratio of the transmissions of the red and violet wing pictures that gives the transmission of the Doppler cancellation so that it is clearly the percentage errors that must be minimized in fitting the theoretical curve to the line profile.

The curve fitting program also yielded an rms error in the fit of the data to the curve. This error was about 7% to 12% in most cases, which compares well with the 10% scatter in the data about the best straight-line fit found by N. R. Sheeley in calibrating Zeeman photos. This reasonably low scatter justifies the use of a simple gaussian fit to the line profile for purposes of calibration of velocities. The gaussian approximation is further justified because the average line profile is itself an approximation to the actual profile of any given solar feature. The value of λ required to make the best fit is a measure of the error of the setting of the micrometer which controls the fine wavelength adjustment of the SHG. A wavelength error here could be expected to be about .0014 nm since that would correspond roughly to the finest divisions (.01mm) of the micrometer. Actual errors averaged .002 nm rms. The effect of such errors in the wavelength is to change the zero velocity transmission. Since the zero velocity transmission can be determined by assuming it to be the average transmission over a large region, the wavelength error will not affect velocity measurement relative to this background. The value of σ is influenced by such factors as slit widths; variation of the line profile from disk center to limb; the sensitivity, exposure,

and especially development (Γ) of the original film; and by scattered light in the SHG and the microphotometer apparatus. The parameters a and b represent the transmission of the profile in the continuum and the intensity of the line, but are sensitive to the exposure and development of the film as well.

One of the advantages of the gaussian curve fitting is that it enables the change of intensity of the cancellation with Doppler shift to be computed for large Doppler shifts and for shifter settings that correspond to non-linear parts of the line profile. The computer program used in the fitting procedure will also print out a table of relative transmissions and densities of the cancellation versus Doppler velocities for the Hα line, if it is given the shifter setting and the direction of the profile with respect to wavelength. The transmission values are normalized to give unity for zero velocity. Figure 12 shows graphs plotted from the computer output for data of July 24, July 31, August 12, and August 26, 1966. All graphs show deviations from linearity at large velocities, but considerable deviations can be found for velocities under 10 km/s. The two curves for August 26, 1966 show the effect of setting the shifter at -5 and -6, thus putting $\Delta\lambda = \pm.070$ nm and at $\Delta\lambda = \pm.084$ nm. In the latter case the deviation from linearity at low velocities is striking.

Mathematical Behavior of the Calibration Curve

An investigation of the behavior of the calibration curve based on the guassian profile as a function of its parameters yielded the

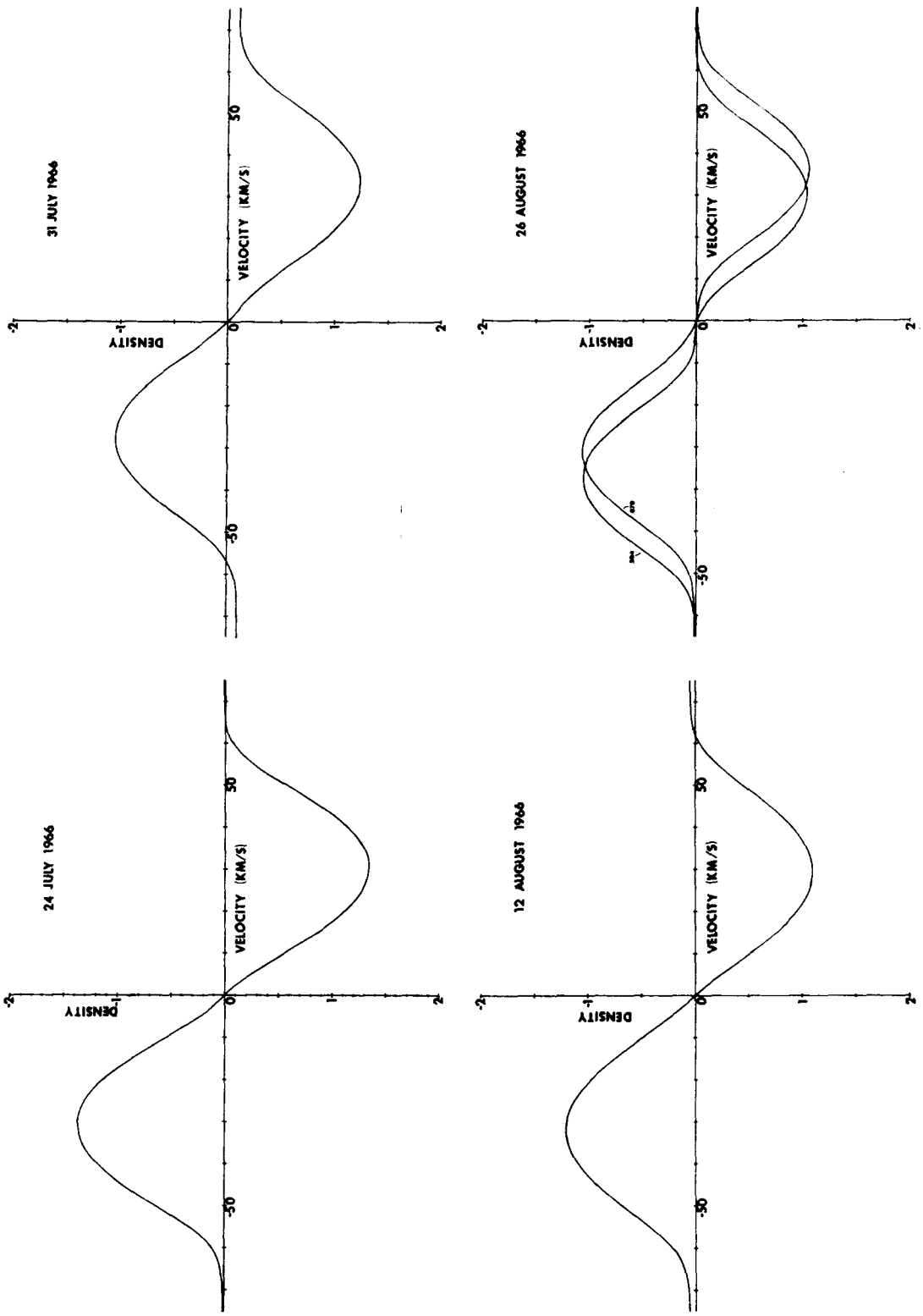

Figure 12. Calibration Curves Computed From the Line Profile Data

graph of Figure 13. The guassian has the form $T(\lambda) = a + b \cdot \exp(-((\lambda-\lambda_o)/\sigma)^2)$ as mentioned above. For this investigation λ_o may be taken as the wavelength of the Hα line exactly. In deriving the calibration curve of cancellation density versus Doppler velocity, λ is replaced by $\lambda_o \cdot v/c$. The calibration curve is then

$$D(v) = \log\left[\frac{a + b\cdot\exp(-((\lambda_o \cdot v/c - s)/\sigma)^2)}{a + b\cdot\exp(-((\lambda_o \cdot v/c + s)/\sigma)^2)}\right] \qquad (28)$$

where D is the relative density, s is the shifter offset, c is the velocity of light, and the other parameters have their usual meanings as previously described. After changing variables to eliminate excess parameters and constants, the above equation takes the simpler form

$$D = \log\left[\frac{1 + (b-1)\cdot\exp(-((v-1)/\sigma)^2)}{1 + (b-1)\cdot\exp(-((v+1)/\sigma)^2)}\right] \qquad (29)$$

where b now corresponds to the ratio of the maximum and minimum film transmissions, and v and σ are measured in units of the shifter offset. The equation is clearly antisymmetric being of the form $f(v)-f(-v)$ upon minor rearrangement. The graph of Figure 13 shows therefore only the curves for positive v. Since the main effect of the parameter b is to give the maximum possible value of D(v), b was given the value 10 so that D(v) would be normalized to a maximum of 1. As the curves of Figure 13 show, the maximum density occurs at velocities corresponding to the shifter setting. At line widths less than .4 the sensitivity to velocities near zero is greatly impaired. At greater line widths than 1.0 the overall sensitivity decreases while the range of sensitivity increases. The curves are of use in estima-

Figure 13. Theoretical Calibration Curves As A

Function of Line Profile Width

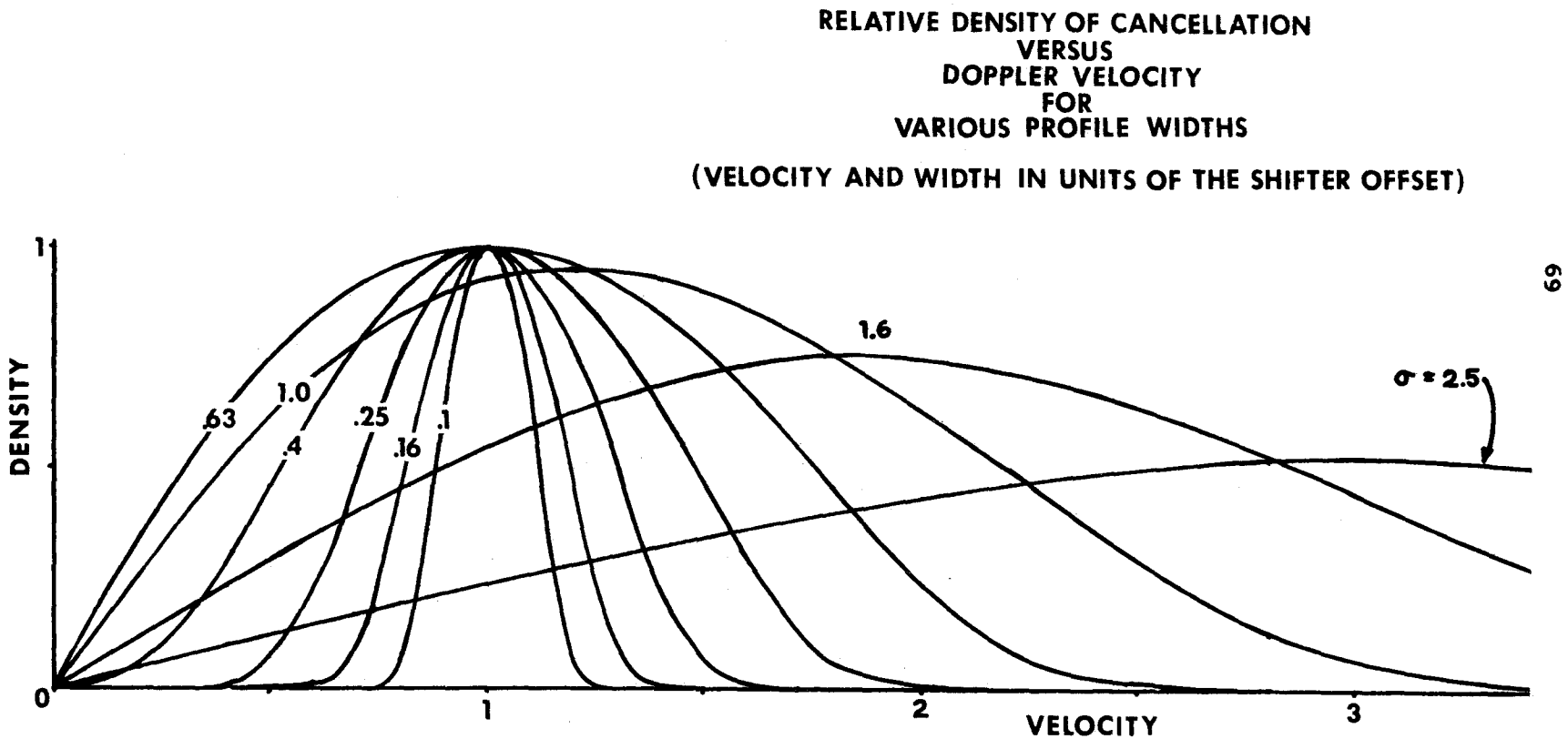

ting the effect of the change of line width from average for an unusual feature of use as a criterion for setting the shifter for various purposes.

Variations in the Profile Width of Solar Features

In order to get an idea of the accuracy of the calibration based on an average line profile, it was of interest to discover how much the line profiles of the dark features and brighter interstices seen in the Hα wings differed from each other and from the average line profile. For this purpose a pair of clean glass plates held the film on which the line profile was recorded. The CIT recording microphotometer scanned the profile making a chart recording of the film transmission as a function of wavelength. This chart recording contained the same sort of information in continuous form that the discrete data taken earlier contained except the integral over y covered a much smaller interval. The co-ordinates of two sets of twenty-five points were recorded. One set contained only co-ordinates of local maxima, the other only co-ordinates of local minima. Fitting a gaussian to all fifty points gave the average profile. Since the dark features in the wings of Hα tend to be found where plage or bright network is found in the Hα core, it seemed that the two sets of data should be dissected and then reassembled so that local minima in the wings would be grouped with local maxima in the core and vica versa. In this way a narrow profile corresponding to dark core features, and a wide profile corresponding to dark wing features were

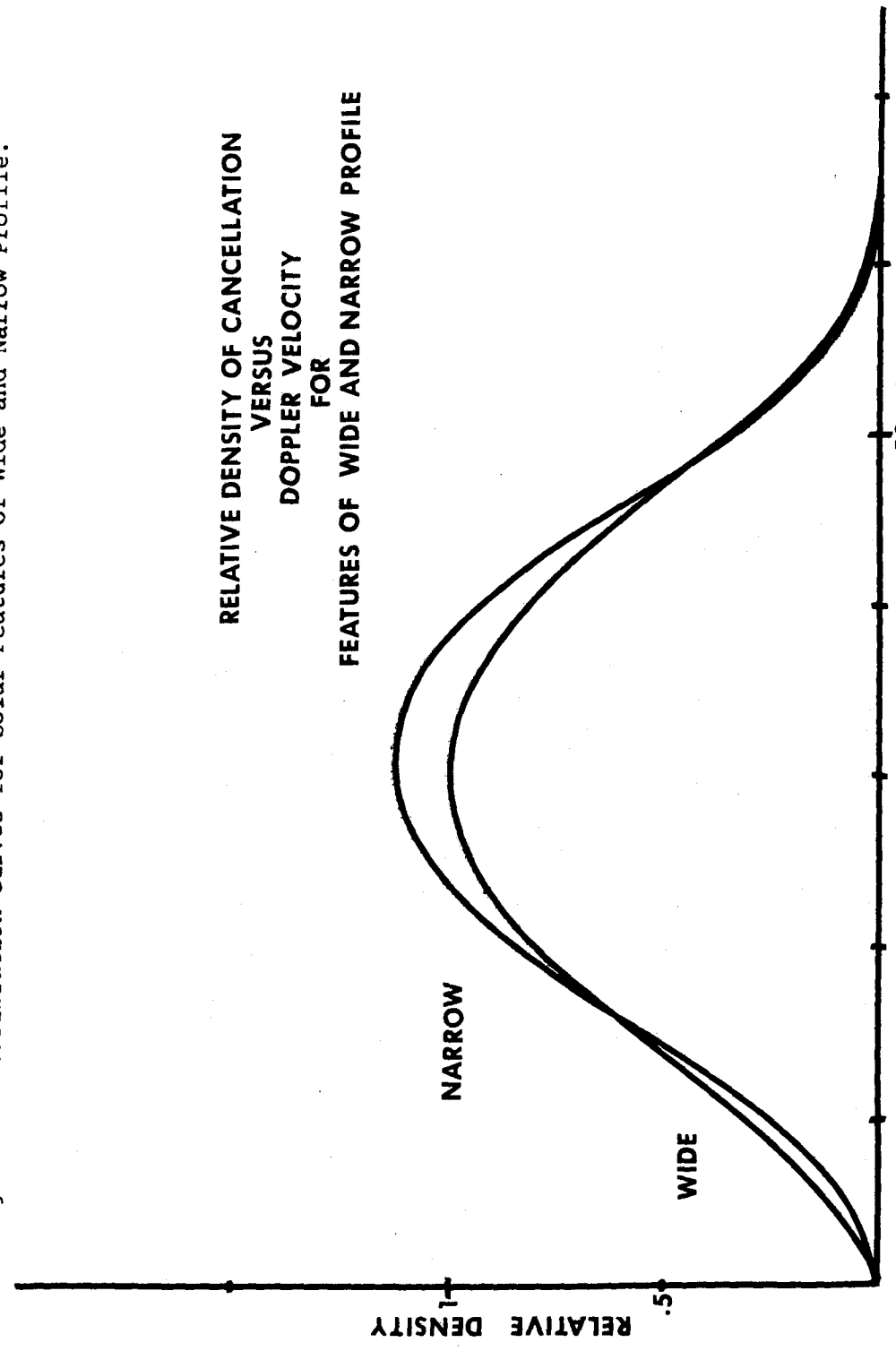

Figure 14. Calibration Curves for Solar Features of Wide and Narrow Profile.

generated. The resultant data are graphed in Figure 14. As can be seen, the calibration curves fall very near each other. Since the rms scatter in the calibration data used in getting average profiles is typically 10% and since there are other uncertainties as well in applying average profiles to particular features, it is not of much use to worry whether an ordinary absorbtion feature has other than an average profile.

Accuracy of Cancellation

On December 26, 1968 a copy of the drive film from the Dual 70 mm Camera was made with alignment for cancelling the drive film itself. The intent at that time was to recopy the slave film and improve its development in order to improve on the Doppler movie for July 5, 1966. The alignment and cancellation should be considered typical for production runs. The development, although quite uniform to the naked eye, showed non-uniformities related to the geometry of the developing reel, when photographed at high contrast. Figure 15 shows prints of a few frames of the self cancellation movie and the Doppler movie of the same day for comparison. The mistake affords a good test of the cancellation machine in normal use, and shows some of the difficulty involved in achieving uniform development.

Seven pairs of measurements on successive images of the frame mask of the 70 mm Camera of the Optical Printer using a comparator yielded the following results:

Mask size 36.936 ± .004 mm

Frame size	37.993 ± .010 mm
Double frame	75.985 ± .004 mm
Odd frame	38.000 ± .004 mm
Even frame	37.984 ± .007 mm

The errors are approximate standard deviations of the data about the mean. The frame size is eight sprockets in these data, so the odd-even effect is related to the fact that the advance uses a sixteen tooth sprocket. Since the scale of the image is .1 mm = 1" arc, the errors in the advance of the 70 mm copy camera are negligible.

After the Film Transport was loaded for cancelling the drive copy with the drive film of July 5, 1966 a microscope having a view field 1.5 mm in diameter at the focal plane was used to estimate the cancellation errors. The results indicate that alignment errors at the center of the frame of .08 mm along the film length and .02 mm along the film width, occurred. In addition, the magnification was 1.002 rather than 1.000. This causes an error of about .12 mm in the usable width of the film. Advancing the film while holding the microscope against the glass pressure plate of the Film Transport brought each successive frame division into the field of view with an apparent jitter of about .05 mm max. This is a compounding of errors in the Film Transport and in the drive advance of the Dual 70 mm Camera and the SHG stops. The alignment error seems very much the same from frame to frame to within about .02 mm or less.

The conclusion follows that alignment errors are typically about .1 mm in a cancellation and that the errors are fairly constant from

frame to frame.

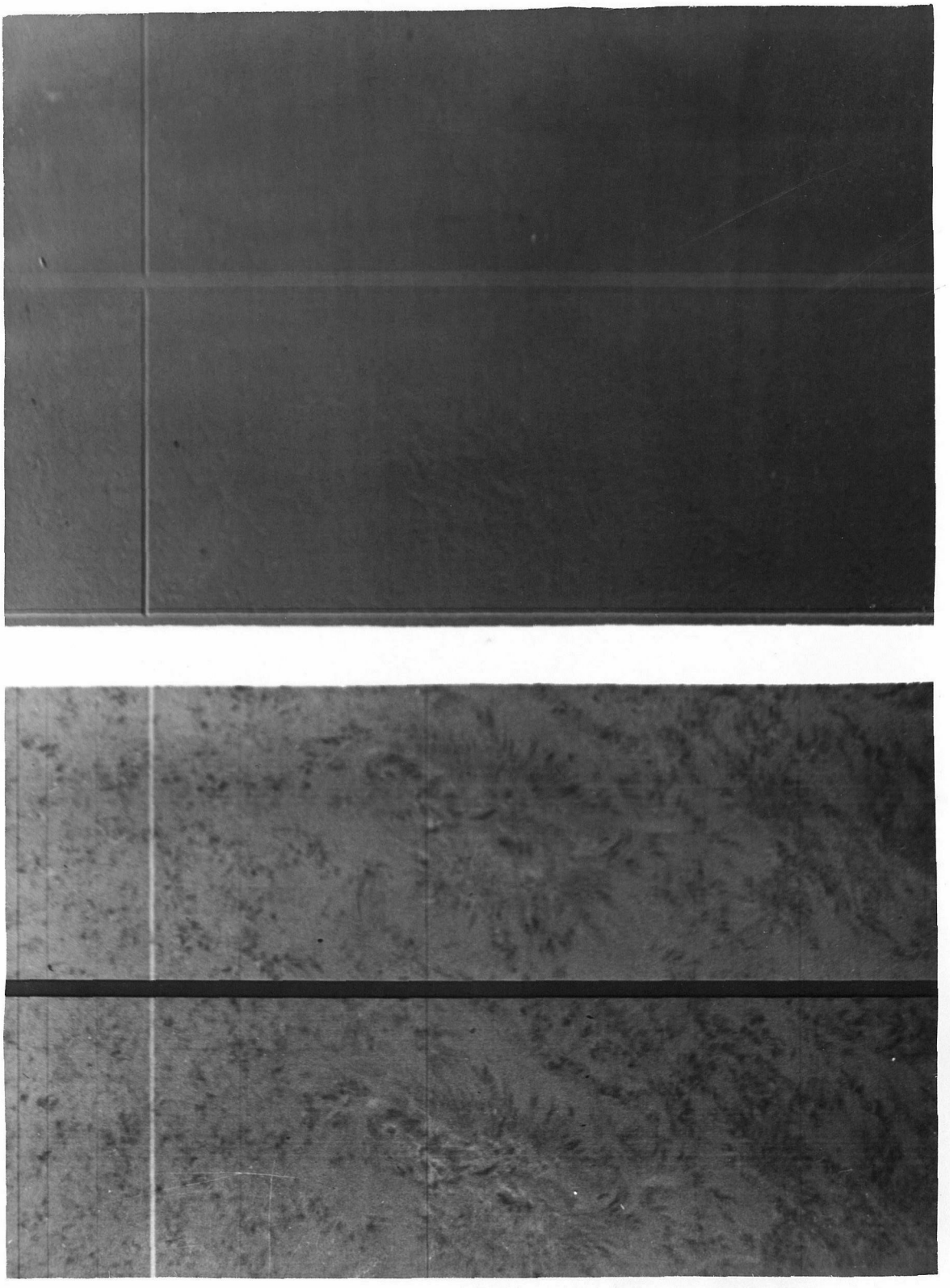

Figure 15. Doppler Cancellation and Self Cancellation From 5 July 1966

Part VII Conclusion

In this section I try to summarize the important contributions of this thesis research. I also indicate some of the possible ways this research might be extended. Finally after considering the many difficulties that were overcome in reducing the data, some suggestions are offered for avoiding them altogether in the future.

Summary

In Part IV it was shown that the arches in plage loop regions have a flow that is downward in both legs and probably upward in the center. The mean height of the arches was inferred from several independent measurements and found to be between two and four Mm. It was shown that if upflow in the center of arches as seen in Ryder's spectrum were a usual phenomenon, then the discrepancy between the heights inferred by different methods would tend to disappear. A model of the arches was explored. The main features of the model were that the subsurface magnetic field erupts from the photosphere lifting the material to form arches, which flows downward without friction , confined to follow the magnetic field lines. The rising field lines presumably cause the sunspots to develop where they enter the photosphere. It was shown that a typical energy release in the eruption of magnetic flux to form a sunspot group was sufficient to lift the entire chromosphere in a plage loop region to a height of three Mm, but insufficient to heat the photosphere near the arch legs to much more than a few degrees Kelvin. The discrepancy between the observed life-

time of the filaments, 2000 s, and the dynamic lifetime predicted by the above model, 300 s, is also discussed. Two alternate explanations are considered. The first is simply that the filaments are optically deep so that several dynamic lifetimes must pass before the gas becomes tenuous enough to be transparent in Hα. The second model is that as a given arch disappears in 300 s another arch just below it is seen in its place. This latter model seems to fit the expected behavior of the magnetic field in a developing sunspot group and to fit some of the descriptions of other observers, and finally leads to the expectation that arches will almost always be seen to be rising in their center.

In Part V a study was made of the velocity fields in the vicinity of sunspots to extend a similar study by Title of the network of the quiet sun. The mean lifetime for upflow events in the network near sunspots was measured as 215 seconds. This value was shown to be consistent with the lower value of Title provided that account were taken of the subjective factors inherent in the measurement. Both observations give a similarly well defined lifetime and both agree that a large majority of the upflow events have a similar history of sudden appearance and slow decay. The downflow in the network gave a mean lifetime of six minutes with a large scatter which also agrees with the observations of Title. A number of very long lived downflow events were also observed. In the active regions themselves, we found that mean lifetimes and scatter of the data about them were about the same for both upflow and downflow

and were also about the same as for upflow events in the network. In all cases several very long lived events were ignored, which may well indicate some other flow mechanisms. However, in all cases except downflow in the network a dominant mechanism seems to be indicated which is probably the same for up-going events in both active and network regions, and perhaps different for downflow in the active regions.

Finally an important part of this thesis work was the successful completion of the automatic cancellation machine itself, and the great amount of practical understanding of electronics and mechanical design which was gained in doing it. The Film Copier has shown that it is practical to cancel movies by projection printing, which greatly simplifies film handling by separating the unexposed and developed films and by not requiring different registration for the original film and its cancellation mate. It has also shown that it is practical to use a stepping motor to position film instead of a geneva. An unexpected bonus from this work has been the versatility of the Film Copier which was easily adapted to making reduction prints from 70 mm to 35 mm and 16 mm, and to projecting 70 mm frames for viewing directly or for microphotometer measurements. This system will prove useful in almost any future cinema application. It will be especially useful in shortening the time between gathering data and viewing cinematically the results, which should greatly aid the observer in gathering precisely the data he wishes.

Future Observations

Further research on the bright loop regions using the present equipment could take several directions. It would be interesting to see if there is any simple quantitative relation between the growth of particular sunspots and the morphology of the arches. It might be that a certain number of arches correspond to a certain umbral area. Perhaps a certain number of arches correspond to a certain magnetic flux. Another possibility is that a particular number of arches appear in a certain area before a pore (small spot) appears. If the Dual 70 mm Camera were operated to give simultaneous spectroheliograms in the Hα core and continuum,then the area of sunspots and morphology of the arches would be easily followed. The Film Copier can easily be used to put the two movies together so that corresponding frames of the two occupy opposite halves of the projection print frame. Zeeman movies should allow the study of the relations between the arches and the magnetic field. The difficulty here is that the Hα line is difficult to use for Zeeman measurements, and most good Zeeman lines do not show the upper chromosphere.

There are two fairly easy methods by which a study of the velocities of the arches could be studied with the present apparatus. The easiest would be to take a short Doppler movie changing the shifter setting with each frame. The most important shifter settings will be far in the wings where exposures can be made in less than forty seconds even in the early morning. Since the individual

filaments undergo changes on a ten minute time scale, the seven or more settings that can be used in five minutes should give a fairly complete and static picture of the velocities. This method has the advantage of requiring no modification of apparatus for obtaining the data and the reduction is likewise standard.

The second method is to modify the exit slit by milling away half of it. If a piece of cardboard were then taped to the beam splitter shutter so that light is blocked from the open side of the exit slit except when the Zapper is used, then a spectrum can be obtained by pressing the Zapper. Moreover, a spectroheliogram can be taken with the other image of the beam splitter. While the spectroheliogram is being made,the spectrogram may be exposed with fiducial marks being left on the spectroheliogram at the location of the spectrogram. If hand timing is required for the spectrogram, the SHG may be halted momentarily and a time exposure made with the appropriate compensating filter in front of the spectrogram.

A more objective method for studying the upflow and downflow events of Part V would be to use the photometer with a small aperture in the movie screen. If this were done in conjunction with a chart recorder, a more easily reduced set of measurements could be obtained without much difficulty. Before this is practical however, the guider will have to be improved as mentioned below.

Suggestions for Improvement of Future Data

For ease of alignment in data reduction, the alignment frames

taken in the line center at the beginning of a run should include using the lateral fiducial marker "Zapper" especially when early morning seeing causes low contrast images. For aid in identifying the exact region of the solar disk where the data are recorded, a continuum light spectroheliogram should be taken. Similarly a few photographs in the core of the Hα line during good seeing would aid greatly in comparing the data with that of many other observers who use Halle´ filters in solar photography.

In taking line profiles for calibration, a better procedure would include an initial line profile with nothing but the micrometer scanner changed. In this way the fiducial marks, put in as the micrometer reaches the nominal setting, would record the wavelength of each movie in the profile and thus the offset of the line shifter. Another direct benefit would be that in the cancellation procedure, these profiles would cancel to give a density-versus-velocity calibration picture. This picture as reproduced in subsequent printing operations would give the calibration of the prints. This procedure would eliminate curve fitting to the line profile.

In gathering Zeeman data initially better results could probably be obtained by using a slower, finer grained, high contrast film such as Shellburst, which does not require special handling and developing. The basic problems of alignment and mastery of the double cancellation procedure could thus be resolved before trying for high time resolution.

Besides the above mentioned recommendations in procedure, a few equipment difficulties need correction in order to improve the future

data. First, an improved guider is needed before cancellation of Doppler movies to obtain acceleration movies will be meaningful. This difficulty will affect doubly-cancelled Zeeman movies too. Second, a vibration of the spectroheliograph when started at high speed will have to be eliminated before higher speeds and better time resolution can be obtained. Third, a small telescope with an Hα filter for visually monitoring flare activity would help in selecting the best sunspot groups to photograph. Alternately, a communication line to an observatory running a flare patrol would accomplish the same end. Either of these would have prevented the halting of the data of August 30, 1966, during the final stages of a class 2 flare. Finally, an automatic device for changing the speed of the spectroheliograph according to the brightness of the sun would give better exposure control especially during breakfast time. In conjunction with this, the difference in spectroheliograph speed in opposite directions should be eliminated. These last modifications would require an automatic time of traverse recorder to keep track of the time resolution. A small movie camera photographing the wall clock once each traverse would be a simple solution.

Appendix I

Design Considerations of the Film Copier

There are two basic methods of making a cancellation movie, and both must deal with the same two problems. One problem is that the Dual Camera has a registration error between the two films which is a function of certain gross adjustments of the two halves of the camera. The other problem is simply developing to unity gamma ($\Gamma = 1$), a unit magnification copy of one film for cancellation with the other.

The method used by Title (8) was to contact print one film. This copy then had the same registration error as the original, but unit magnification was automatic and the procedure was quite easy once the film was loaded. The copy was developed to unity gamma and run manually through the film cancelling machine along with the opposite original. The error in registration was removed in this cancellation machine by using the two sets of epoxy bosses to register the two films independently.

When the design of the Film Copier was under consideration, a great deal of time was spent thinking of a way to automate this cancellation machine. The main stumbling block was that it required a sense of touch to get the film to lock onto the epoxy bosses properly. It was deemed a delicate task requiring a lot of feedback. Beyond that, the system required two of these film movements all mounted in a small space, and spatially adjustable with respect to each other.

The method used by the Film Copier to make a cancellation movie is to make a unit magnification projection print in which the registra-

tion error is removed in copying. The resulting film when developed to unity gamma, can be cancelled with the opposite original by bi-packing them in register through the Film Transport. The apparatus for this is shown in Figures A1 through A8. The disadvantage here is that success is dependent on correct alignment of a previously correctly developed copy. The advantage is that correct alignment is straightforward, and that cancellation is trivial if the copy is done correctly.

Appendix II

Operating Controls of the Film Copier

The Optical Printer and Transport Unit may be operated either together as a whole or independently. Plugging in the umbilical cable causes them to operate together provided both are turned on. The following description explains the operation: first of the Transport Unit alone, next the Optical Printer alone, and finally the two together.

Figure A1 shows a photograph of the front panel controls of the Transport Control. The power switch is on the right hand side of the chassis. The Fast-Slow knob controls the clock rate and thus the speed of the stepping motor. The Reverse Switch selects the direction of the stepping motor. The Run Button causes the stepping motor to step at the clock rate. If the Step Button is pushed and then released, the stepping motor steps once moving 1/200th of a circle in angle. The Frame Button causes the film to be moved one frame. The length of one frame is determined by the setting of the switches of the Steps Counter. The values of all the switches set to the left must be summed to determine how many steps form one frame. Multiples of twenty-five steps correspond to multiples of four sprocket holes. The switches of the Exposure Counter are set in the same manner as the Steps Counter. This counter, however, is not used independently of the Optical Printer with one exception. If it is set to 0, the Transport will move frame after frame until some other number is selected. The Auto-Manual Switch controls the mode of operation. It disables the push buttons

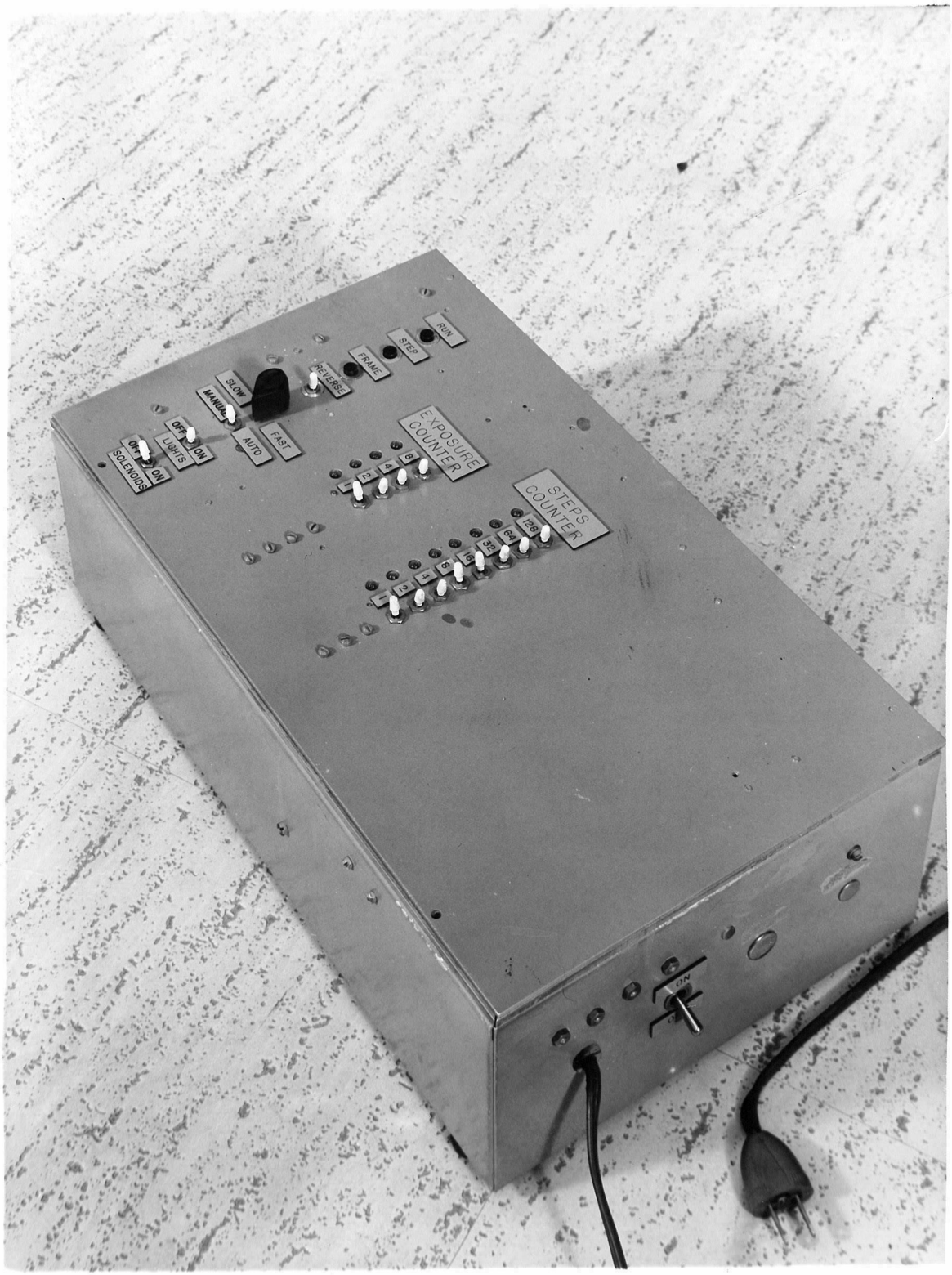

Figure A1. The Front Panel Controls of the Transport Control

and Reverse Switch in the automatic mode. The Solenoids Switch has three positions: on, neutral and off. If the switch is on, the solenoids will press the film whenever it is not moving. If the switch is off, the solenoids will remain off at all times. In the neutral position, the solenoids will remain off in the manual mode, but press the film in the automatic mode. The Lights Switch allows the indicator lights to be extinguished without turning off the power switch.

Figure A2 shows a photograph of the Optical Printer. The power switch is on the right side. The Automatic, Light and Expose Controls are on the left side where the umbilical cable from the Transport Unit attaches. The Expose Button causes the Optical Printer to take a photograph and advance the film. The Automatic Switch does the same thing, but may be left on for multiple photographs. The Light Switch turns off the light between photographs if desired. The Frames Counter, on the right of the front panel, counts once for each four sprocket holes of camera film advanced. It prevents exposure after the number, preset behind the red window, is reached. This last feature may be overridden by the toggle switch under the counter. The Photo Timer is on the left of the front panel. The two toggle switches set the order of magnitude of the exposure time. For example, the standard setting of 1 x 1 may be multiplied by a factor of .1 by using a setting of .01 x 10. These factors are not very accurate, but could be calibrated. The two knobs of the phototimer should each be read like the hour hand of a clock with 10, 11, and 12 replaced by 0.

Figure A2 The Optical Printer

A. Camera Mounting Position

B. Cable Connection to Camera

C. Photo Timer

D. Knobs to Set Number of RC Times Per Exposure

(Shown Set To Twelve)

E. Switches to Select C

F. Photocell Plugs in Here

G. External Photocell and Viewing Device in Storage

H. Power Switch (See H Figure A3)

I. Frame Counter

J. Frame Counter Override Switch

K. Light Source

L. Side Panel Controls

M. Umbilical Cable to Transport Unit (not shown)

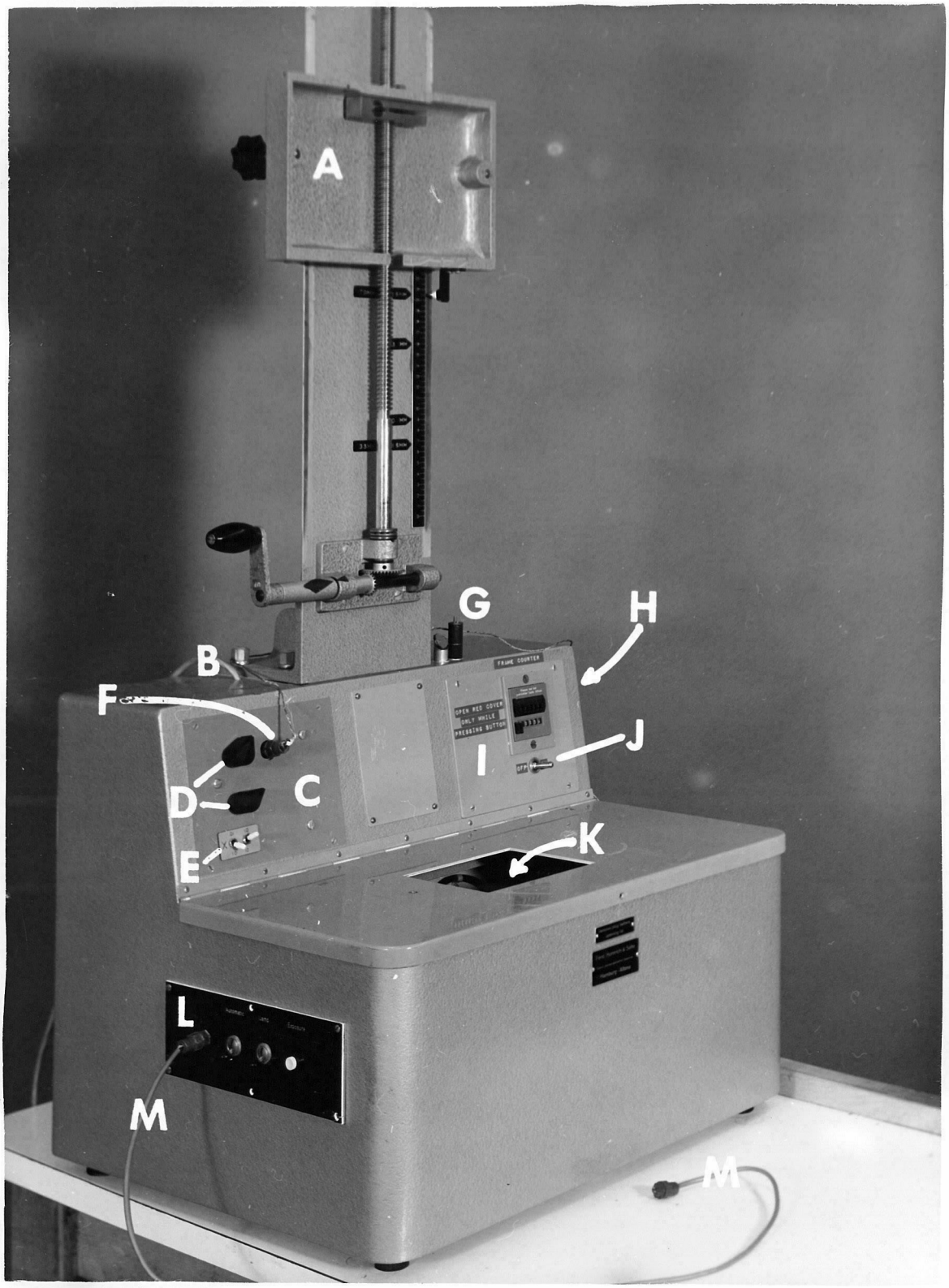

Figure A2. The Optical Printer

The upper knob and lower knob form a two digit number with the upper knob being in the ten's place. This two digit number is accurately proportional to the exposure time and may be set from 00 to 99.

The cameras have two external controls. On the bottom left of the camera is a push button that advances film. On the top left is a red-handled switch which may be set to forward, off or reverse. The switch is ordinarily kept at the forward position. The off position disconnects the advance motor allowing exposure without film advance. The reverse position runs the advance motor backwards. This latter feature is used if the film jams by winding around the sprocket. The pressure plate of the 70 mm camera may be raised for loading film by raising the film tensioning device on the left of the camera until it trips a microswitch. With the 35 mm camera, opening the access door to load film trips a similar microswitch.

When the Optical Printer is connected to the Transport Unit, they operate together in two different but similar ways, depending on the setting of the Auto-Manual Switch of the Transport Control. In the manual mode the Transport Unit may be operated with no effect on the Optical Printer. On the other hand, manual operations of the Printer will be counted by the Exposure Counter of the Transport Control. When the number of exposures counted equals the number set on the switches of the Exposure Counter, the film in the transport will advance a frame, and the Exposure Counter will reset. In the automatic mode the Transport Control will cause the printer to take exposures continually as if the automatic switch on the printer

were on except when the Film Transport is advancing film. This last exception is important and is why the automatic switch on the printer is not equivalent to that on the Transport Control.

Appendix III

Detailed Procedure for Cancelling Movies

The procedure and apparatus for producing a cancellation movie is indicated schematically and photographically in figures A3 through A8. Starting with original movies A and B, the three main steps may be summarized as follows:

(1) Make a contact print, -A, of one of the alignment frames of movie A. (Figure A3)

(2) Register print -A on the reflex window of the 70 mm camera. Then put movie B in the transport and maneuver it until its image aligns with -A. Print the movie B and develop it to unity gamma yielding -B. (Frames A4 → A6)

(3) Bi-pack -B on top of A in the transport and print the result at suitable reduction yielding -(A-B). (Figures A7,A8)

A more detailed procedure is discussed in the following paragraphs. Although the procedure seems complex, most of the details will seem obvious to anyone who has familiarized himself briefly with the apparatus. Hopefully, the uninitiated can plunge ahead with this explanation and a little common sense and make a good movie the first trial.

(1) Using the contact printing frame and a small length of 70 mm film, make a contact print of the alignment frames of movie A. Any frame that is the same in both movies, A and B, will serve as an alignment frame. For Shellburst film an exposure of 1 second with the 135 mm lens at f/22 and the Omega enlarger raised all the way up is appropriate. Development of this film for about five minutes in D-76

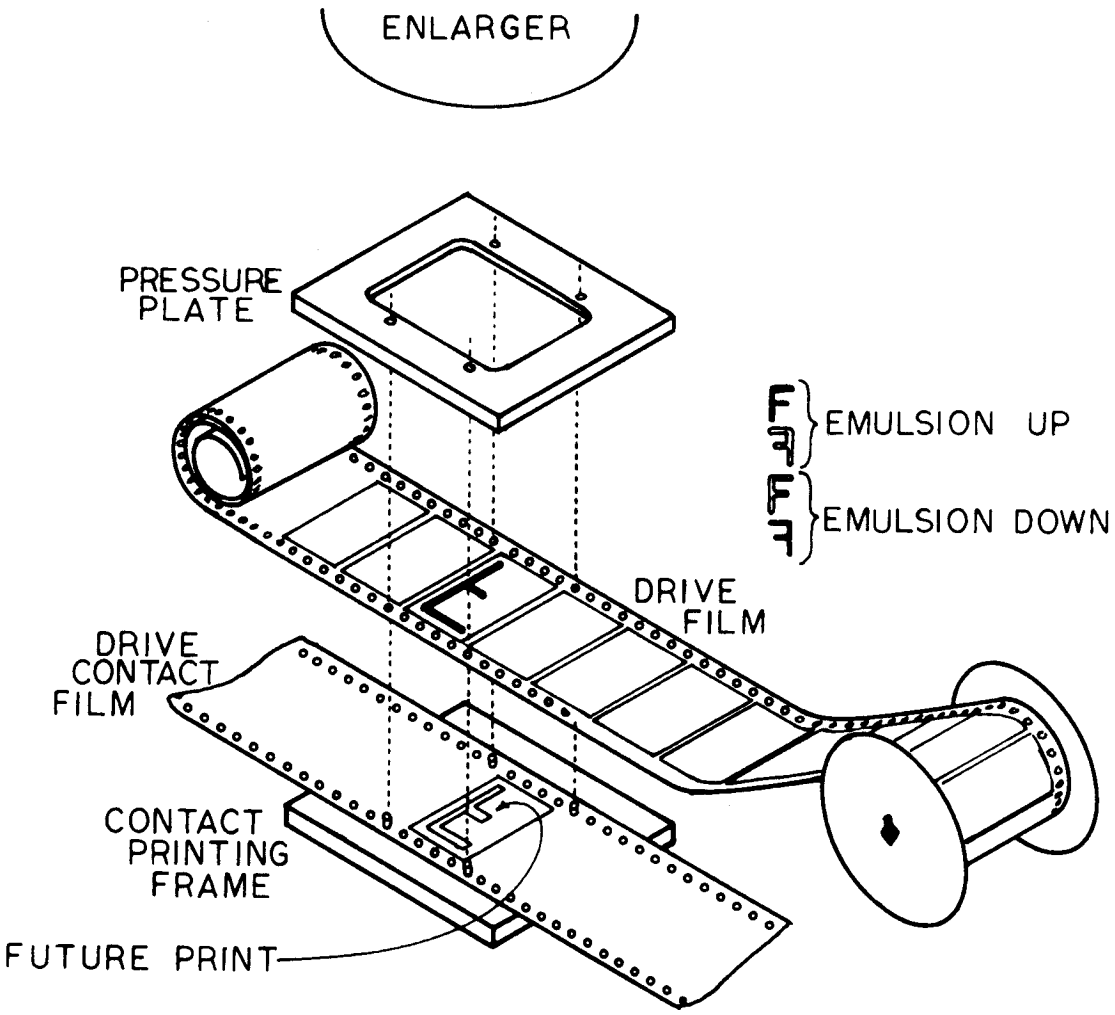

Figure A3 Step 1, Contact Printing Shown Schematically

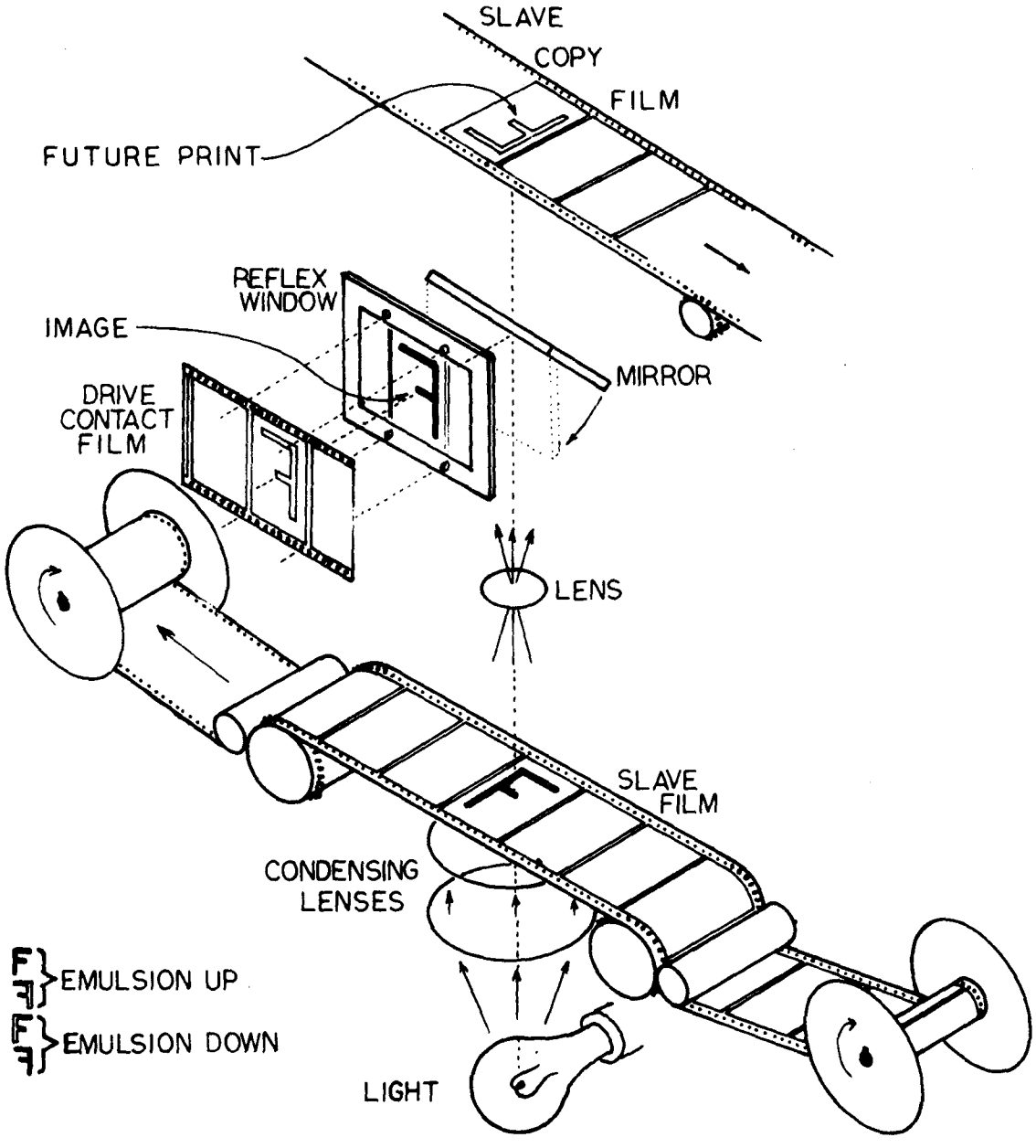

Figure A4 Step 2, Unit Magnification Alignment Copying

Shown Schematically

Figure A5 The Film Copier As A Unit Magnification Copier

A. Red Handled Switch Used For Film Advance Control
   Switch S7 of Figure A33

B. Manual Film Advance S8

C. 70 mm Camera

D. Reflex Mirror Control Knob (black)

E. Focus Stop Screw For Unit Magnification

F. 1 of 2 Thumbscrews For Adjusting Image at the Reflex Mirror

G. Fiducial Marks For Setting Camera Distance For Unit Magnification

H. Power Switch

I. Film Take-Up Motors and Reels

J. Door Enclosing Extra Condensing Lens Used in Unit Magnification
   Printing

K. Film Supply Holder

OP Optical Printer

P. Internal Photocell Connection

R. Reflex Window With 70 mm Contact Print Attached

T. Transport

TC Transport Control

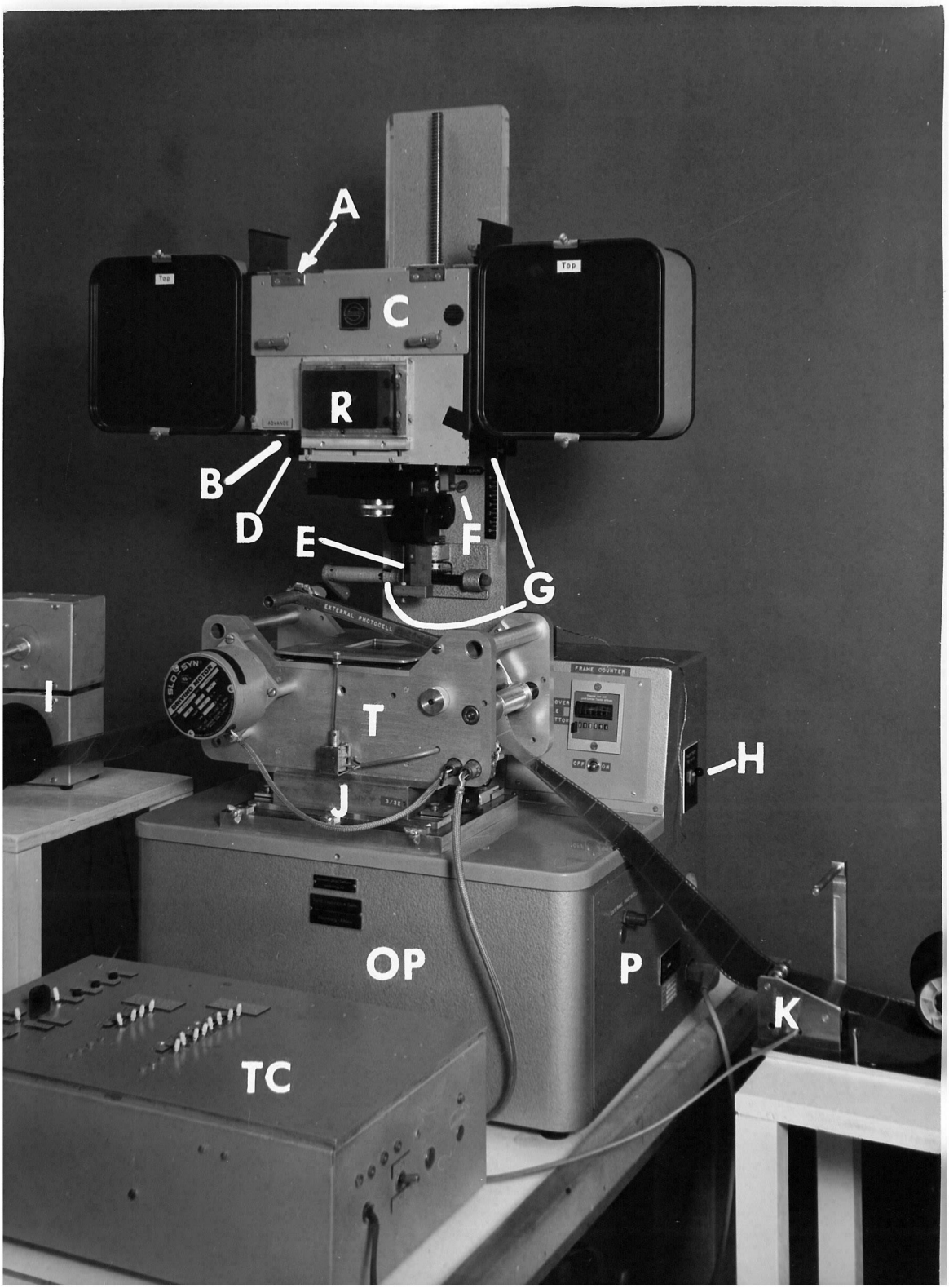

Figure A5. The Film Copier as a Unit Magnification Copier

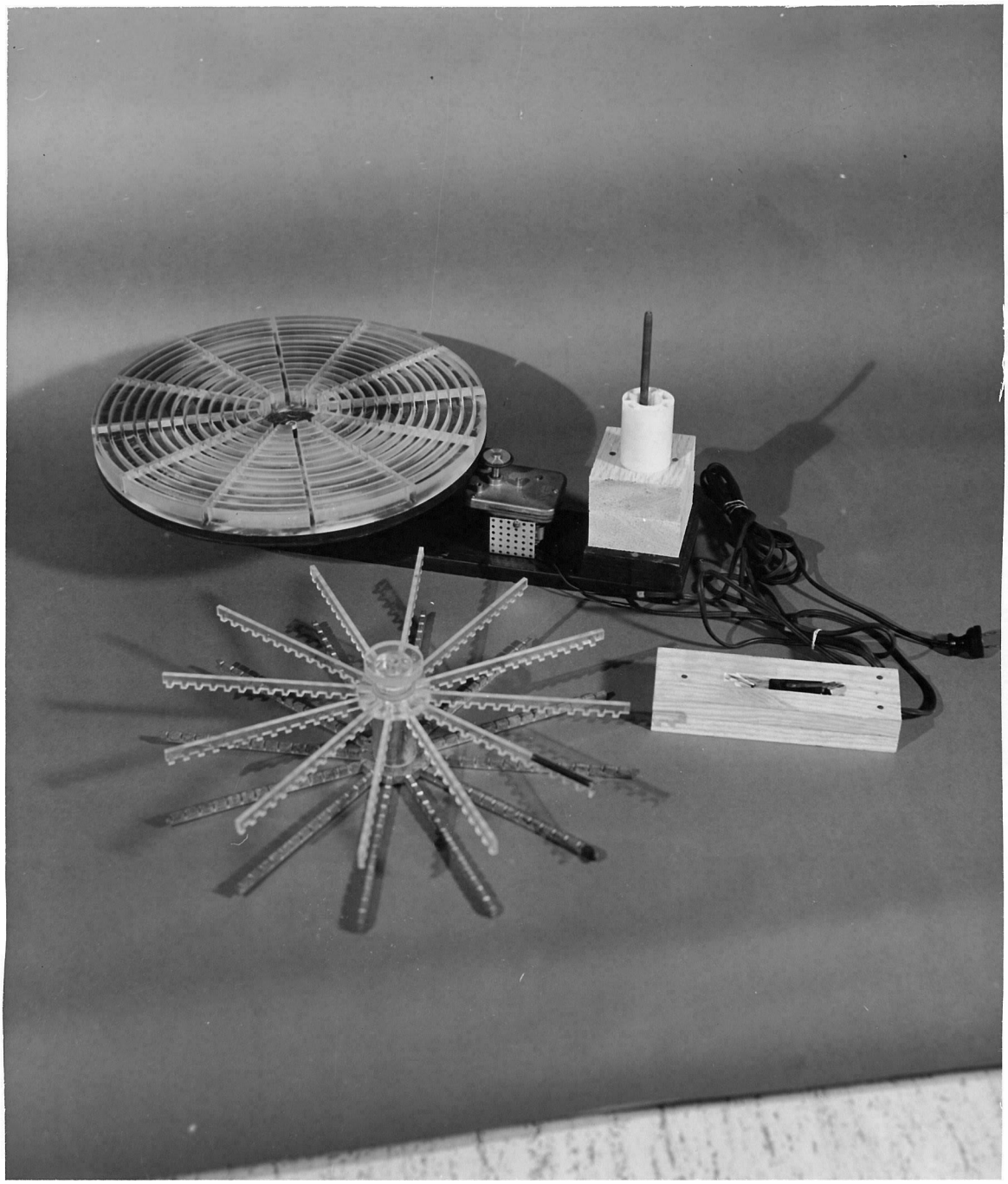

Figure A6. Special Developing Reel System

Figure A7 The Film Copier As A 35 mm Cancellation Copier

A. Red Handled Switch Used For Film Advance Control
   Switch S7 of Figure A33

B. Manual Film Advance S8

C. 70 mm Camera'

D. Door Enclosing Extra Condensing Lens Used in Unit Magnification
   Printing

OP Optical Printer

P. Internal Photocell Connection

T. Transport

TC Transport Control

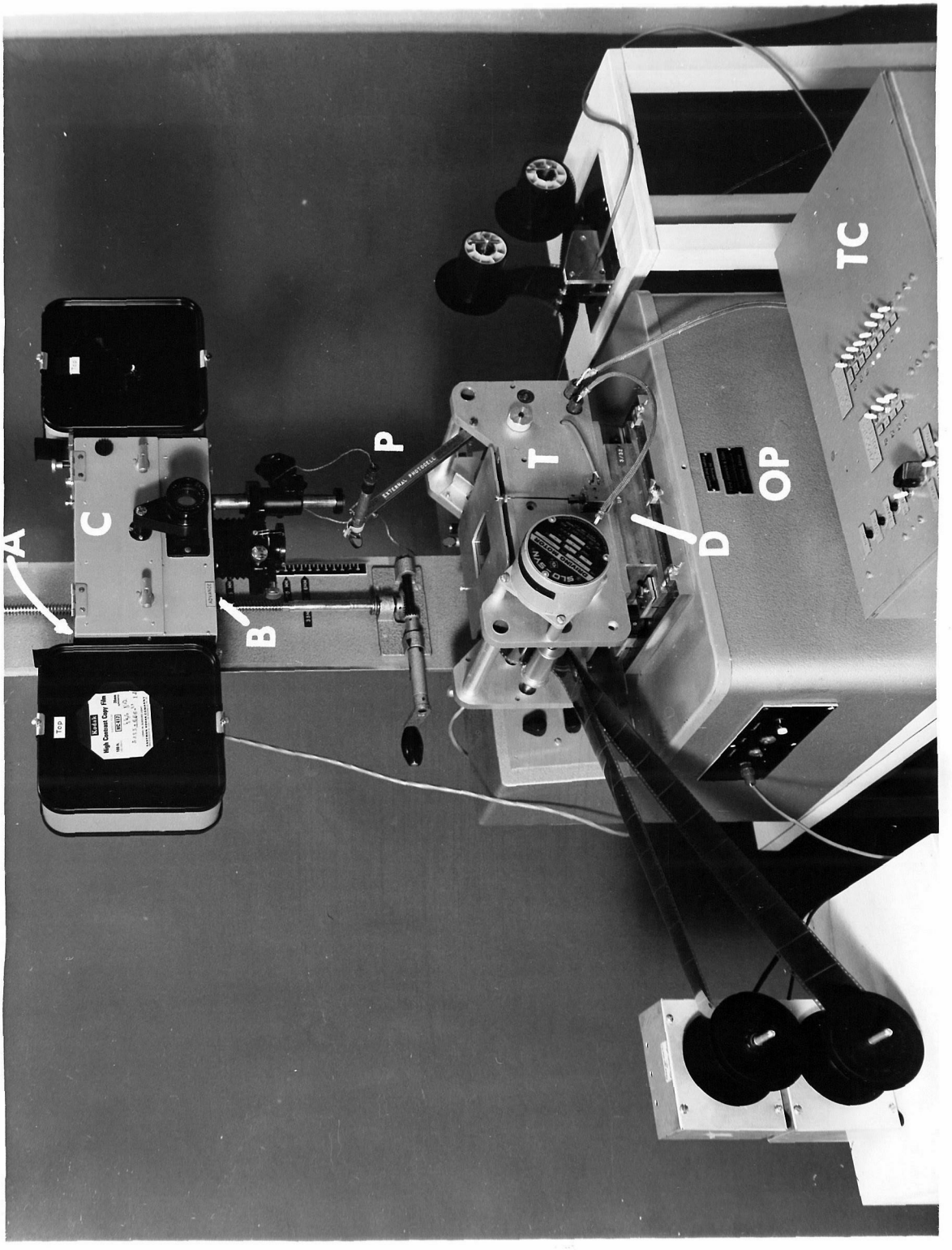

Figure A7

Figure A8 The Film Copier With the 16 mm Camera

A. Solenoid Controlling Shutter and Advance

B. Relay Interfacing the Optical Printer to Solenoid A

C. 16 mm Camera

D. Power Supple for Solenoid A

E. Connection to Power Supply D

OP Optical Printer

W. Thumbscrew to Remove and Swing Camera Out for Winding

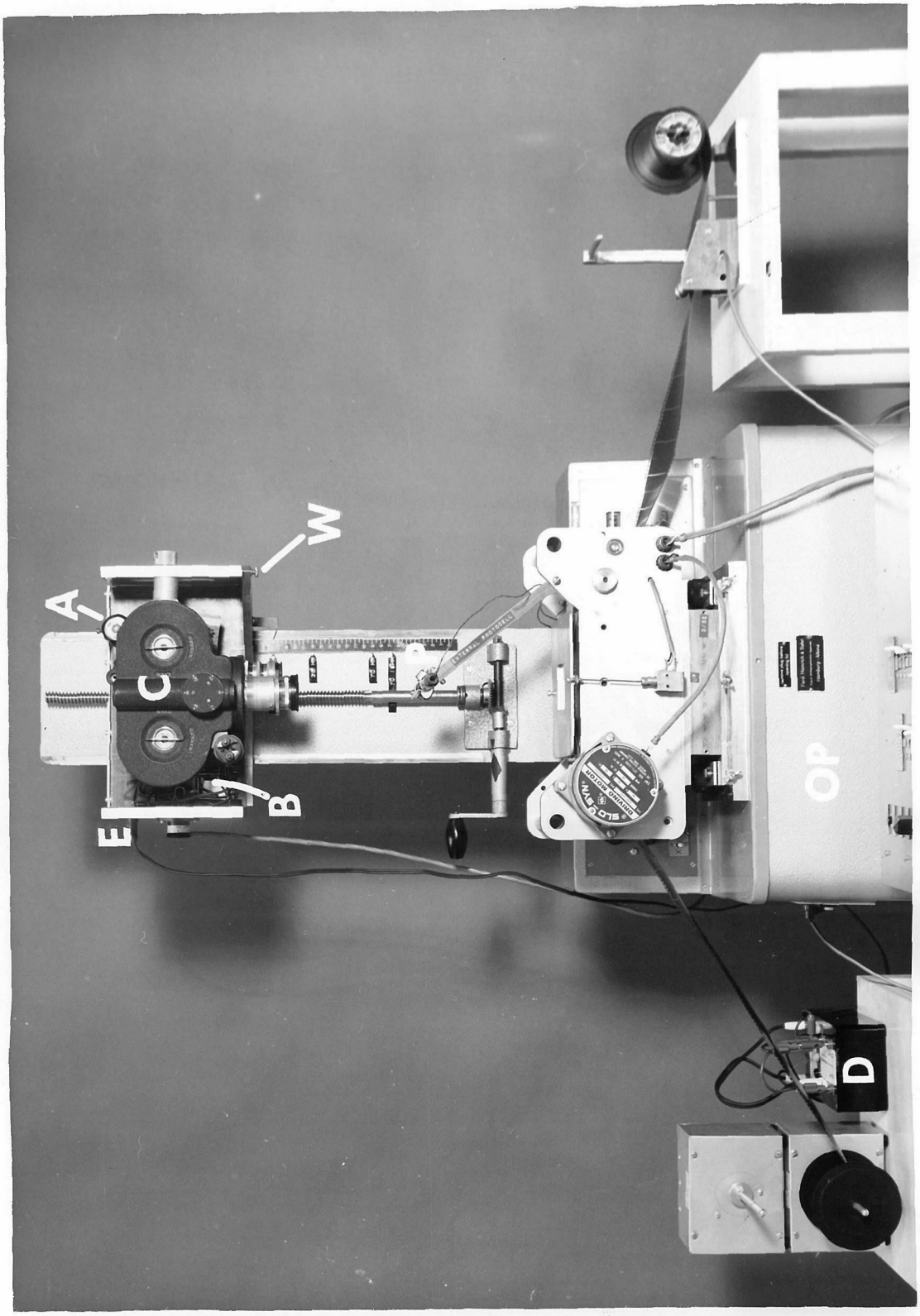

Figure A8

at room temperature yields unity gamma contrast. Achieving exactly unit contrast is not critical here.

(2) Installation of the 70 mm camera on the Optical Printer and setting up for one to one (unit magnification) printing includes the following:

a. The camera film must be started on the take-up spool.

b. The umbilical cable should be connected between the Phototimer and the internal photocell P as as shown in figure A5.

c. The third condensing lens must be installed in the bottom of the transport causing an image of the enlarging lamp to be cast approximately on the camera lens.

d. The Exposure Counter is set to 1.

e. The Steps Counter is set to 50.

f. The Solenoids Switch is set to neutral or on, not off.

g. The exposure should be set. For Shellburst and the present photocell, the settings N=1, X=1 and 10, and the lens at F/22 yields good densities with any enlarging bulb.

h. The camera must be set to unit magnification. Usually the lens will be already focused against the stop. The camera-to-subject distance is correct when the scale pointer is at 9.0 cm with the marks on the crank-shaft and bearing aligned.

With the 70 mm camera set-up, film B is threaded through the Film Transport with its emulsion up. Lifting away the pressure plate of the Transport Unit and use of the Fast-Slow knob of the Transport Control are helpful in this film threading. The Film Supply Holder

should be plugged in at this time if desired. When the contact print, -A, is placed on the register pins of the reflex window of the camera, the image of the corresponding frame of movie B may be maneuvered to produce cancellation with -A. The three screws facing the front at the base of the Film Transport move the image in the vertical direction and rotate it slightly about an axis parallel to the optical axis. Two thumbscrews, one on either side of the lens board, move the image in the horizontal direction. Care should be taken not to change the adjustment of the screws that move the reflex window since this would destroy the relationship between the reflex window registration pins and the film sprocket inside the camera. Proper alignment can only exist when the film is in tension between the two sprockets of the Transport. Prudence dictates that the registration be checked by tapping on the camera lens board and by backing up the Film Transport a few frames and then advancing it again. If the registration returns after this, one may feel confident that the operation of the camera will not change the alignment.

Assuming proper alignment and that the film in the Transport is at the first frame, then there remains only to turn out the light, remove the reflex mirror from the light path, advance a frame in the camera, and switch to automatic. The film coming out of the Transport should be threaded onto a spool on the take-up machine which should then be turned on. If the Film Supply Holder is used, the Film Copier will stop at the end of the film, so that no monitoring will be necessary. If the machine is operating properly, it will

be moderately noisy and monotonously repetitive. Occasional buzzing (120 Hz) of the solenoids of the Transport Unit is all right if moderate.

When all frames of the slave film have been copied, the camera should be advanced twenty frames or so, to give some trailer. The exposed film is next removed, using scissors on mylar film and loaded on the special developing reel shown in figure A6 . The loading is easiest if the film is wound from center outward with the emulsion out. The loading is quite straightforward, but requires some skill. Previous practice in the light with scrap film is a must. The pieces of tape on different parts of the assembly are tactile index marks for use in the dark.

For best results in development, the nitrogen burst system should give a short, high pressure (∿20psi) burst so that a raft of bubbles is formed, avoiding large scale currents. It is also helpful to occasionally lift the developing reel out, turn it, and resubmerge it, avoiding stirring motions. Development for about five minutes in D-76 at room temperature yields unity contrast ($\Gamma = 1$). Changes in developer temperature may be compensated by changing developing time at about 15 s/°C. The developer should be replenished with D-76R according to directions on the package. If the developer seems to change strength with use, adjust the replenisher to compensate.

(3) Installation of the 35 mm camera on the Optical Printer and setting up for reduction printing includes the following:

a. The camera film must be started on the take-up spool.

b. The external photocell should be plugged in and set-up as a spot photometer on the area of interest.

c. The third condensing lens must be removed from the bottom of the Film Transport, thus casting the lamp image at the higher position of the lens of the 35 mm camera.

d. The Exposure Counter is set according to the number of movie frames to be projected for each original 70 mm frame.

e. The Steps Counter should be set to 25 or 50 according to whether the original data was taken in 18 mm or 36 mm long frames.

f. The Solenoids Switch is set to neutral or on, not off.

g. The exposure should be set.

h. The desired reduction must be set, and the camera focused.

If the 16 mm camera is used in place of the 35 mm camera, procedure (b) may require modifications, and procedure (h) should be done first. In addition the 16 mm camera must be wound and the external power supply plugged in.

Once the film -B is found to give a good cancellation with film B, it may be threaded into the Transport bi-packed in register with the film A. The bi-packed film should give good cancellation except for the desired signal. The smaller cameras have shutters so that when the first frame is in position, only switching to automatic is necessary. The resulting movie is the required cancellation movie, -(A-B).

Development of a reduction print is not critical. If developing times are long enough ($\sim$10 minutes) uniformity is assured and a

Nikkor reel may be used. In the case of 16 mm film, hand development without a reel in a large tank will work as long as the film can be kept from sticking to itself. This generally means that every ten feet of film requires another gallon of developer in the tank to provide room for it to coil freely. For projection the 16 mm film should be of a "positive" type such as "Fine Grain Release Positive". Positive film does not use reversal development, but merely has a low base "fog" density suitable for projection. Positive films are also generally one-tenth the cost of negative films and may be processed under a safe light.

Appendix IV

Construction of the Film Copier

The Optical Printer was purchased in the fall of 1966 and construction of the Transport Unit was begun. It was assumed that interfacing would not be too difficult and that the most progress could be made by proceeding with the Transport Unit. When the Printer finally arrived, it became necessary to make extensive modifications of both an electrical and mechanical nature. Unfortunately, not all of these problems were immediately seen, so that corrective measures were not taken on a grand enough scale to achieve the best results. Instead, an almost endless series of patch-ups was begun, always with the thought that the end was in sight but ending in frustration as some new difficulty became apparent.

Since the Optical Printer was designed for slide copying, rather than movie cancelling, a number of modifications were necessary and expected. Beyond that, several unexpected deficiences needed correction. A discussion of some of the major difficulties follows.

The 70 mm camera came with an ordinary ground glass reflex viewing window. There was no provision for mounting film at the window, as required during the unit magnification copy procedure. After removing and carefully measuring the original window mount, a new mount with register pins and with contours flush with the ground glass was milled.

The optical axis of the camera was not perpendicular to the bed for mounting the Film Transport. Although this error angle was only about five milliradians, it led to an image whose magnification was

not constant but varied by a factor of about 1.002 over the frame width. Shimming the ways of the optical bench where they mounted to the wood chassis solved this problem. The reflex mirror was mounted on a sheet metal stamping which was somewhat twisted and did not return to exactly 45 degrees. This meant that the image focal plane did not coincide with the ground glass surface of the reflex window when it coincided with the film plane. Adjustable stops were installed, adjusted, and cemented at the best adjustment. These stops removed most of the twist in the mirror and its mount, and brought the mirror angle very close to 45 degrees. The resulting change in focal plane made necessary the milling of a new reflex window mount. The front of the camera was rebuilt at this stage, to incorporate a screw-adjustment of the new reflex window mount. A dove-tail arrangement in the new mount allowed independent adjustment of the mount in the direction of film motion which was giving the most difficulty. After minor shimming of the reflex window in its mount, coincidence of the image focal plane and the ground glass surface was achieved.

The reflex mirror of the camera was also the shutter since exposure times were expected to be longer than .5 second. With each exposure the mirror banged back and forth. After some months this caused maladjustment of the mirror again. As a remedy the mirror was readjusted and the solenoid replaced with a bi-stable, spring-loaded device allowing the mirror to be set either extreme. A manual knob controls the mirror. Designing a substitute shutter proved too difficult with the given spatial and electrical restrictions. Electrical modifications were made to operate the enlarging light instead of

using a shutter.

The original procedure for adjusting the mount was to photograph a target with the camera and then put the photo on the register pins of the reflex window. If the target was not moved in the meantime, the reflex mount could be moved until the photograph cancelled the projected image of the target. At this position the register pins on the mount are at the reflected position of the sprocket holes of the camera film.

Actually, this simple procedure had to be modified because the bi-packed films in the Film Transport are not pin registered. They are sprocket registered and the sprocket teeth slant. It is thus necessary to use the following procedure: First, set the camera to make a unit magnification print. Second, contact print a target picture in pin register and put this print on the reflex window pins. Third, put the target in the Film Transport, align the projected image with the contact print on the reflex viewer and take a camera picture. Fourth, bi-pack this picture with the original in sprocket registration and view through the reflex viewer. The translation of the reflex window mount is that translation necessary to cause the contact print to move from coincidence with the target image to coincidence with the image of the camera picture of the target.

Although the 70 mm camera had a pin registered movement, it was only designed to register two bi-packed films as in making contact prints. The register pins did not register the film exactly in the camera; the geneva was supposed to do that. The geneva was so badly machined that it caused a wobble of the sprocket of a few thousandths

of an inch. Since the registry of the film was the same for even numbers of advances of the sprocket, an insidious alignment problem arose. The alignment procedure would seem to work since, as luck would have it, an even number of advances was typically used for the alignment photograph. Later testing, after an odd number of advances, would indicate malalignment. A good geneva was purchased from Precision Instrument Company and an entire advance mechanism designed and fabricated to fit in the 70 mm camera.

The electrical system of the Optical Printer was mostly electromechanical. A 220 volt, 50 Hz timing motor and some cams and microswitches controlled its operation. These components were housed in the wooden chassis. The operation of the Optical Printer itself was good except that at 60 Hz the timer motor allowed too little time for the complete advance of the 70 mm camera. This could be solved by pausing briefly between pictures.

After mechanically interfacing the Optical Printer with the Transport Unit using a relay and a microswitch, the internal radio-frequency interference (RFI) problem arose. This internal RFI problem was not solved until the electrical system of the Optical Printer was replaced by a low voltage electronic one, designed to interface with the Transport Unit. RFI from outside sources was stopped by filtering the line and putting all the new Optical Printer electronics in grounded metal chasses connected by shielded cable.

The original data as taken on Mount Wilson have density variations in them from time to time as changes in solar intensity at the telescope and SHG speed occur. As new settings are used and types of

data are obtained, different densities from film to film occur. In order to achieve uniform density in the 35 mm copies of the data, a photocell exposure timing system was designed and built. Later this was modified to avoid including light beyond the picture edges in the photocell measurement.

The Film Transport itself was designed and built in the fall of 1966. The use of a stepping motor in place of a geneva movement was a mechanical simplification, but an electrical complication. This mechanical simplification is somewhat illusory, since the exact position of the stepping motor sprocket is influenced by changes in the film tension. Thus, a tensioning device that is precise must be employed. Moreover the device must be able to take-up at least one step worth of slack film because angular momentum of the sprocket causes a momentary overshoot of a fraction of a step as the motor halts.

It was necessary to modify the Film Transport to include a pressure plate to hold the film to be copied flat. This problem of film curl is particularly bad when the films are to be held emulsion to emulsion.

Besides the electrical problems mentioned earlier, some other problems peculiar to fast digital electronics occurred. If an electronic counter is to count operations of a push button or other switch, then account must be taken of contact bounce in the switch. It is impressive for the uninitiated to see a counter count 3, 4 or 5 counts randomly at the flick of a switch. This problem is easily controlled with a set-reset flip-flop described in Appendix V. Another problem in circuits involving flip-flops is that their internal state is de-

pendent on their history as well as the states of their inputs. It is a good idea to have an indicator light for each flip-flop so malfunctioning ones may be spotted easily. The most frequent cause of flip-flop problems is spurious trigger pulses. Another difficulty was that of trying to spot malfunctions in circuitry while an automatic clock was busy pulsing the system. This was solved by building an alternate manual clock. In designing complex digital circuits, it is well to remember that the system has 2^n states where n is the number of flip-flops. It is well to consider what each state will cause to happen, including those states which are not used in normal operation, for they may be used in abnormal operation with disastrous results.

If the entire system were built again from the beginning, I would make several recommendations. The first would be to build rather than buy both the Optical Printer and the Film Transport. Second, both should mount to a solid metal plate. Third, the 70 mm camera should have a transparent pressure plate and opening at the back for direct viewing of the image at the film plane. In this way the reflex window with its registration pins and mirror would be eliminated. In its place would be the registration mechanism of the camera itself. Fourth, the lens should have X and Y, as well as Z motions for shifting the image on the film as well as focusing. Fifth, the Film Transport or the camera should have a small rotational degree of adjustment about the optic axis. Sixth, film transport should have pin registry to avoid the registration difficulty of the slanting sprocket teeth which shows up in bi-packing film. Finally, the transport should allow film to be loaded and unloaded in the middle of a roll.

Appendix V

Film Copier Design Details

This section explains the operation of the internal parts of the Film Copier. It is hoped that enough detail and explanation has been given that a person, able to operate the Film Copier when it is in order, could repair it without too much difficulty if it malfunctions. On the other hand, complete explanation would be too lengthy and thus unclear. The text assumes familiarity with the operating controls.

A. Logic Circuitry and Symbols

Figure A10 shows some of the major symbols used in circuit schematics representing logic circuits. The logic value "true" is called 1 and is represented electrically by a high (>1 volt)voltage and the logic value "false" is called 0 and is represented by a low (ground) voltage. The outputs of the symbolized devices are a function of the inputs, and a logical equation is given for this function.

Figure A10 Logic Circuit Symbols

Symbol	Name	Logical Function
	Amplifier	$A(a) = a$
	Inverter	$A(a) = \bar{a}$
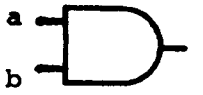	AND gate	$A(a,b) = a \cdot b$
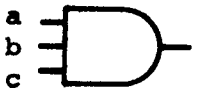	AND gate	$A(a,b,c) = a \cdot b \cdot c$

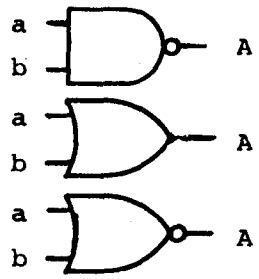

NAND gate $A(a,b) = \overline{a \cdot b}$

OR gate $A(a,b) = a + b$

NOR gate $A(a,b) = \overline{(a + b)}$

A small circle on an input or output of a symbol means that the input or output is inverted from what it would have been. The most common circuit element used in the Film Copier is a n-input NOR gate which is implemented electronically as shown in figure A 11 The inverter can be considered as a one input NOR gate and is implemented that way electronically.

Figure A 11 Electronics of a NOR Gate

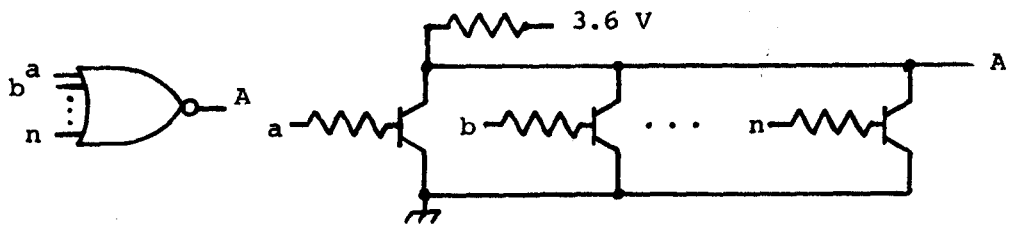

Another important class of logic devices is the flip-flop. Two kinds are used in the Film Copier; the first is the set-reset, or S-R flip-flop, and the second is a variant of the J-K flip-flop.

The S-R flip-flop is symbolized below.

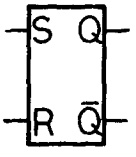

S and R are inputs and Q and $\bar{Q}$ are outputs. An S-R flip-flop is usually constructed from two 2-input NOR gates as shown in figure

Figure A12 Implementation of the S-R Flip-Flop

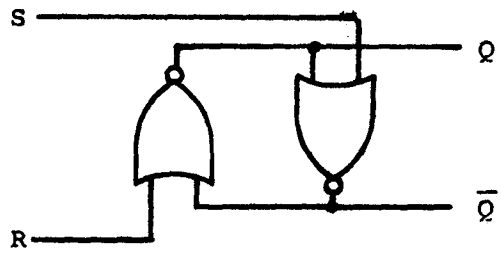

Truth Table

S	R	Q	$\overline{Q}$
1	1	0	0
1	0	1	0
0	1	0	1
0	0	X	$\overline{X}$

As shown in the truth table of figure A12 there are two stable states of the flip-flop when the inputs S and R are both 0. Either of these states may be attained by momentarily causing a 1 on either S or R. The state where both S and R are 1 is generally avoided, since it is usually desired that $\overline{Q}$ have the opposite value of Q as its label implies. S-R flip-flops can be made from NOR gates having 3 or more inputs, thus providing extra independent S or R inputs.

The J-K flip-flop is a triggered flip-flop of great versatility. The inputs are usually labeled J,K, and T, and the outputs Q, and $\overline{Q}$. The outputs may change state only when the T input is changed from 0 to 1. The new state attained will depend on the values of J, K, and Q itself. Figure A13 shows the symbol for a J-K flip-flop and a truth table summarizing its properties. The subscript on Q indicates how many trigger pulses have been received. Before the nth trigger pulse, Q might have a value of either 1 or 0. Let X be that value. $\overline{Q}$ has a value opposite to Q at all times.

Figure A13 The Canonical J-K Flip Flop Truth Table

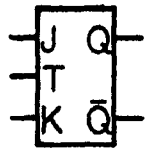

J	K	Q_{n-1}	Q_n
0	0	X	X
1	0	X	1
0	1	X	0
1	1	X	$\overline{X}$

If J and K are affected at the time of the trigger pulse, this will not affect the outcome of the transition because the flip-flop uses the values of J and K that just precede the trigger pulse. It is often convenient to use another symbol instead of Q such as the name of the flip-flop if it has one. For example, a flip-flop labeled A would have outputs A and $\overline{A}$. The J-K flip-flop may have set and/or reset inputs in addition. These behave as for a normal S-R flip-flop and take precedence over the J-K type operation except when both S and R are 0. The actual J-k flip-flops used have inverters on the inputs J,K, and T and on the outputs Q and $\overline{Q}$. If we take J, K, and T to be the values on the input leads and Q and $\overline{Q}$ to be the values on the output leads, then the truth table below follows:

Figure A14

J	K	Q_{n-1}	Q_n
0	0	X	$\overline{X}$
1	0	X	1
0	1	X	0
1	1	X	X

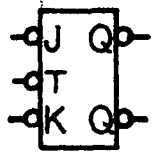

where transition is caused by T going from 1 to 0. In addition a reset lead is available forcing the Q output to a value of 0. The labeling system used by the manufacturer is shown in figure A15 however, the system in figure A14 is used extensively in the diagrams in this appendix because it seems strange to have an output labeled 1 whose value may be 0 or 1.

Figure A15 Another Labeling System For the J-K Flip-Flop

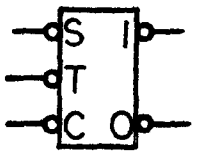

S (set) = J

T (trigger) = T

C (clear) = K

"1" = Q

"0" = $\overline{Q}$

Occasionally a lead in a circuit diagram will be labeled with a logic value. This means connection to a power supply or ground, possibly through a resistor. Toggle switches are shown as in figure

Figure A16 Toggle Switches

SPST SPDT DPDT 4PDT

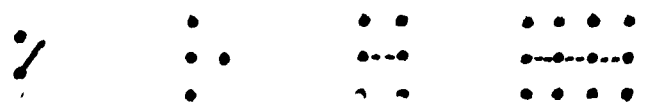

Push button switches, microswitches, relay contacts, and any other switch having normally closed and normally open contacts are symbolized as in figure A17 usually with contacts shown in normal position.

Figure A17 Switches With Normal Positions

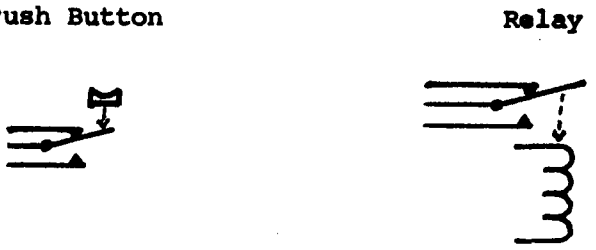

Lines which cross without a node are not connected. A special symbol resembling an arrowhead indicates an input to or output from a circuit according to its orientation.

Figure A18 Connection Symbols

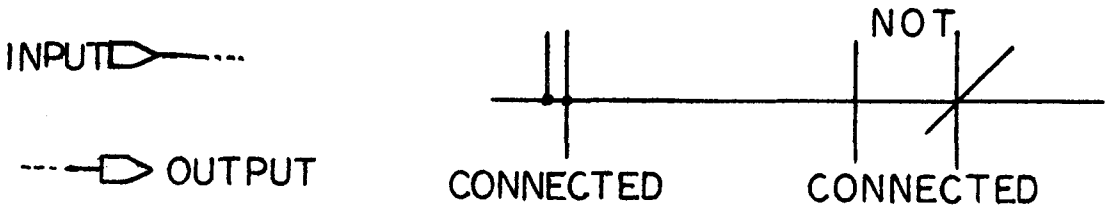

B. The Film Copier

The Film Copier consists of two independent parts, see Figure A19 the Optical Printer and the Transport Unit. A cable connected between them will cause them to operate together. In this mode of operation the Transport Unit signals the Optical Printer to make exposures and then receives a signal back at the completion of each exposure.

The Optical Printer consists of a Camera Control and an interchangeable pair of cameras, one for 35 mm film, the other for 70 mm film. The Camera Control signals the camera shutter to open and the film advance to operate. The camera in return signals the number of frames advanced and the completion of advancement.

The Transport Unit consists of a Transport Control and the Film Transport itself. The Transport Control directly controls the motor and solenoids of the Film Transport. In addition, it controls operation of the Optical Printer when used in the automatic mode. An optional Film Supply may be plugged into the Transport Control box. When this is done, the signal which causes the Optical Printer to make an exposure must pass through a microswitch which interrupts the signal if the Film Supply is out of film.

(1) The Optical Printer

Figure A20 shows a block diagram of the Transport Unit. The Fast-Slow knob controls the pulse rate of the clock which sends timing signals to the Transport Sequence Control. The Sequence Control can send stepping signals to the Motor State Control which in turn deter-

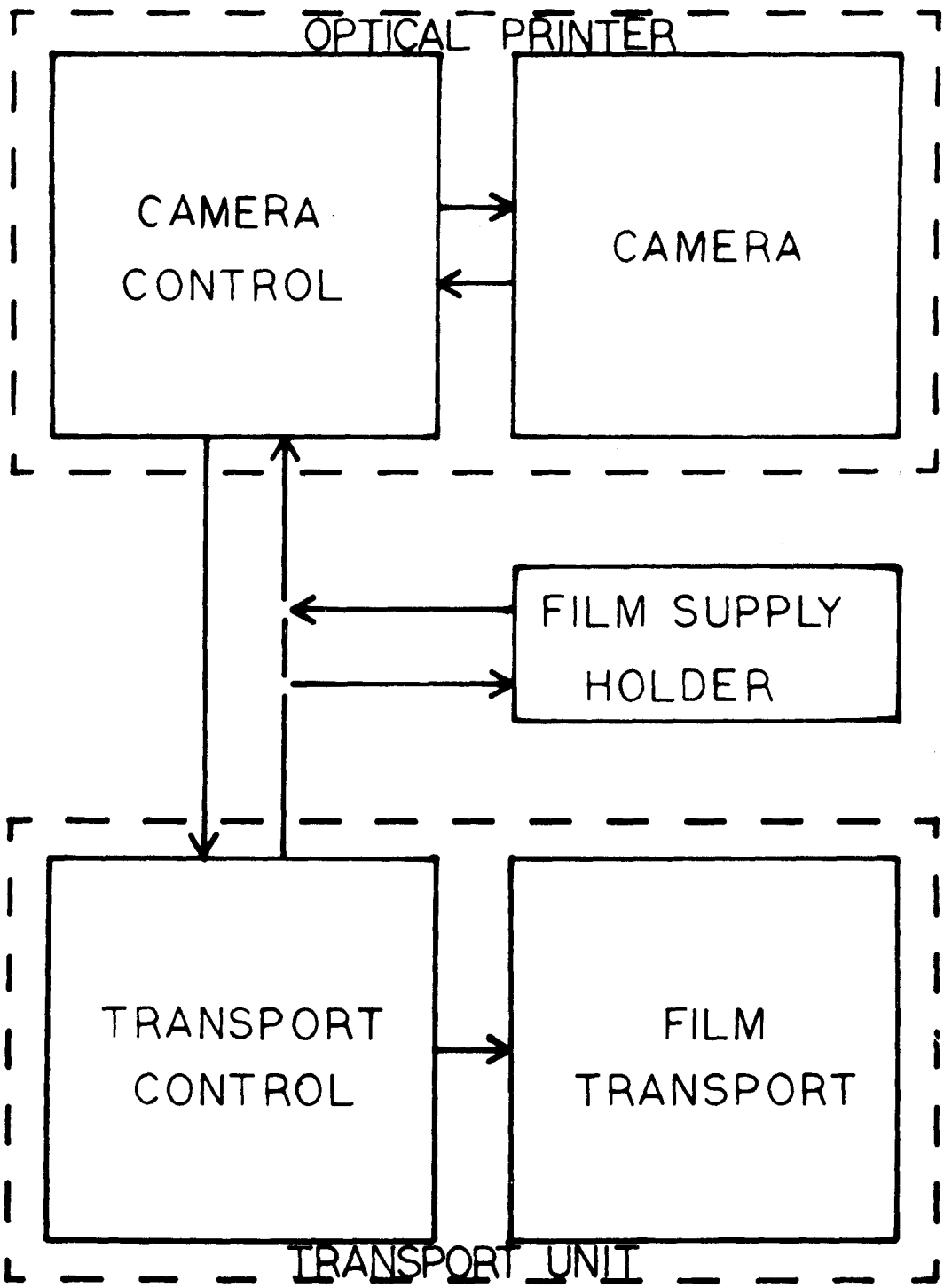

Figure A19 **The Film Copier**

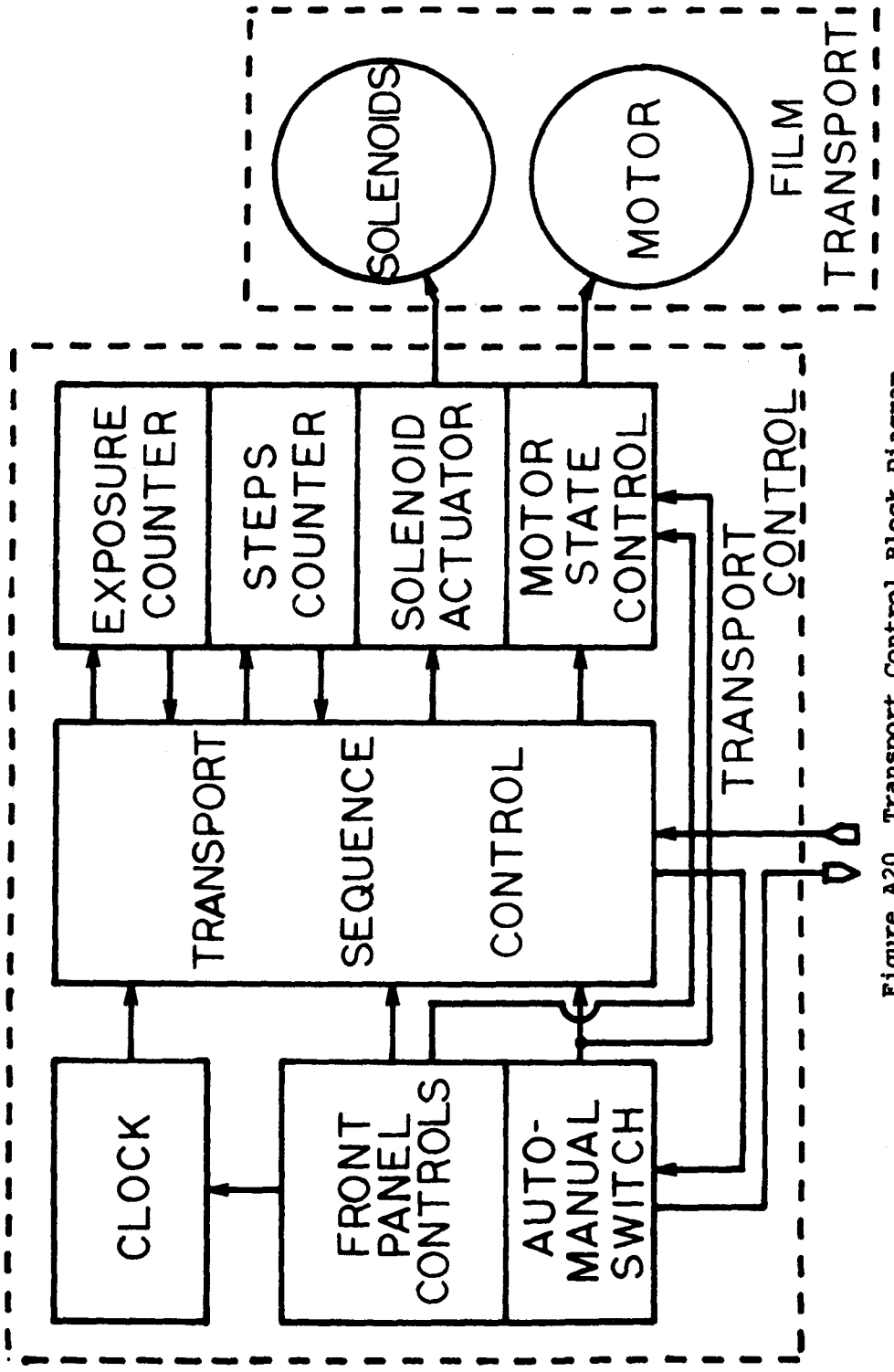

Figure A20 Transport Control Block Diagram

mines how to phase the current in the stepping motor windings in order to step. The direction of the step is determined by the reverse button on the front panel and the Auto-Manual switch.

The Auto-Manual switch controls the mode of operation of the Transport Unit. In the manual mode, signals to the Optical Printer are blocked and the front panel controls are enabled. Operation of front panel controls causes signals to be sent to the Transport Sequence Control, where logic circuits combine them with clock signals to generate stepping signals and to release the film (solenoids) when the film is moved. When the front panel controls are idle in the manual mode, the Sequence Control will have automatically reset the Exposure Counter, and be awaiting signals from the Optical Printer. If the Optical Printer is operated manually, it will send signals to the Sequence Control, which will relay them to the Exposure Counter. When the Exposure Counter has counted enough exposures, it will signal the Sequence Control to advance the Stepping Motor.

(a) Transport Control Power Supply

The Transport Control has two DC power supplies. The 35 V, 2A supply powers the stepping motor, the indicator lights and clock. The 3.6V, .5A supply powers the integrated circuitry. Figure A21 below is a schematic diagram of the power supplies.

The basic circuit is similar in both supplies; a transformer feeds a full wave diode bridge whose rectified output is ripple filtered by a very large capacitor. In the 3.6 V supply this filtered power is regulated by a zener diode controlled emitter follower circuit.

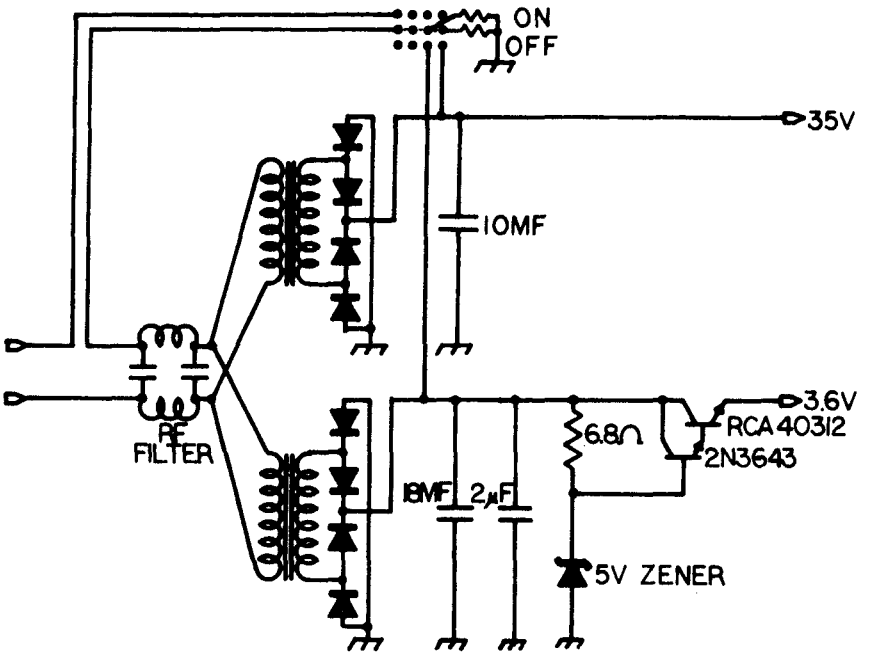

Figure A21 Transport Control Power Supply

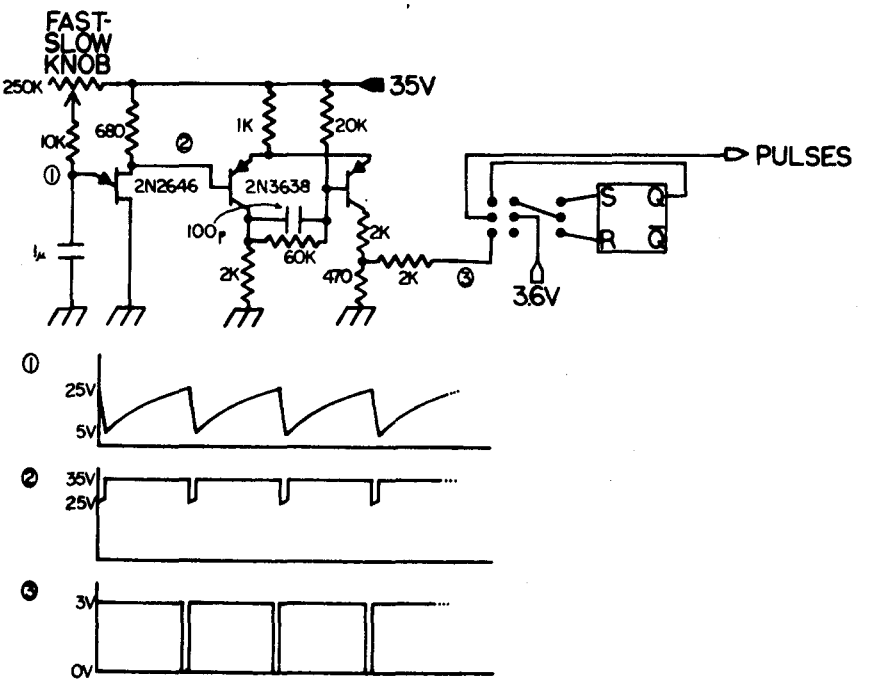

Figure A22 Transport Control Clock

The 2 μf capacitor is for RF filtering, as is the LC network on the input line.

(b) Transport Control Clock

There are 2 clocks in the Transport Control; one is a pulse generator of adjustable frequency, the other is a manually switched S-R flip-flop. A toggle switch inside the chassis choses between the two clocks. The manual clock is chosen for debugging purposes and the pulse generator for normal operation.

The pulse generator is a unijunction transistor oscillator[2] feeding a Schmitt trigger[3]. The resulting clock signal as a function of time is graphed below the circuit diagram.

(c) Transport Sequence Control

The clocking causes the two J-K flip-flops of the Sequence Control to sequence cyclically through four internal states. These states are decoded and cause the following sequence of events:

01 Camera operation and exposure counting

00 Resetting step counter

10 Transport operation and step counting

11 Resetting exposure counter

When a counter is set to count a certain number, N, of pulses; then its gate circuit has an output of 0 unless the number, N, has been reached. Thus resetting a counter to 0 will cause the gate to go to 0 unless N = 0. On the next sequential state after resetting, the counter will be set to count and further states will be prevented

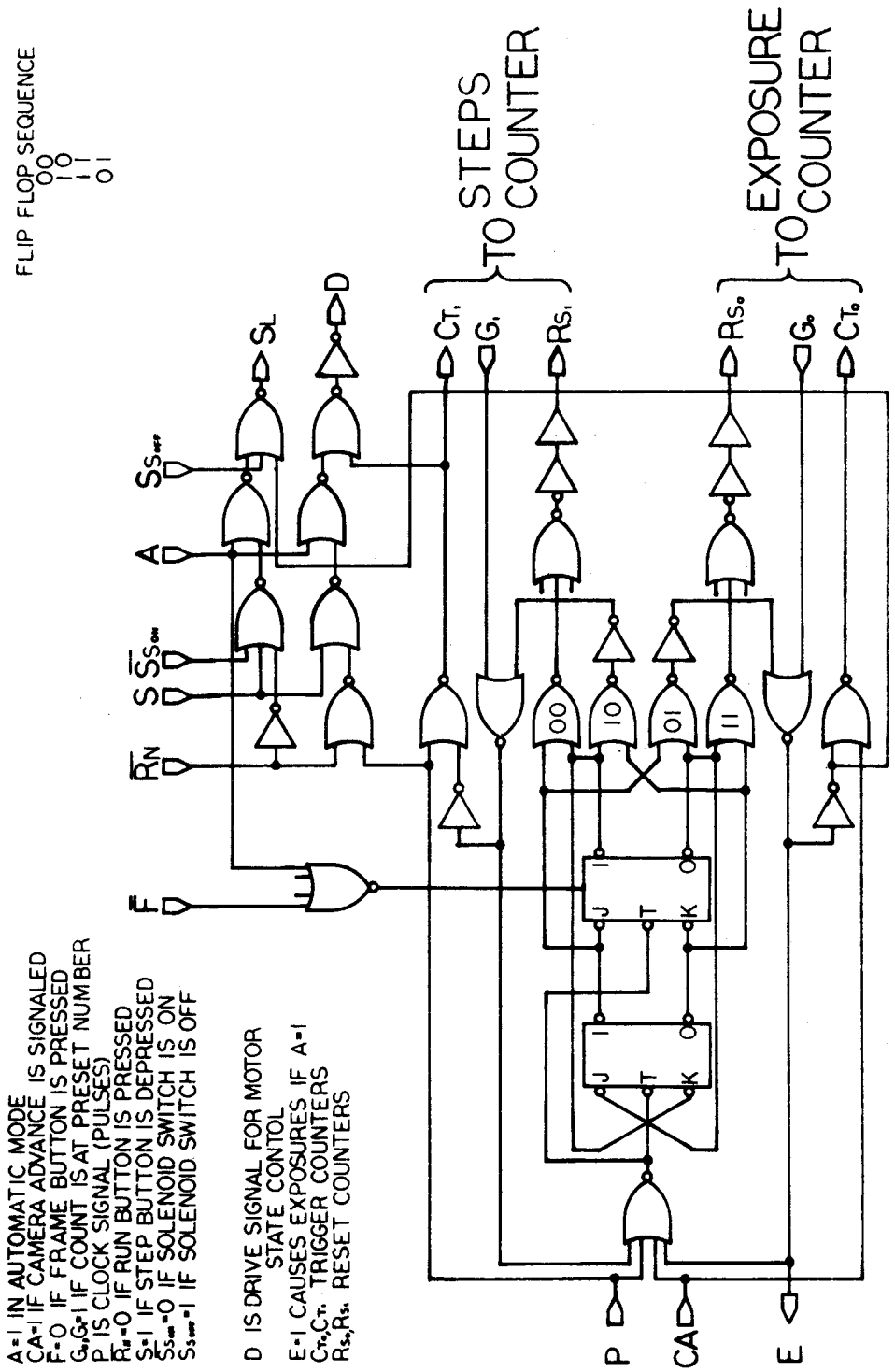

Figure A23 Transport Sequence Control

until the gate goes to 1. The clock changes the states and causes the Step Counter to count and the stepping motor to step. It cannot however cause the Exposure Counter to count. Thus, if the camera does not expose, the sequencer will stop in the 01 state waiting. In this state a signal is sent to the camera sequence control to expose. This signal is interrupted if the Auto-Manual switch is at manual or the Film Supply Holder is empty.

In the manual mode the sequencer will stop waiting for camera cycles to count. The frame button is enabled in this mode to reset a flip-flop forcing a transition from 01 to 00. The pulse generator will then cause the next step to 10, followed by counting, and then an attempt to go to 11. As long as the frame button is pressed, only the 00 and 10 states are possible. When the frame button is released, sequence control will be able to go to 11 and stop at 01 again.

The remaining logic circuits control the driving pulses to the Stepping Motor State Control and the operation of the solenoids so that the Run and Step buttons are disabled in the automatic mode and so that the solenoids release the film when the stepping motor is moving it.

(d) The Motor State Control

The stepping motor is of the bi-filar type having four windings which we may label A, $\overline{A}$, B, and $\overline{B}$. These windings must be turned on and off in the following sequence of states or its reverse:

	0	1	2	3
A	ON	OFF	OFF	ON
$\overline{A}$	OFF	ON	ON	OFF
B	ON	ON	OFF	OFF
$\overline{B}$	OFF	OFF	ON	ON

The pattern immediately suggests that A and $\overline{A}$ should be controlled by the opposite outputs of a flip-flop, and similarly for B and $\overline{B}$. The sequence can be generated by alternately flipping the A flip-flop and then the B flip-flop. The following figure shows the two arrangements of two J-K flip-flops which give the above sequence and its inverse.

Figure A24 The Basis for the Motor State Control Design

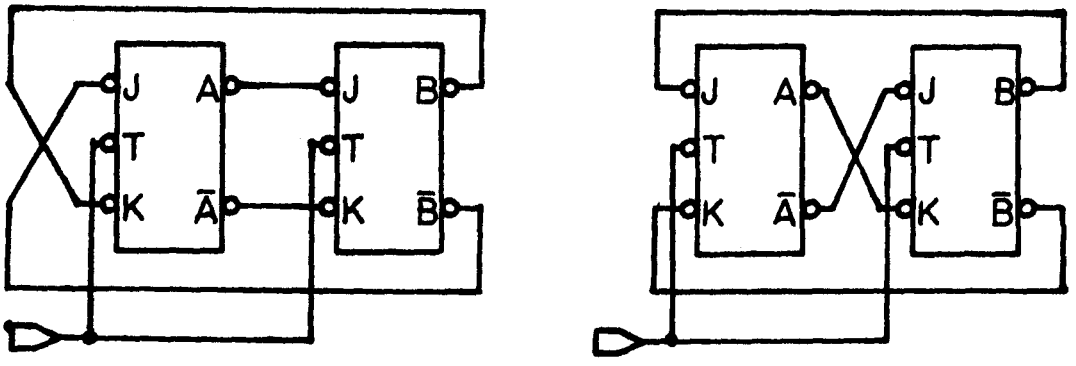

The 200 positions of the motor may be labeled each according to its electrical state; 0,1,2, or 3. The result is that position N has electrical state N (mod 4). There are 50 positions corresponding to each state. The motor always goes to the nearest position corresponding to a given state when states change. Clearly a change, from say state 0 to state 2 in a time small compared to the reaction time

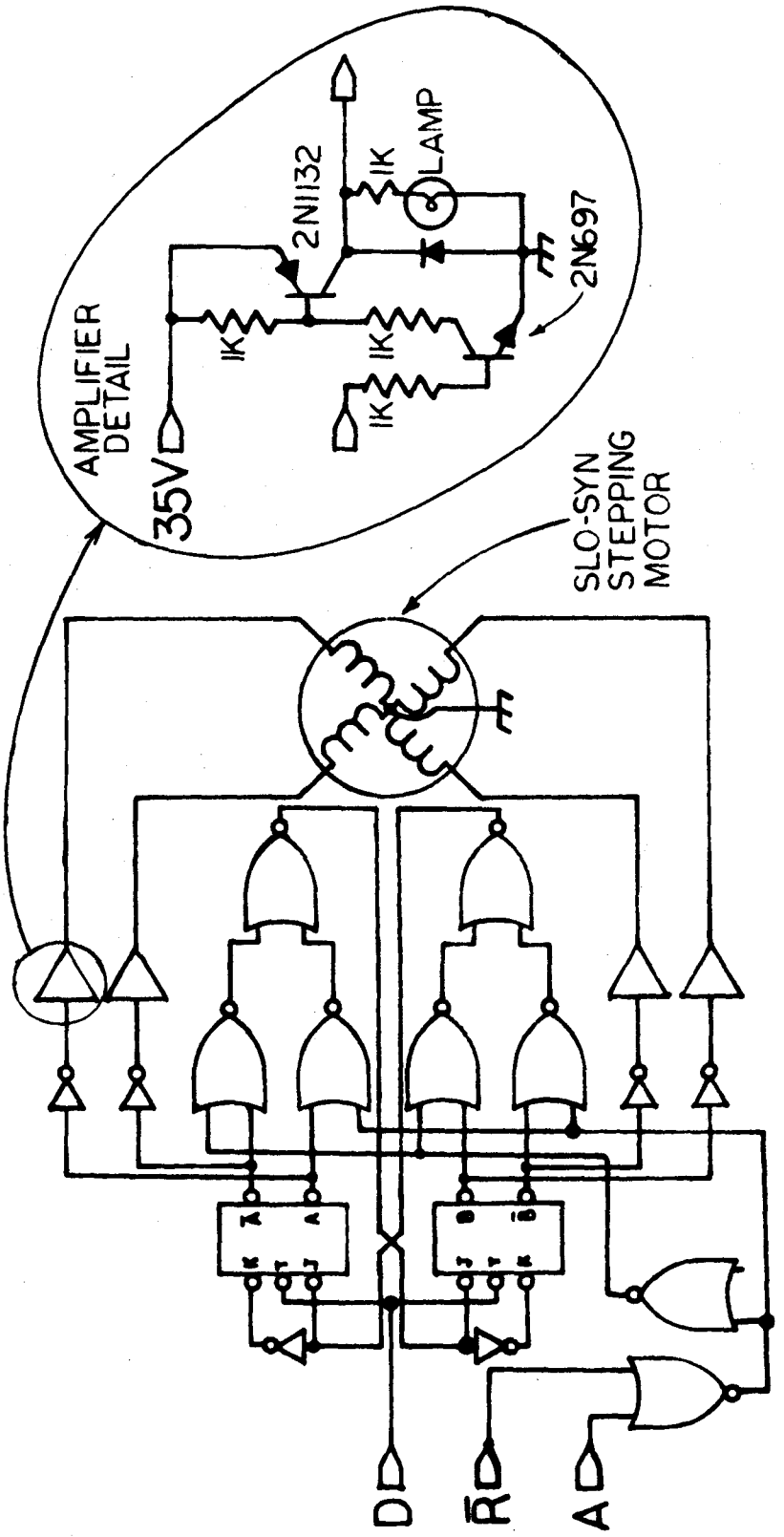

Figure A25 The Motor State Control

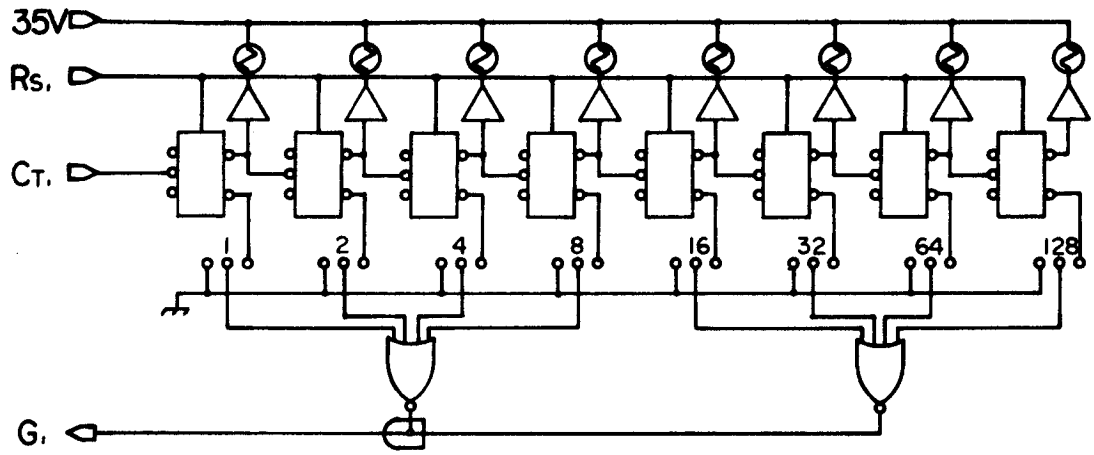

Steps Counter

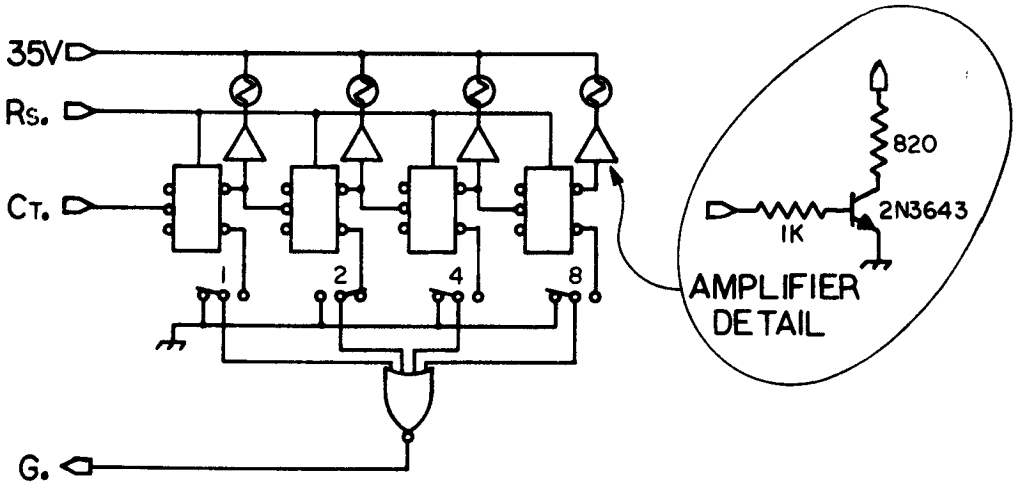

Exposure Counter

Figure A26 Counting Circuits

of the motor, will lead to ambiguity as to which position corresponding to state 2 is closest to state 0.

Figure A25 shows the actual implementation of the above ideas for the Motor State Control. The NOR gates allow switching between the two connection schemes shown in Figure A24. The flip-flop outputs are amplified in several stages to 35V, at .3A. The diodes prevent inductive voltage surges, when windings are turned off. The indicator lights are arranged in the pattern $A\overline{BAB}$ in a circle on the circuit card. The pattern of the lights shifts clockwise when the motor steps forward and counter-clockwise when the motor steps back.

(e) Counting Circuits

Figure A26 shows the counting circuits for the Exposure Counter and Steps Counter respectively. The counter gate will detect any number, N, of trigger pulses, if the panel switches are set to sum to N. The value of any switch is 0 if set to the left and equal to the value shown above it if set to the right. A counter will also detect certain numbers higher than the number set on the switches. This is not a problem in actual practice since the counter stops at the first detection and is reset to zero before the next count. The Exposure Counter is shown set for N = 2. Analysis of the gate circuit shows that it will detect N = 2, 3, 6, 7, 10, 11, 14, and 15. The outputs of the two NOR gates of the Steps Counter are simply wired together. This has the same result as if they were wired to an AND gate, as symbolized.

The solenoids operate the film pressure plate of the Transport. Since they are 110 V AC solenoids, it was necessary to interface with the logic circuitry. This interface had to be done in such a way as to avoid inductive voltages when the solenoids were turned off. The resulting circuit is diagrammed schematically in figure A27 below.

Figure A27 Solenoid Circuitry

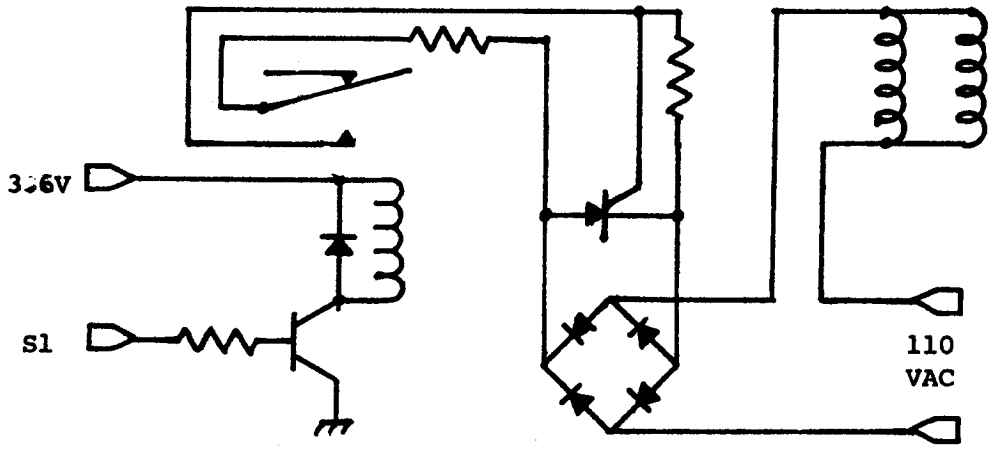

(2) The Optical Printer

Figure A28 shows a block diagram of the Optical Printer. The input from the Transport Unit has the same effect as manually pushing the Expose button on the left side of the printer. The enlarging lamp may be turned on manually, but will be turned on electronically if necessary during film exposure. The same signal turns on the lamp, opens the camera shutter, and sets the photo timer into operation. The photo timer signals the end of exposure time,causing the Camera Sequence Control to cease exposure and start advancing

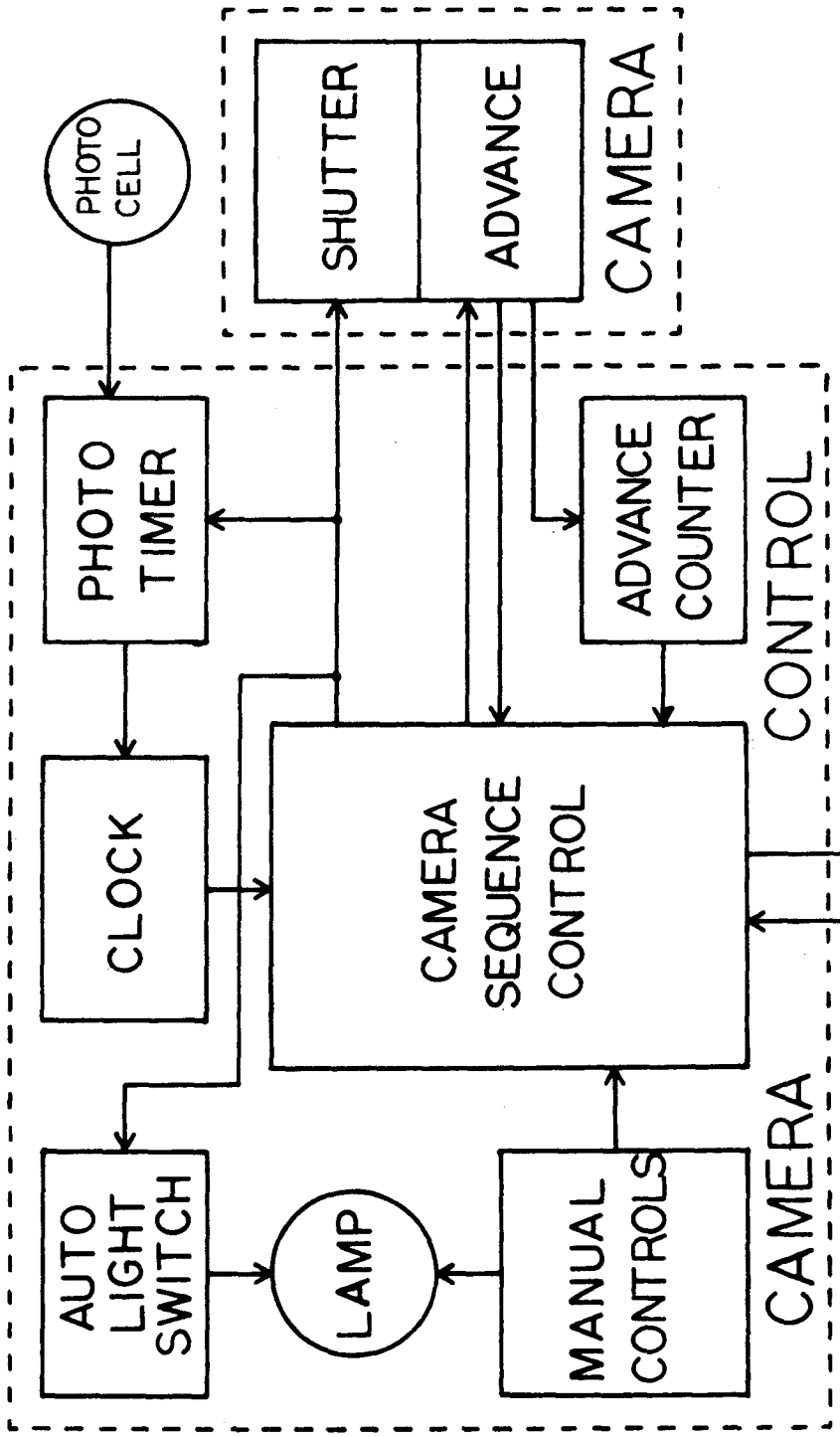

Figure A28 Optical Printer Block Diagram

film. The signal to advance film also informs the Transport Unit that the exposure is complete. Since the advance speed and number of frames advanced is different with different cameras, the camera must signal both the number of frames advanced and the end of advancement itself. The first signal goes to the Advance Counter on the right front panel of the Camera Control. The Advance Counter will halt further exposures after a pre-selected number of advances, which is usually selected to correspond to the camera running out of film. The Camera Sequence Control awaits the end-of-advancement signal before allowing the next exposure to begin.

(a) Optical Printer Power Supply

The Optical Printer has two DC power supplies. The 15V, 5A supply powers the camera, phototimer, advance counter, and electronic light switch. The 4.5V, .6A supply powers all integrated circuitry.

The DC power supplies are very much alike in configuration as can be seen in figure A29 below. The basic circuit is a transformer which feeds a full wave diode bridge whose rectified output is filtered by a very large capacitance. This filtered DC power is voltage regulated by a Zener diode controlled emitter follower circuit. The power supplies contain RF filters in, hopefully, strategic locations.

(b) Optical Printer Clock

Figure A30 shows the circuit schematic for the clock. The four main parts are a UJT oscillator, a Schmitt trigger, a frequency shifter, and a gate. The oscillator and trigger function as they do in the

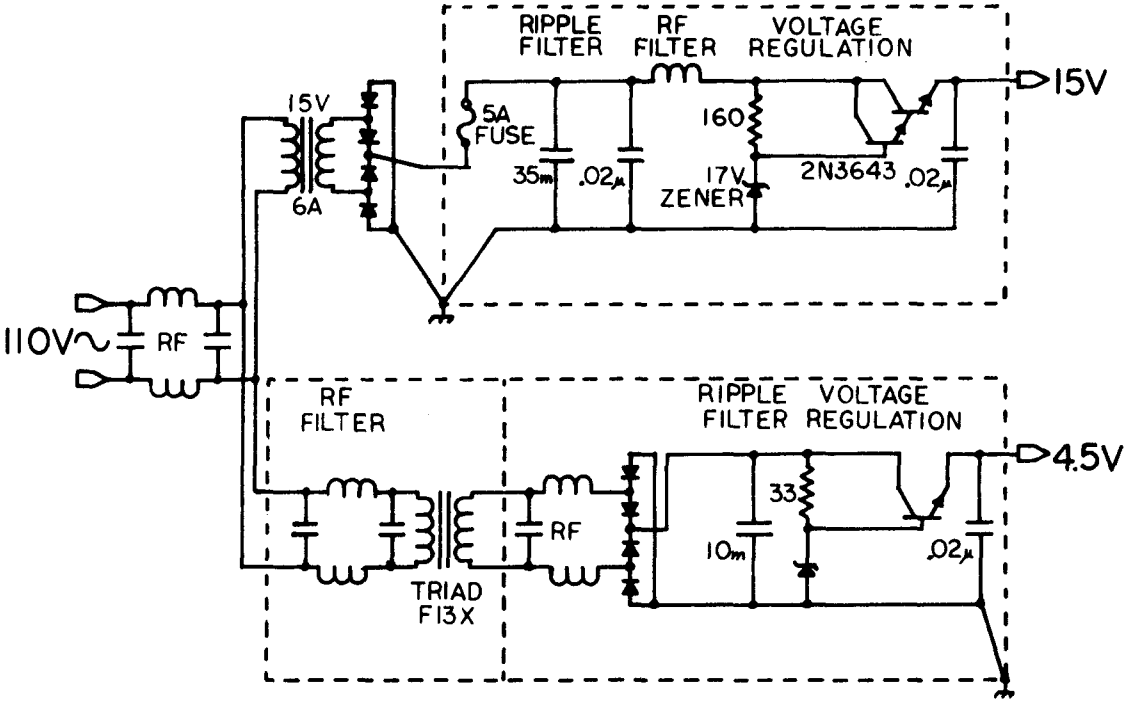

Figure A29 Optical Printer Power Supply

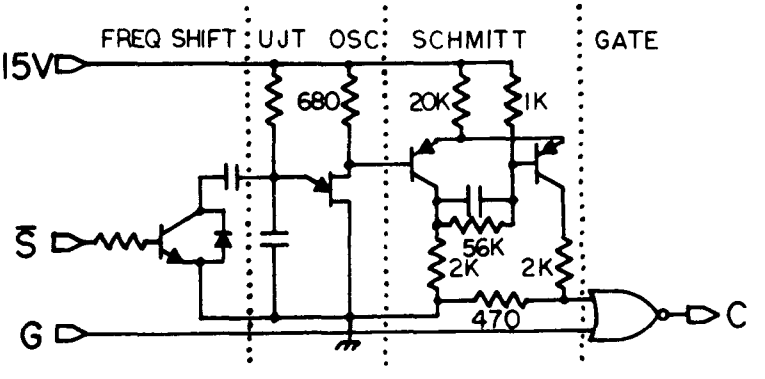

Figure A30 Optical Printer Clock

Transport Control Clock. The frequency shifter switches a timing capacitor of the oscillator, shifting the usual 5 Hz to about 500 Hz. The gate controls the output pulses to the Camera Sequence Control.

The clock puts out 5 Hz normally. When exposure begins, the S input to the frequency shifter goes to 0, boosting the frequency. Simultaneously the G input to the gate goes to 1 blocking the next pulses. When the desired amount of light has been measured, the gate input returns to 0. The next pulse then escapes within 1/500 second,ending the exposure and returning the frequency to 5 Hz.

(c) Camera Sequence Control

There are two J-K flip-flops in the Camera Sequence Control and thus four internal states. These are decoded and cause the following actions in sequence as clock pulses are received:

0) Wait for expose signal and film advance completion

1) Expose frame

2) Dummy

3) Advance film and signal Exposure Counter in Transport Control

The expose button and the automatic switch on the printer cause an S-R flip-flop to be set. When reset, the 0 state above will be stable. The 2 state would be stable but it sets the flip-flop. State 3 resets so that only state 0 is stable. The S-R flip-flop may not be set during film advance or shortly thereafter, since the relay R and the capacitor C assure that the advance is done before the next exposure begins. The photo timer controls clock pulses thus assuring

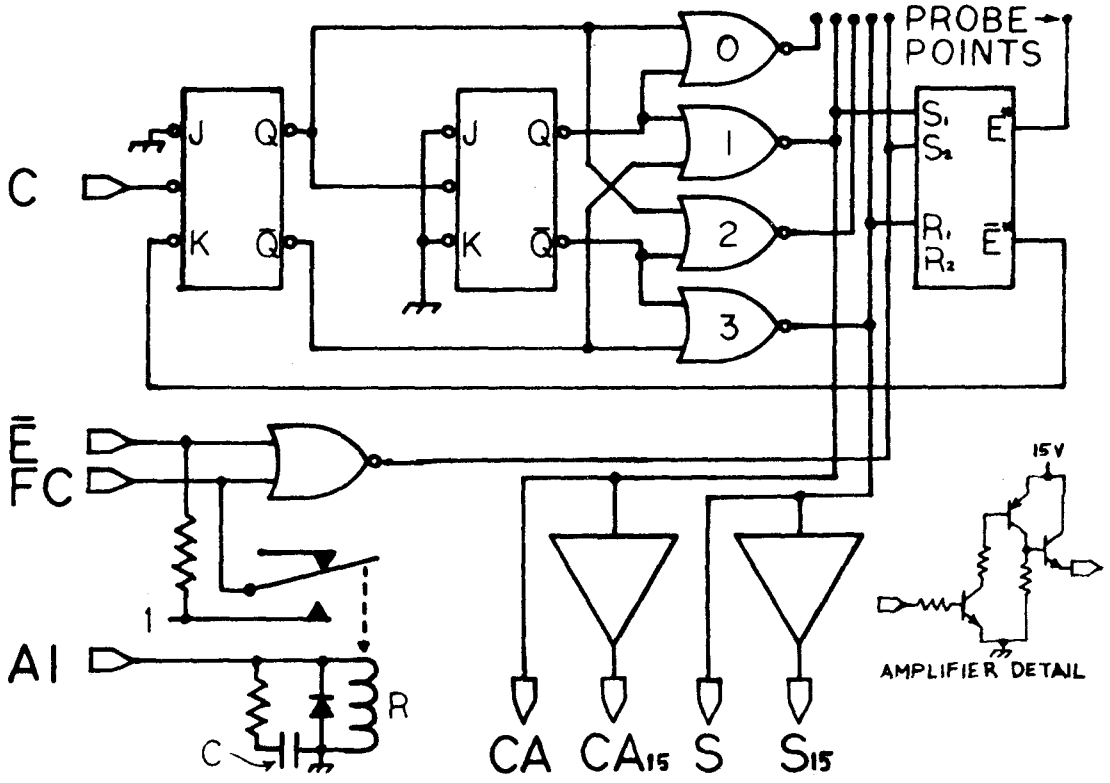

Figure A31 Camera Sequence Control

that exposure is finished before advance may begin.

(d) The Photo Timer

Figure A32 below shows the circuit schematic for the Photo Timer. There are two UJT oscillators, called measurer and perturber. The basic equation governing the exposure measurement is the following:

$$\text{Flux} = \int I(t)dt = kC \ln(V_p/V_v) = \text{const}$$

where C is the timing capacitance, V_p and V_v are peak and valley emitter voltages. I is the light intensity on the photo cell and k is defined by

$$k = I \cdot \text{photo cell resistance} \approx \text{const}$$

The capacitor C will charge until it reaches the voltage V_p at which time the UJT will fire spontaneously unless I is too small. In the latter case, a perturber pulse will precipitate the firing. Any required amount of flux may be measured by adjusting C, and counting a suitable number, N, of firings of the flux measuring circuit. There is a choice of four capacitors, and some logic circuitry allows a choice of N = 0 to N = 99. The black spots on the different stages of rotary switches indicate switch positions for which conduction occurs.

(e) The Cameras

Figure A33 shows a schematic diagram of the 35 mm and 70 mm copy cameras. The 70 mm copy camera operation is just like that of the 35 mm copy camera including labeling with the following exceptions. Switch S4 keeps the advance motor from starting before the register pins have cleared the film sprocket holes. The register pins are part of the pressure plate which is lifted by the pressure plate

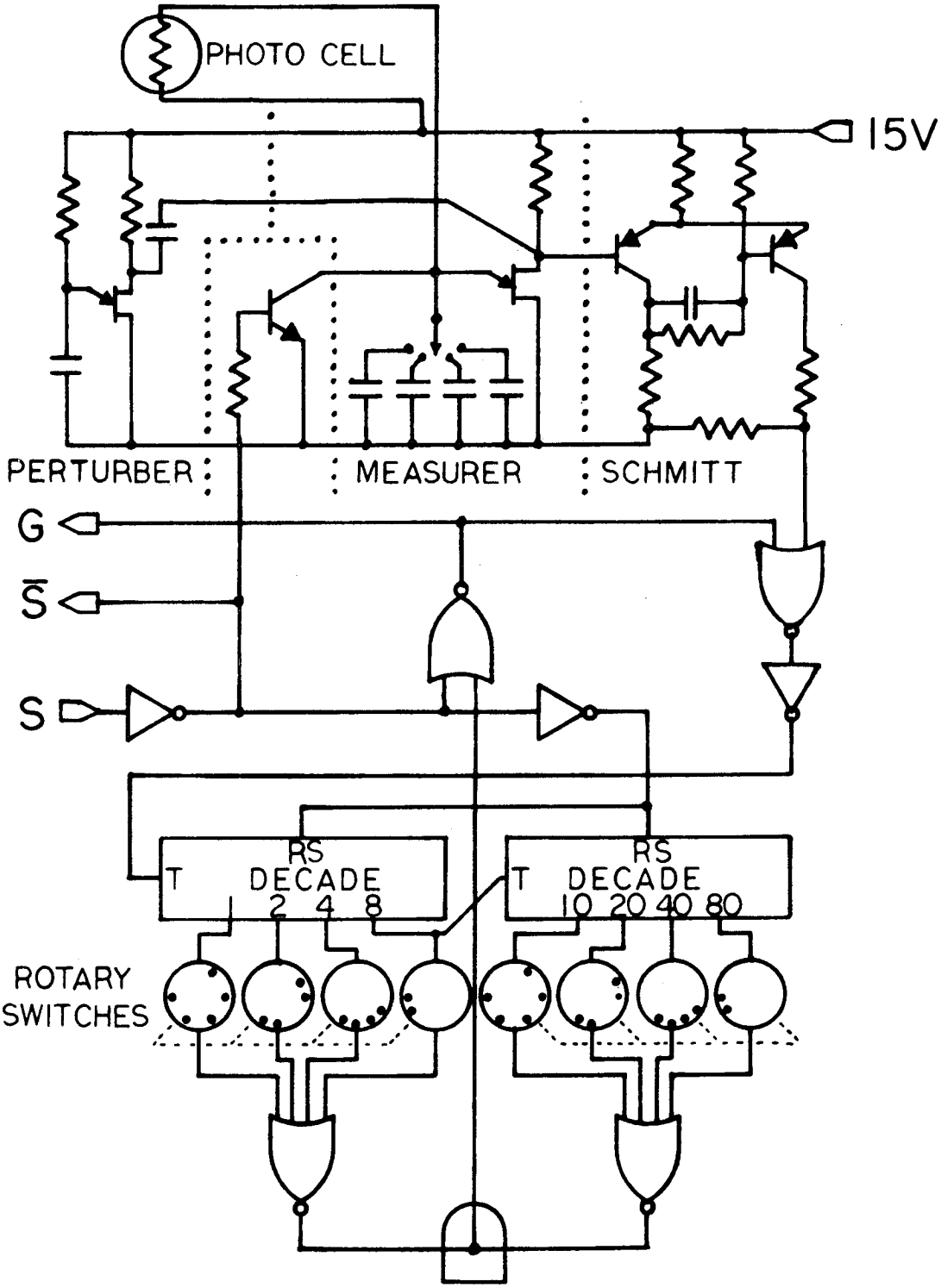

Figure A32 The Phototimer

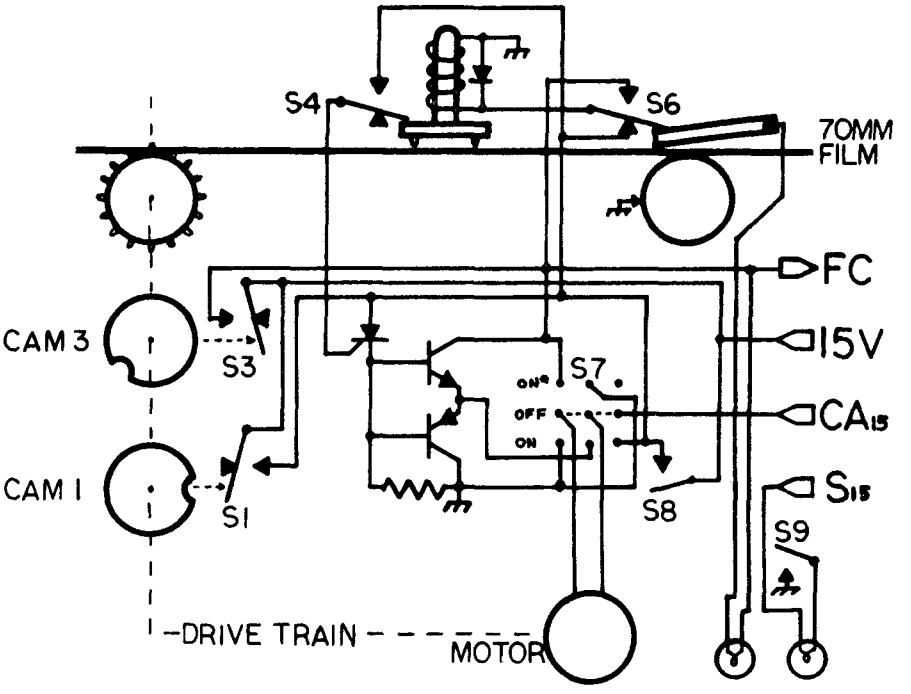

70mm Camera

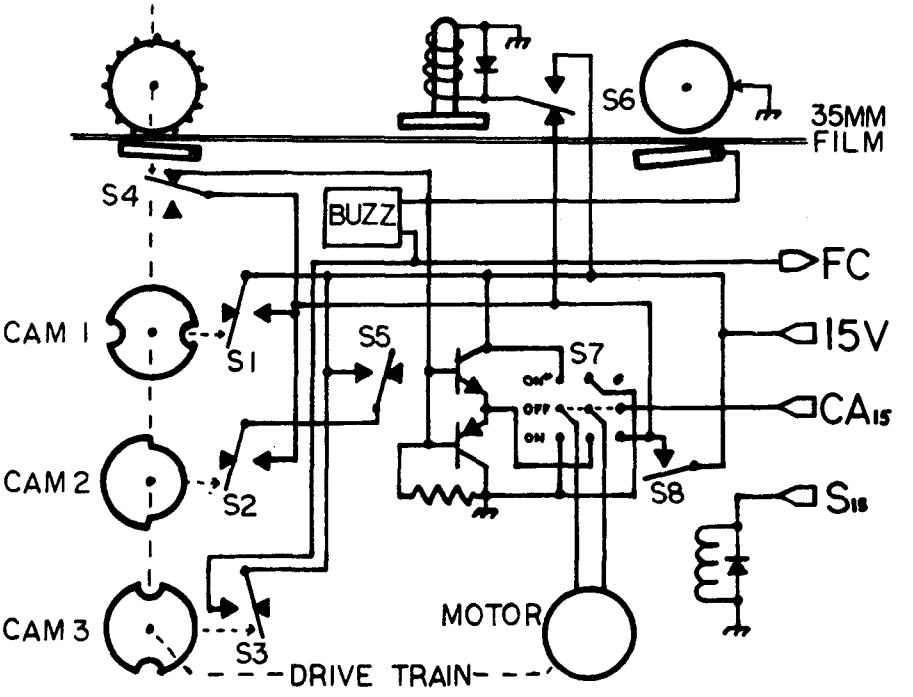

35mm Camera

Figure A33 The Cameras

solenoid. The effects of contact bounce in switch S4 are eliminated by the SCR. The buzzer has been replaced by a warning light. Since the shutter is hand operated, the shutter signal now actuates a warning light if the shutter is not opened for exposure.

To understand the operation of the film advance, assume the camera is initially quiescent. In that case all switches may be set as shown. A brief 15 volt signal coming through the advance input or the switch S8 will lift the pressure plate solenoid through S6 and start the advance motor through S4 and the double emitter follower circuit. The motor turns the three cams. Cam 1 keeps the motor advancing after the initiating signal is gone until it has turned an integer number of half revolutions. Cam 2 keeps the motor advancing past the first half revolution, provided switch S5 is closed. Switch S5 is controlled by the size of frame exposed. Cam 3 sends signals to the frame counter and to the buzzer.

The buzzer will buzz on this signal if its ground lead is connected through the pressure roller. Switch S4 opens if film becomes tangled around the sprocket. When this happens, the motor may only be run backwards using switch S7. Switch S6 lifts the pressure plate solenoid when the camera is opened for film loading.

The shutter input signal (15V) actuates the shutter solenoid opening the shutter. The diode prevents an inductive voltage surge when the solenoid is turned off.

The double emitter follower circuit dynamically brakes the motor when the 15 V signal in the advance line disappears. The PNP emitter follower section tends to short to ground at this time, loading the

motor now turned generator.

REFERENCES

1. Leighton, R. B. Ap. J. 130: 336-380. 1959.

2. Leighton, R. B. Nuovo Cimento (Supp.). 22: 321-325. 1961.

3. Leighton, R. B., Noyes, R. W. and Simon, G. W. Ap. J. 135: 474-499. 1962.

4. Noyes, R. W., Ph.D. Thesis, California Institute of Technology, 1963.

5. Simon, G. W., Ph.D. Thesis, California Institute of Technology, 1964.

6. Simon, G. W. and Leighton, R. B. Ap. J. 140: 1120-1147. 1964.

7. Sheeley, Jr., N. R., Ph.D. Thesis, California Institute of Technology, 1965.

8. Title, A. M., Ph.D. Thesis, California Institute of Technology, 1966.

9. Bruzek, A. I. A. U. Symp. 35: 293-298. 1967.

10. Bruzek, A. Solar Phys. 2: 451-461. 1967.

11. Bruzek, A. Solar Phys. 8: 29-36. 1969.

12. Zirin, H. Private Communication, August 1969.

13. Weart, S. R., and Zirin, H. Pub. Astron. Soc. of Pacific. 81: 270. 1969.

14. Ellison, M. A. Monthly Notices Roy. Astron. Soc. 104: 22. 1944.

15. Babcock, H. W. Ap. J. 133: 572-587. 1961.

16. Hyder, C. Private Communication, August 1969.

17. de Jager, C. Handbuch der Physik. 52: 80-362. Springer-Verlag, Berlin. 1959.

18. Kuiper, G. P. (ed.), The Solar System. Vol. 2. University of Chicago Press, Chicago. 1953.